zone as a boundary between two layers.

As to a resistive layer of more than 5,000Ωm, it shows a westward dipping to the west of Station No. 75. In general, this layer, except for the second layer of Station No. 77, is the deepest layer modeled in this section. A resistive layer of 1,000–5,000Ωm is considered to reflect compact amphibolite distributed at shallow depths and it is found as three small blocks, i.e., between Station No. 78 and No. 79, between Station No. 81 and No. 83, and to the east of Station No. 86.

Several fault structures are presumed to the east of Station No. 76: the most noticeable one being those between Station No. 80 and No. 81, between Station No. 77 and No. 78, and between Station No. 79 and No. 80. Several blocks of amphibolite seems to be regulated by these faults.

SECTION–F

A sort of highly resistive concave structure can be found in this section, which shows a resistive layer of more than 1,000Ωm distributed in the depth of about 50m in both ends of the section, trends toward the center of the section, where the resistivity layer of less than 1,000Ωm reflects the schist seen thickly distributed from Section–D. As in Section–E, the highly resistive is also distributed from the surface and trending more widely towards the E-W direction.

2–3–4 Resistivity Plan Maps

In order to obtain the information of the resistivity structure at probable depths of the existing ore deposits or mineralization zones, interpreted resistivities at 100m, 300m and 500m, were plotted on plan maps as shown in Figs. III–15 through III–17.

100m DEPTH

As shown in Fig. III–15, resistivities lower than 1,000Ωm are found around the center and the east of the survey area.

The one at the center forms a resistivity belt extending toward the N-S direction and divides, consequently, the survey area. In the middle this resistivity belt is so distributed that reflects effects of a fault structure, while at both edges the existence of a widely distributed conductive layer is suggested. Another conductive zone, being arranged in the NE-SW direction within a high resistivity zone, is found at the west of the survey area, which may be caused by a fault and fractured zone.

On the other hand, resistivities higher than 1,000Ωm are widely distributed to the west and east of the survey area. The one at the west forms a large resistive zone which may correspond to

a homogeneous high-resistivity layer (rock). And the other one at the east shows a tendency to arrange toward the NE-SW direction, and a distribution being subdivided by NW-SE structural lineaments. Most of Alvo are actually located in this high resistivity zone of more than 1,000Ωm.

There are many local resistivities higher than 1,000Ωm in the whole survey area, which may correspond to compact amphibolite and/or basement rocks.

300 m DEPTH

This plan map shows a strong resistivity contrast, with resistivities of less than 1,000Ωm and those of more than 10,000Ωm seen partly scattered.

Resistivities of lower than 1,000Ωm are found to the north, to the center and to the south of the survey area. With the exception of the east, they give origin to a resistive zone which is seen connected along the N-S direction in the plan map of 100m depth. However, in this map, the mentioned zones seem to be divided by higher resistivity zones. Resistivities at the east show almost the same distribution as those on a map of 100m depth, but reflecting more clearly the structural lineaments of the N-S and NE-SW directions.

Low resistivity zones of lower than 100Ωm seem to be distributed more widely than those on a map of 100m depth, suggesting the existence of local conductive layers, which may correspond to a fault and fractured zone.

Distribution of resistivities higher than 10,000Ωm seems to be increased in the whole area comparing with a map of 100m depth.

500 m DEPTH

This map shows a stronger resistivity contrast than the above 300m depth plan map and some interesting distributions considered to reflect in a better way the geological structure.

Resistivities of less than 1,000Ωm are concentrated around the center of the survey area. Among those, the most interesting distributions, which may reflect geological structure, are (1) the one trending in the N-S direction at the center of the area, (2) the one found scattered along the NW-SE direction at the northeast of the area, and (3) the one trending in the NW-SE direction at the southeastern corner of the area. The first one at the center shows almost the same distribution as above 100m depth map and forms a low resistivity zone being arranged in the direction of NNE-SSW to N-S. The second at the northeast, suggesting to reflect a structural line of NW-SE direction, is composed of four scattered small zones arranging in the NW-SE direction and has a tendency to be connected to the first one at the south of the survey area. Therefore, it can be said that most of resistivity zones of less than 1,000Ωm may be caused by the fault structures.

Resistivity distributions of more than 1,000Ωm, being thought to reflect highly resistive rocks, are subdivided by low resistivities corresponding to structural lines, but increase those extents in comparison to above 300m depth map so that it can be said highly resistive rocks are distributed more widely and more compact in the depths.

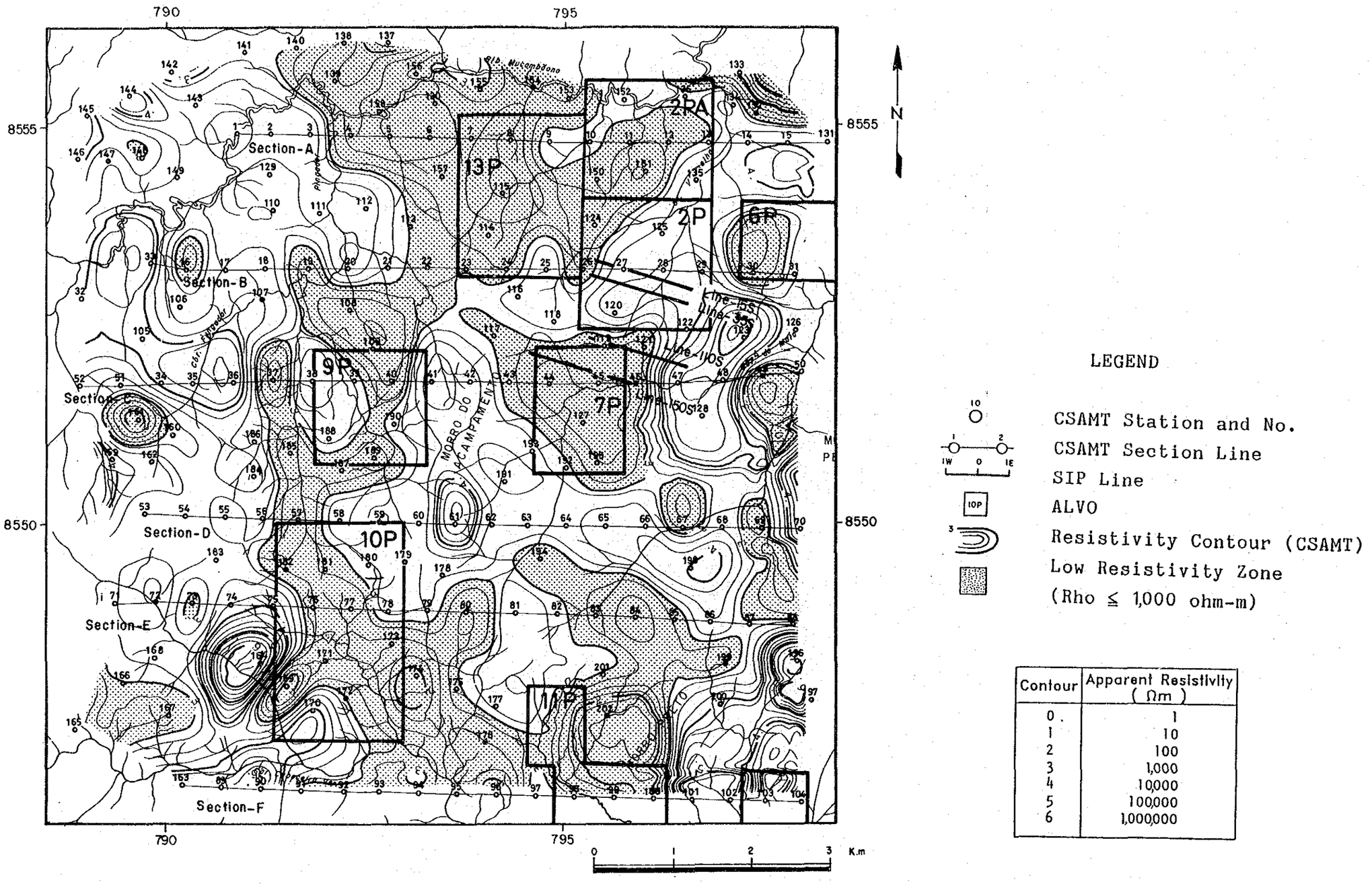

LEGEND

- CSAMT Station and No.
- CSAMT Section Line
- SIP Line
- ALVO
- Resistivity Contour (CSAMT)
- Low Resistivity Zone (Rho ≤ 1,000 ohm-m)

Contour	Apparent Resistivity (Ωm)
0	1
1	10
2	100
3	1,000
4	10,000
5	100,000
6	1,000,000

Fig. III–15 Resistivity Structure Map [CSAMT (–100 m)]

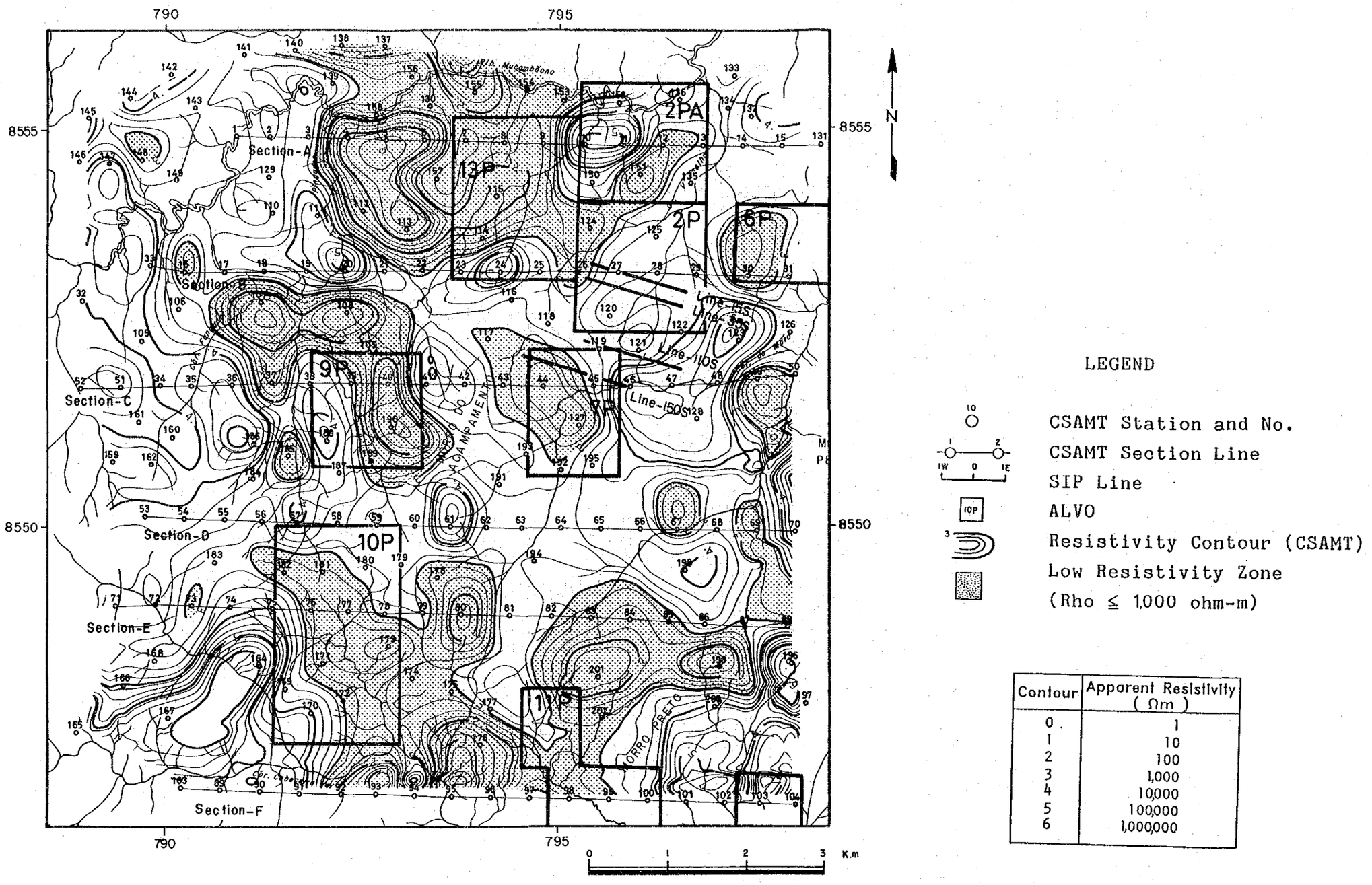

LEGEND

- CSAMT Station and No.
- CSAMT Section Line
- SIP Line
- ALVO
- Resistivity Contour (CSAMT)
- Low Resistivity Zone (Rho ≤ 1,000 ohm-m)

Contour	Apparent Resistivity (Ωm)
0	1
1	10
2	100
3	1,000
4	10,000
5	100,000
6	1,000,000

Fig. III–16 Resistivity Structure Map [CSAMT (–300 m)]

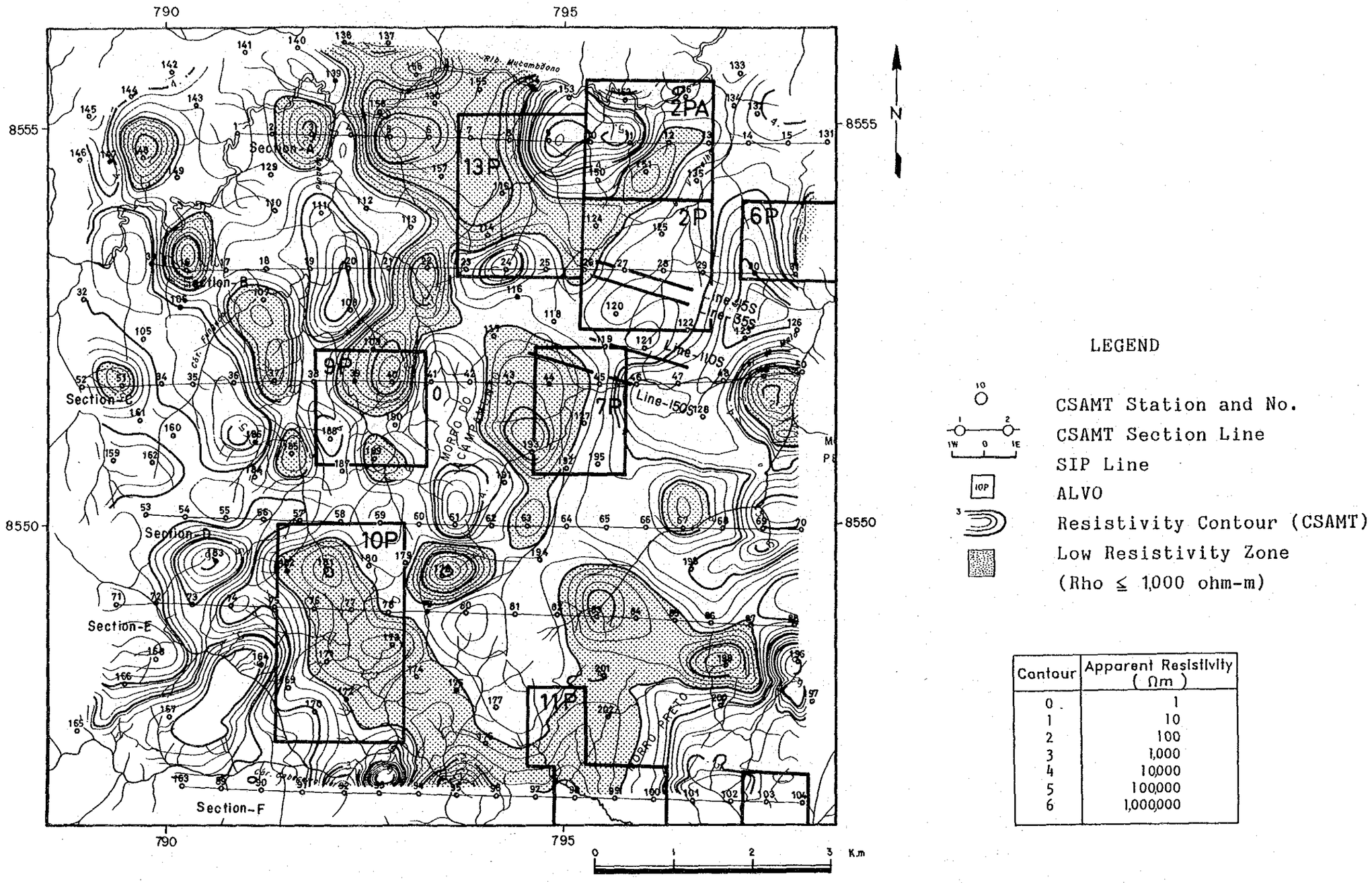

LEGEND

- CSAMT Station and No.
- CSAMT Section Line
- SIP Line
- ALVO
- Resistivity Contour (CSAMT)
- Low Resistivity Zone (Rho ≤ 1,000 ohm-m)

Contour	Apparent Resistivity (Ωm)
0	1
1	10
2	100
3	1,000
4	10,000
5	100,000
6	1,000,000

Fig. III–17 Resistivity Structure Map [CSAMT (–500 m)]

2–4 Discussion

In general the CSAMT method has been utilized in the reconnaissance and/or semi-detailed survey. However, it has been used in the detailed surveys with significant success.

Analysis fails in when a discontinuity on apparent resistivity – frequency curve appears, which is caused by a strong resistivity contrast between neighbouring two layers. And when there is a low resistivity body at the ground surface, a conductive layer is analyzed as a thicker layer because this body will affect the apparent resistivity values of low frequency region. All of these conditions were taken into consideration in order to clarify the continuity of the formation bearing the C-1 ore deposit and the resistivity structure in the survey area.

By the close analysis of the data taken at frequencies higher than 128 Hz, it was detected a decreasing tendency in the resistivity distributions as going from the west to the east of the survey area in such a way to permit to distinguish three defined areas: a high resistivity zone distributed all over the west part and extended along the N-S direction, a middle resistivity zone between 150 to 600Ωm located around the center, and a low resistivity zone in the east of the survey area.

At the frequencies lower than 128 Hz, where the high resistive distributions can be amply distinguished, the low resistivity zones suggest the structure lines along the N-S direction. The high resistive zone in the west part is considered to reflect the homogeneous high resistivity rocks (layer) with a resistivity distribution showing no change from the surface to the analyzed deeper part. Since the resistivity increases as the frequency is lowered, it seems that high resistivity zone at the shallower part may be caused by the schist-amphibolite, and the one at the deeper part may reflect the basement rocks. The high resistivity zone reflecting the basement rocks shows a wider distribution in depths, and being including scattered high resistivities at the center of the area, continues to the one to the east of the survey area, which is found only in depths.

As a result of 1-D model calculation, at the east of the area, a two-layer structure is found; the first low resistivity layer with a thickness of 100m and the second high resistivity layer of more than 1,000Ωm which may reflect amphibolite and the basement rocks.

The schist, which originates in the resistivity structure above the 1,000m depth, has quartz intercalated and a developed schistosity. In the case that a folding structure is seen notably in the area, when the measurement conditions are different on the same geological formation, the resistivities obtained may not be same.

In general, the resistivity structure of the survey area indicates that the structure is dominated by two folding structures. One with its axis along the E-W direction is extended for about 4-5 km and presumed to be the resistive layer of more than 10,000Ωm. The second one has

its axis extending along the N-S direction. At the center of the survey area, the high resistivity layer is the deepest under the influence of two folding structures different in directions.

The resistivity structure around the C-1 ore deposit shows two-layer structures, the first layer, being less than 100Ωm with a thickness of about 50m and the second, higher than 400Ωm. In this regards, the C-1 ore deposit seems to be originated in the first layer. However, the C-1 ore deposit is located in a gradual zone where folding axis exists along the NE-SW direction, and where the resistivity contrast were so weak that led to the consideration that the similar ore deposit or mineralization zone may take place in this NE-SW trending resistivity zone.

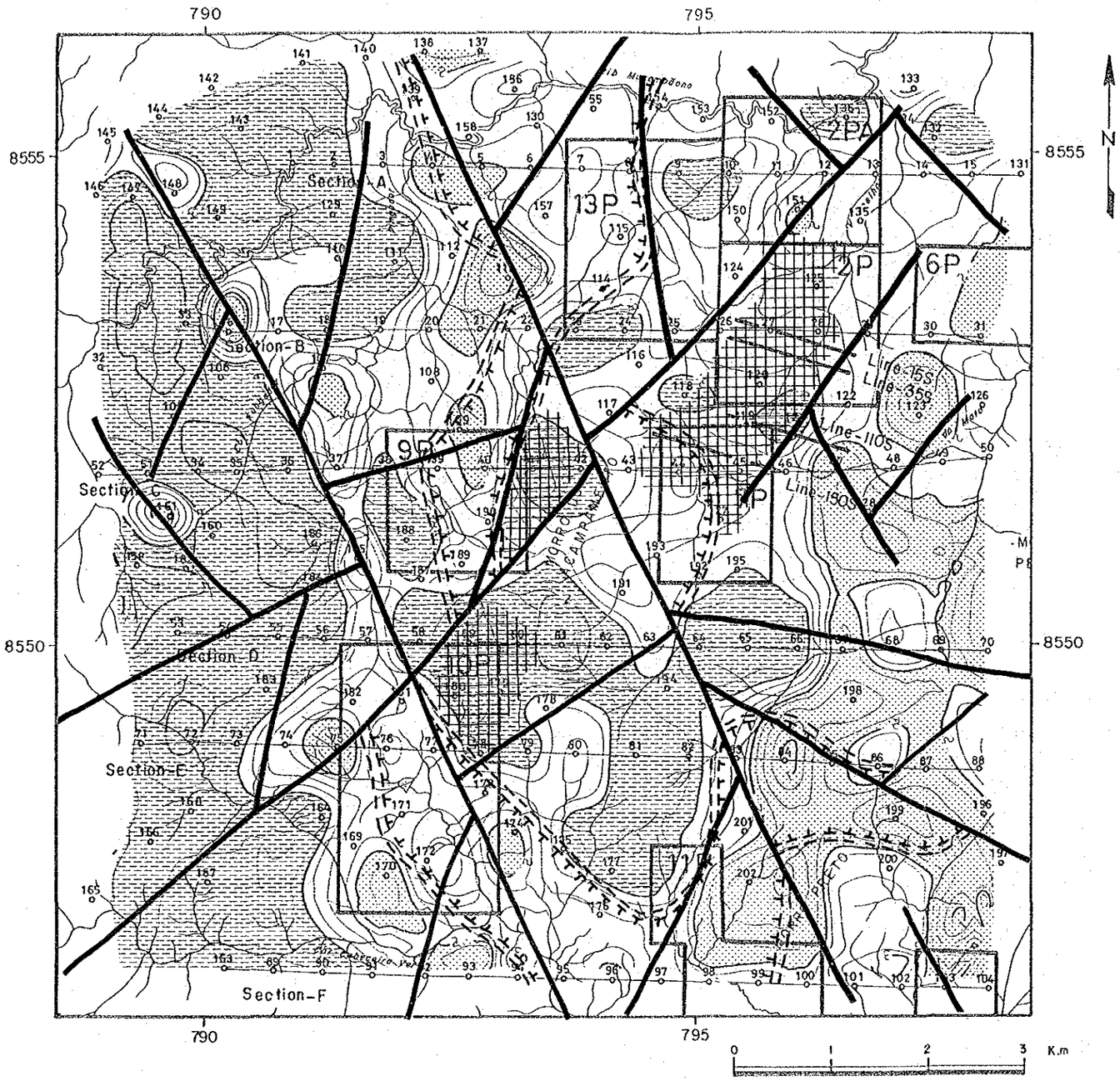

LEGEND

- CSAMT Station and No.
- CSAMT Section Line
- SIP Line
- ALVO
- Resistivity Contour (CSAMT)
- Low Resistivity Zone (Rho ≦ 100 ohm-m)
- High Resistivity Zone (Rho ≧ 1000 ohm-m)
- Inferred Tectonic Line
- Low Resistivity Zone (CSAMT)
- Promising Zone for Ore Researve

Contour	Apparent Resistivity (Ωm)
0	1
1	10
2	100
3	1000
4	10000
5	100000
6	1000000

Fig. Ⅲ−18 CSAMT Interpretation Map

CHAPTER 3 SIP SURVEY

The SIP (Spectral Induced Polarization) method was carried out in order to clarify the spectral response of the existing ore deposit, which will be useful not only to pursue a deeper understanding of the C-1 ore deposit, but also as an index of survey for another area.

3–1 Introduction

The SIP geophysical survey is an electrical method which measures the transient phenomenon (Induced Polarization) caused by the electro-chemical nature of the minerals and/or rocks. The conventional IP method measures the phenomena at only two frequencies (in general 0.3 and 3.0 Hz), while the SIP technique measures the amplitude of the receival signal, of the phase difference, etc. in a wide band frequency from 0.1 to 100 Hz, permitting in such way to clarify the nature of the IP anomalous source by analyzing the frequency response (spectral response) of the layer or ore deposit.

The location map of the survey lines are indicated in the Fig. III–19.

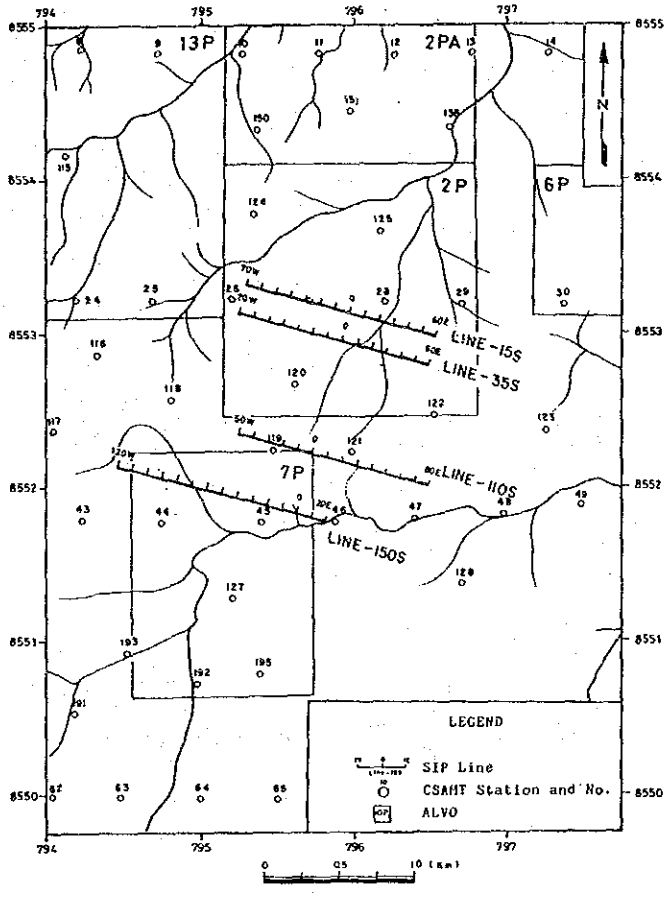

Fig. III–19 Location Map of SIP Survey

3-2 Field Methodology

The designed survey lines were located in the field by means of an open traverse method using compass and measurement tapes. The stations were placed at intervals of 50 m on each survey line, and the receiver lines were set at 25 m apart and parallel to the main survey line. The electrode configuration adopted was a dipole-dipole array as shown in Fig. III-20. The specifications and amounts of the survey are indicated in Table III-2.

Table III-2. Specifications and Amounts of SIP Survey

Method	Line Length	Measuring Points	Measuring Interval and n-factor	Electrode Configuration
SIP	1.3 km x 3 lines 1.4 km x 1 line (Total 5.3 km)	117 points 40 points (Total 161 points)	a = 100 m n = 1 ~ 5	Dipole - Dipole

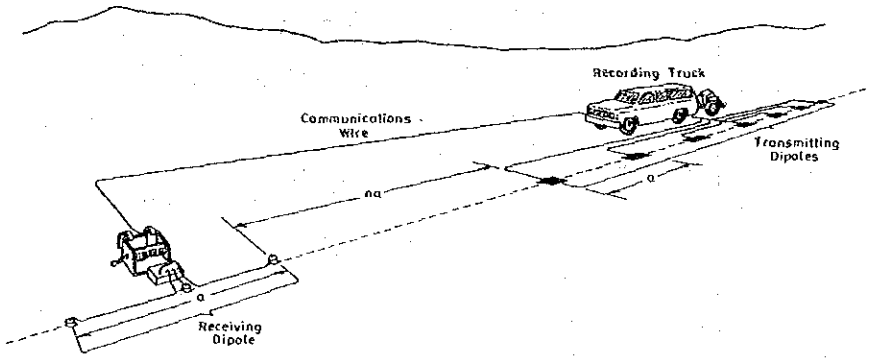

Fig. III-20 Electrode Configuration

The survey was carried out by using the equipment utilized for the CSAMT survey. As mentioned before, this system was manufactured by Zonge Engineering and Research Organization Inc., U.S.A. and its multitype use allowes the possibility to be used for different kinds of electric survey by only exchanging programs to the system (see Section 2–1–2).

A diagram of SIP survey system is illustrated in Fig. Ⅲ–21.

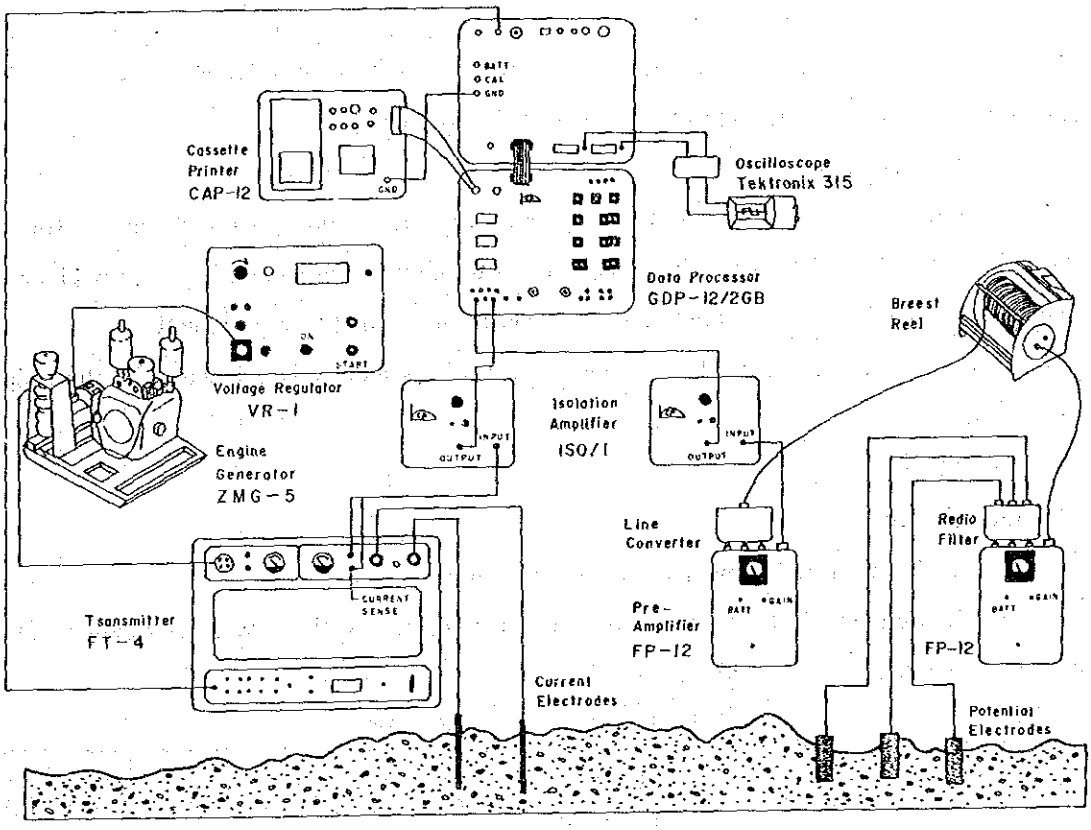

Fig. Ⅲ–21 Diagram of SIP Survey System

3–3 Method of Analysis

3–3–1 Data Processing

The measured data were input to a data processor incorporated to the equipment, which calculate the necessary information to interpret the geoelectrical structure by using the following maps and diagrams, peculiar in the SIP method.

1) Phase Spectrum Diagram

This diagram gives, for every frequency, the phase shift obtained between the transmitter and receiver station. The phase difference versus the frequency are plotted on a log-log chart.

2) Magnitude Spectrum Diagram

It shows the change in the potential difference by plotting on a log-log chart the potential data normalized at the lowest frequency against the frequency.

3) Cole-Cole Diagram

This diagram expresses the magnitude (amplitude) corresponding to a change in the frequency and in the phase difference. The diagram is obtained by plotting in a complex plane the logarithm of the imaginary component versus the logarithm of the real component.

The real (Re) and imaginary (Im) components can be respectively calculated by the following equations:

$$Re = M \cos\phi$$

$$Im = M \sin\phi$$

Where M is amplitude, and ϕ the phase difference.

The calculation for both components are normalized for the lowest frequency. These calculations are indicated in Fig. III–22.

(Hz)	(Ratio of Magnitude)	(Normalized Magnitude)	(Phase Shift)	(Real P.)	(Imag. P.)
0.125	$M_1/M_2 = M_4$	$M_4/M_4 = N_4 (= 1)$	ϕ_4	$N_4 \cos\phi_4$	$N_4 \sin\phi_4$
0.375	$= M_5$	$M_5/M_4 = N_5$	ϕ_5	$N_5 \cos\phi_5$	$N_5 \sin\phi_5$
0.625	$= M_6$	$M_6/M_4 = N_6$	ϕ_6	$N_6 \cos\phi_6$	$N_6 \sin\phi_6$
0.875	$= M_7$	$M_7/M_4 = N_7$	ϕ_7	$N_7 \cos\phi_7$	$N_7 \sin\phi_7$
1.125	$= M_8$	$M_8/M_4 = N_8$	ϕ_8	$N_8 \cos\phi_8$	$N_8 \sin\phi_8$
1.375	$= M_9$	$M_9/M_4 = N_9$	ϕ_9	$N_9 \cos\phi_9$	$N_9 \sin\phi_9$

Fig. III–22 Complex Resistivity Calculations

4) 3-Point Decoupling Phase Diagram

Three point decoupling phase is an approximate phase at DC current, calculated by assuming a second order polynomal between frequency and phase, with the phases being at three different frequencies, i.e., at 0.125, 0.375 and 0.625 Hz.

This relation is illustrated in Fig. III−23.

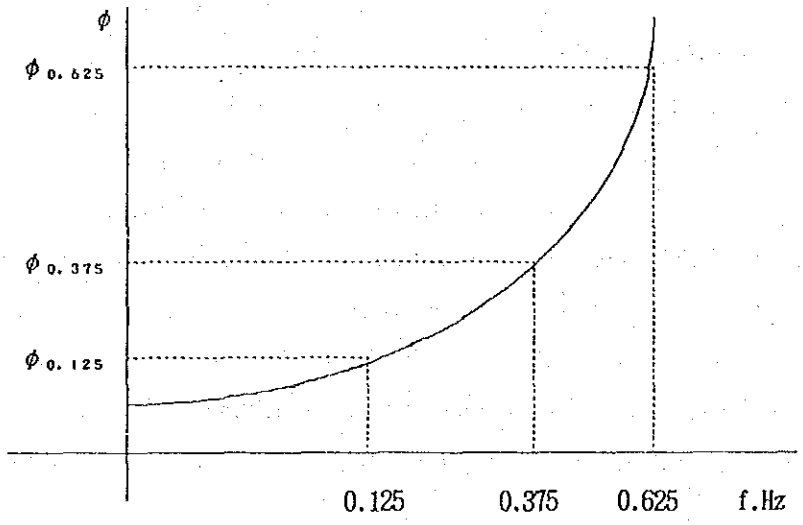

Fig. III−23 3-Point Decoupling Phase

An approximate value of C used in the above diagram make use of the following equation :

$$C = \frac{15}{8}\phi_{0.125} - \frac{10}{8}\phi_{0.375} + \frac{3}{8}\phi_{0.625}$$

Where $\phi_{0.125}$, $\phi_{0.375}$ and $\phi_{0.625}$ are the phases obtained at the frequencies of 0.125, 0.375, and 0.625 Hz, respectively.

This quantitative relation was first proposed by Hallof and Pelton and is to be useful for decoupling effect considerations.

The complex impedance, Z (ω) adopted in the SIP method is given by the Cole-Cole dispersion model as

$$Z(\omega) = Ro\left\{1 - m_1\left[1 - \frac{1}{1+(i\omega\tau_1)^{C_1}}\right] - m_2\left[1 - \frac{1}{1+(i\omega\tau_2)^{C_2}}\right] + m_3\left[1 - \frac{1}{1+(i\omega\tau_3)^{C_3}}\right]\right\}$$

Where the terms in square brackets corresponds, the first, to the IP response ($C_1 < 0.5$), the second to the response for the EM coupling effect of a homogeneous earth ($C_2 > 0.5$), and

the third, to the response of the EM coupling effect for a conductor.

Also in the same equation, m_i is the chargeability of the rock, τ_i the time constant, C_i the frequency dependence, and Ro the value of Z (ω) at zero frequency.

These last four parameters are called the Cole-Cole parameters, which, through the above equation, make possible to choose the most suitable parameters to permit the separation of the measured IP responses from the distortions due to inductive coupling effects.

3–3–2 Physical Property of Rocks

The measurement of the IP properties of the rocks collected in the survey area have the purpose to correlate the observed data taken in the field with the resistivity, phase shift, magnitude, and spectral response of the rock samples distributed in the surveyed area. Since the measuring conditions in the laboratory are not the same as those in the field, it may happen that the measured values in the samples does not necessarily reflect the observed values in the field.

A total of 48 samples were collected in the field, where 34 of them were collected in the surveyed area and the rest were core samples obtained in drilling carried out by CPRM. Since six of these samples were spoiled, the laboratory measurements were carried out for the remaining 42 samples.

A diagram of the measurements are indicated in Fig. III–24 and the results are detailed in Table III–3.

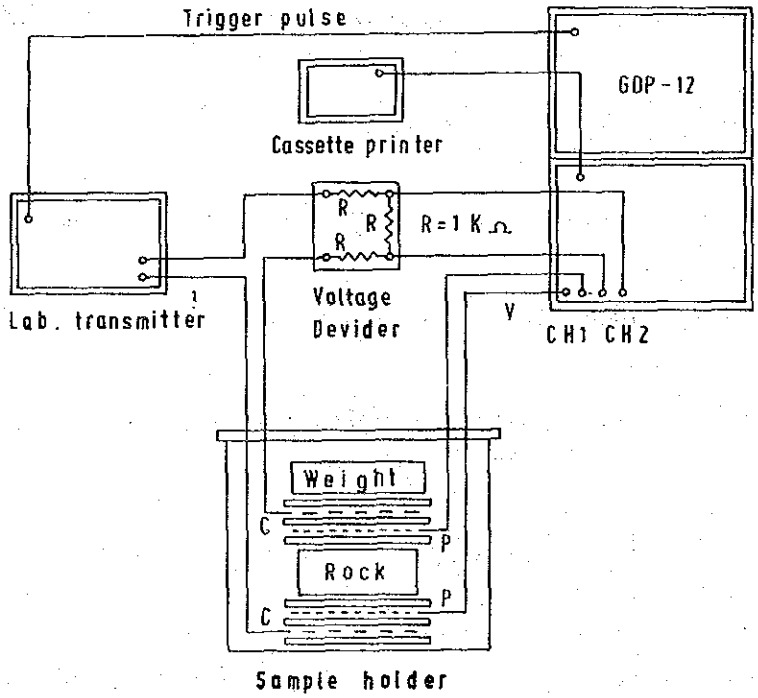

Fig. III–24 Electrical Properties Measurement System

(Amphibolite)

Sample Name		Geological Horizon	Resistivity (Ω m)	P.F.E (%)
NI	0011	Pip_3	3134	1.4
	0053	Pip_3-Pip_4 (xt_2)	11750	0.0
	0056	Pip_4	1222	0.7
	0060	Pip_3	5838	1.2
	0065	db	1671	1.2
	0067	Pip_4	50560	0.3
TS	0011	Pip_4 (xt_2)	1620	1.0
	20069	Pip_3	11970	1.7
8 Samples			10971	0.9 (1.0)
PM-68 (36.7 m)		(xt_1)	3892	8.0
PM-23 (49.6 m)			15460	5.4
PM-93 (46.7 m)			10640	6.2
PM-93 (67.9 m)			41700	10.6
PM-34 (85.4 m)			14620	0.5
PM-31 (89.0 m)			16770	9.6
PM-24 (73.5 m)			13263	7.6
PM-19 (50.0 m)			16250	0.6
8 Samples			16574	6.0 (7.8)

(Schist)

Sample Name		Geological Horizon	Resistivity (Ω m)	P.F.E (%)
NI	0017	Pip_4 (xt_2)	5695	1.4
	0035	Pip_4 (xt_3)	3664	2.4
	0037	Pip_4 (xt_2)	19200	1.5
	0038	Pip_4 (xt)	5571	1.1
	0039	Pip_5	11178	3.0
	0040	Pip_4 (xt_3)	297	1.3
	0046	Pip_5	572	2.4
	0059	Pip_4 (xt_1)	6148	1.9
	0062	Pip_2	646	2.3
	0068	Pip_4 (xt_2)	2225	1.4
	0069	Pip_4 (xt_2)	556	3.7
	0078	Pip_2	6143	0.3
TS	0001	Pip_4 (xt_2)	306	0.8
	1031	Pip_4	7146	1.0
	1032	Pip_4	1372	2.8
15 Samples			4714	1.82

Table III－3　Electrical Property of Rock and Core Samples

The measurements carried out for each sample were conducted at two different traversal directions since the schistosity in the samples may present different properties depending on the measured direction. These two values were averaged for every sample.

In order to obtain a good correlation to assist in the understanding of the electrical structure, the 31 samples of amphibolite and schist were considered as follows.

Amphibolite samples amounted to 16: 8 of them collected in the survey area, and the other 8 were selected from core samples. The electrical measurements of amphibolite gave an average resistivity of 13,896Ωm and P.F.E. value of 3.52%. However, only the rock samples collected in the area gave an average value of 11,190Ωm, which is considered to be lower than the total average. While the average resistivity in the core samples gave a value of 16,602Ωm, which is considered to be higher than the total average. The P.F.E value in the core samples is six times higher than those obtained for the samples collected in the area. All of these differences can be understood if we consider that the rock samples on the surface are mainly affected by weathering and cracking, while the core samples are mainly compact and near the deposit. On the other hand, the resistivities measured along the two directions in each sample, were determined within a difference in the order of about 10%-20%. It leads to the consideration that the amphibolite distributed in the area can be considered as the homogenous rocks.

Regarding the schist samples, 15 rock samples were collected in the area, with an average resistivity value of 4,714Ωm, which is about 34% less than that of amphibolite. They can be arranged into two classes: one with resistivity higher than or equal to 1,000Ωm, due probably to the fact that they have a lot of quartz and few cracks and the other, which is low in quartz and exposed to weathering or alteration of other kind, with values lower than 1,000Ωm. The average in their P.F.E values resulted in 1.82% with a few high values as compared with the background values of the survey area. The phase spectrum showed a remarkable pattern in the high resistivity rocks, especially in amphibolite, which gave strong negative coupling at the high frequency range. Typical type of spectrum considered to reflect amphibolite and schist are indicated respectively in Figs. III−25 and III−26.

The type of spectrum determined for amphibolite and schist showed almost the same patterns. However, in both of them, the following features were found:

1) The spectral pattern shown by amphibolite indicates a convexity pattern with a maximum phase difference in the range from 1.0 to 10Hz.
2) In relation to schist, when the resistivity measured were high, a negative coupling appeared at the high frequency range.

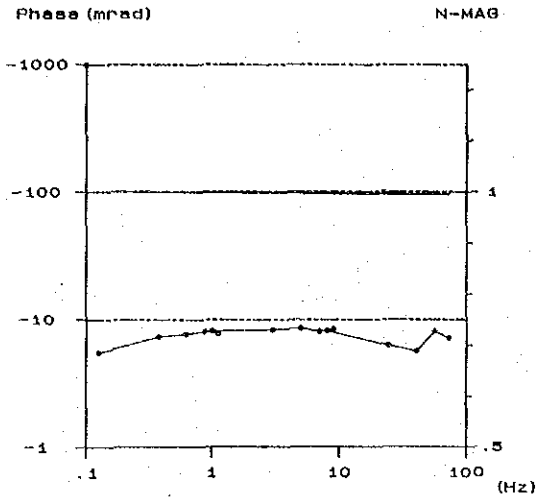

Sample No TS0011
ROCK NAME amphibolite
RHO: (Ohm-m) 2448
P.F.E. 1
PHASE 5
3-P.D.PHASE 3

No. 23

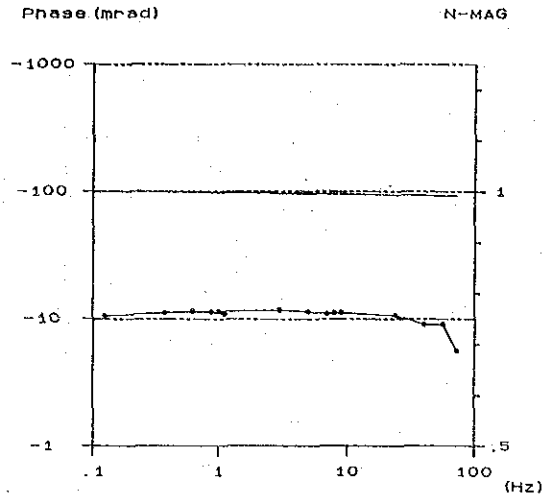

Sample No : NI0011
ROCK NAME : amphibolite
RHO : 3134 (ohm_m)
P.F.E. : 1.4 (%)
PHASE : 10 (-mrad)
3-P.D.PHASE : 10 (-mrad)

No. 36

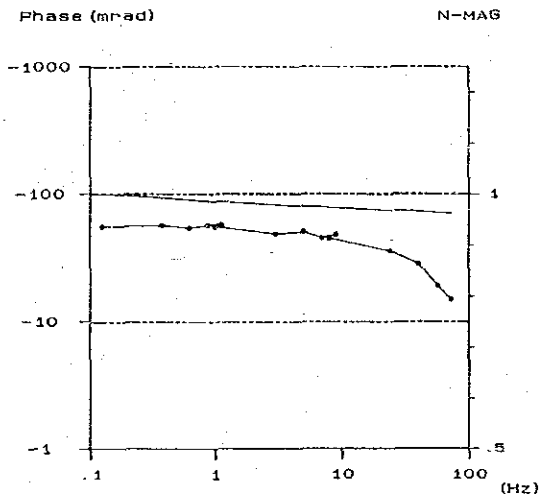

Sample No : PM-68
ROCK NAME : amphibolite
RHO : 3892 (ohm_m)
P.F.E. : 8 (%)
PHASE : 55 (-mrad)
3-P.D.PHASE : 53 (-mrad)

No. 54

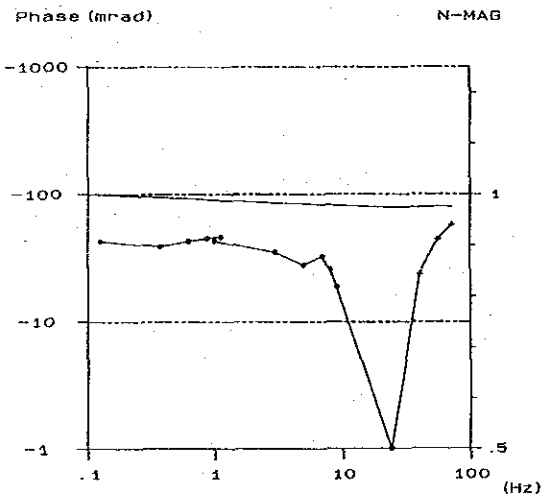

Sample No : PM-93
ROCK NAME : amphibolite
RHO : 10640 (ohm_m)
P.F.E. : 6.2 (%)
PHASE : 42 (-mrad)
3-P.D.PHASE : 47 (-mrad)

No. 55

Fig. III－25 Spectrum of Rock Samples (Amphibolite)

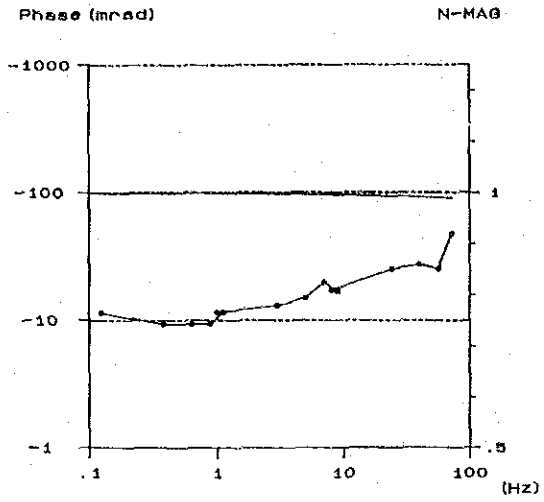

Sample No NI0038
ROCK NAME mv-bt-feld-qtz-schist
RHO: (Ohm-m) 5571
P.F.E. 1.1
PHASE 11
3-P.D.PHASE 13

No. 9

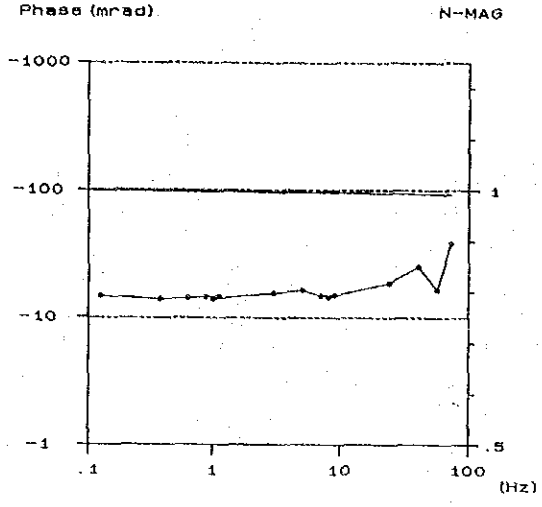

Sample No : NI0037
ROCK NAME : mv-bt-feld-qtz schist
RHO : 19200 (ohm_m)
P.F.E. : 1.5 (%)
PHASE : 14 (-mrad)
3-P.D.PHASE : 15 (-mrad)

No. 13

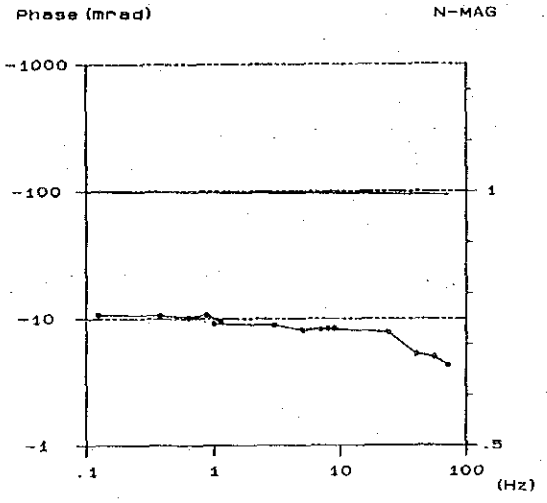

Sample No : NI0068
ROCK NAME : gnt-bt-mv-feld-qtz schist
RHO : 2225 (ohm_m)
P.F.E. : 1.4 (%)
PHASE : 10 (-mrad)
3-P.D.PHASE : 10 (-mrad)

No. 41

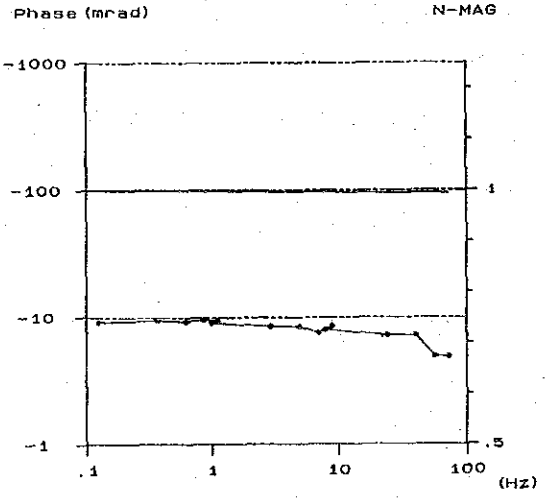

Sample No : NI0040
ROCK NAME : mv-bt-feld-qtz schist
RHO : 566.3 (ohm_m)
P.F.E. : 1.3 (%)
PHASE : 9 (-mrad)
3-P.D.PHASE : 8 (-mrad)

No. 43

Fig. III－26 Spectrum of Rock Samples (Schist)

3) Two types of spectral pattern were detected in schist. In one of them, the phase difference increased only at high frequency ranges, but constant at low frequency. In the other one, the phase difference decreased as frequency increased.

3–3–3 Model Calculations

Model calculations were made for the four SIP survey lines, obtaining a satisfactory fit between the observed and the calculated by the modeling. In these calculations, it was also taken into consideration the results obtained from the previous CSAMT survey, the results of the electrical properties measured for the samples, geological information, and drilling results.

The results of the model calculations are presented in Fig. III–27 through III–30. In what follows are given the results of the interpretation on the modeling.

- **LINE–15S**

From the assumed model for this line, it is found that the PFE value is a little higher, however, the resistivity calculated approximates to the observed value.

To model the IP anomalous source, the following codes were utilized: Code 1 (Resistivity = 100 Ωm, PFE = 3.5%), Code 2 (500 Ωm, 3.5%), Code 5 (300 Ωm, 3.5%) and Code 7 (1,500 Ωm, 6.0%).

Resistivity model for the structure is assumed composed by schist of less than 500 Ωm and amphibolite of higher than 1,500 Ωm. The resistivity values used were based on a difference of resistivity between schist and amphibolite, being the latter 3 times as much resistive.

As a result of this, a syncline structure due to folding between Stations 30E and 00 at around 150 m depth is presumed to distribute amphibolite, whereas schist is presumed to dip westward from the assumption model corresponding to schist.

Code 1 corresponding to the C-1 ore deposit is supposed to be the boundary between schist and amphibolite beneath Station 00 at depth of 30m-150m. Code 2 and Code 5, which correspond to the dissemination zone less than 150m depth, are supposed to dip westward within schist. Below those, Code 7 is used which agrees with the dissemination zone due to amphibolite and which is supposed to dip vertically.

From model calculation, the PFE value detected is a little higher than measured value, meaning that the dissemination zone originated within schist may be of about 3.0% of PFE value.

- **LINE–35S**

The resistivity structure in this line is almost the same as that in Line-15S. However, the value used for the resistivity layer for amphibolite is higher than that in Line-15S.

The C-1 ore deposit which is considered to continue from Line-15S is given the definition of Code 1 (100Ωm, 5.0%), and the dissemination zone around the C-1 ore deposit are given those of Code 2 (500 Ωm, 3.5%), Code 5 (300 Ωm, 3.5%) and Code 7 (2,000 Ωm, 6.0%).

As a result, the resistivity of less than 500 Ωm supposes that the resistivity used in the model is presumed to reflect the same geological structure as that of Line-15S. The model corresponding to amphibolite assumes value of resistivity of 2,000 through 4,000 Ωm, being higher than the obtained in Line-15S, and the Code 8 (4,000 Ωm, 0.0%) assumed reflects a resistive layer dipping westward.

Code 1 is assumed at about 10m depth from the surface compared with Line-15S and shows a stronger IP effect with almost the same distribution form as that in Line-15S except for the depth from 10 to 60m which gives a wider distribution.

The dissemination zone of this line, with a width of about 600m, is seen to be due to amphibolite at the lower part of 150m depth.

Code 6 is found between Stations 30W and 60W at a shallow part of less than 50m. This resistivity (Code 6) is also found at less than 50 m between Stations 30W and 60W at Line-15S, suggesting this fact that a continuous low resistivity layer is distributed around the surface.

From the above, the C-1 ore deposit is presumed to be dipping smoothly toward Line-15S but decreasing in scale.

• **LINE–110S**

In this line, several code blocks corresponding to resistivities higher than 1,500 Ωm are assumed beneath Stations 40W to 20W. They are assumed dipping eastward, so that around them are widely distributed code blocks corresponding to the resistivity of less than 1,000 Ωm. The resistivity structure modeled shows a little different structure than those of Line-15S and Line-35S.

Five kinds of codes, namely, Code 4 (400 Ωm, 2.0%), Code 5 (100 Ωm, –0.5%), Code 6 (400 Ωm, 0.5%), Code 7 (400 Ωm, –1.0%) and Code 9 (200 Ωm, 0.5%) are assumed in order to detect the basin shape of resistivity distribution of less than 300 Ωm and with a negative IP anomaly of between Stations 20W and 10E.

Code 2 (1,500 Ωm, 2.5%), Code 3 (1,500 Ωm, 4.0%) and Code 1 (2,000 Ωm, 5.0%) are assumed in order to model an IP anomaly of about 2.0% shown between Stations 30W and 10W from the surface to depth and eastward.

As a result of the above, the resistivity distribution of the central part of this line fits approximately well the observed distribution, but at the west of this line, resistivity between

Stations 20W and 10W resulted higher than the observed values. It is explained by the facts the resistivity of Code 3 is higher and that the supposed area of Code 6 is narrower.

On the other hand, the distribution form of IP anomaly approximates the observed distribution form, but it makes necessary to change the PFE values of Code 3 to 3.5%, and to expand the assumed area of Code 1 westward.

• **LINE–150S**

High resistivity zone is clearly distinguished in this line, showing a resistivity of less than 1,000 Ωm at the center of the line forming the basin shape distribution.

Code 7 (2,000 Ωm, 3.0%), Code 8 (2,000 Ωm, 4.5%) and Code 9 (2,000 Ωm, 1.5%) are assumed in order to fit the resistivity of higher than 1,000 Ωm. On the other hand, in the center of this line, the assumed Code 1 through Code 6 are seen to correspond well with the distribution zone given by the observed values.

IP anomalies of higher than 2.0% are shown at two locations, that is, at the west end of this line and beneath Station 10W, where Codes 7 and 8 were assumed.

As a result, apparent resistivity distribution is nearly approximated to the observed distribution form, although the resistivity value is a little higher than the observed.

IP anomaly distribution form at the west end of this line gives a good fit with Code 8, showing an IP anomalous source.

On the other hand, in order to reflect a weak IP anomaly dipping westwards under Station 10W, Code 7 block dipping westward is to be assumed from 75 m depth to the depth.

It results in a good fit. These two IP anomalies are due to the high resistivity. The IP anomalous source dipping westward under Station 10W is presumed to be due to the dissemination zone.

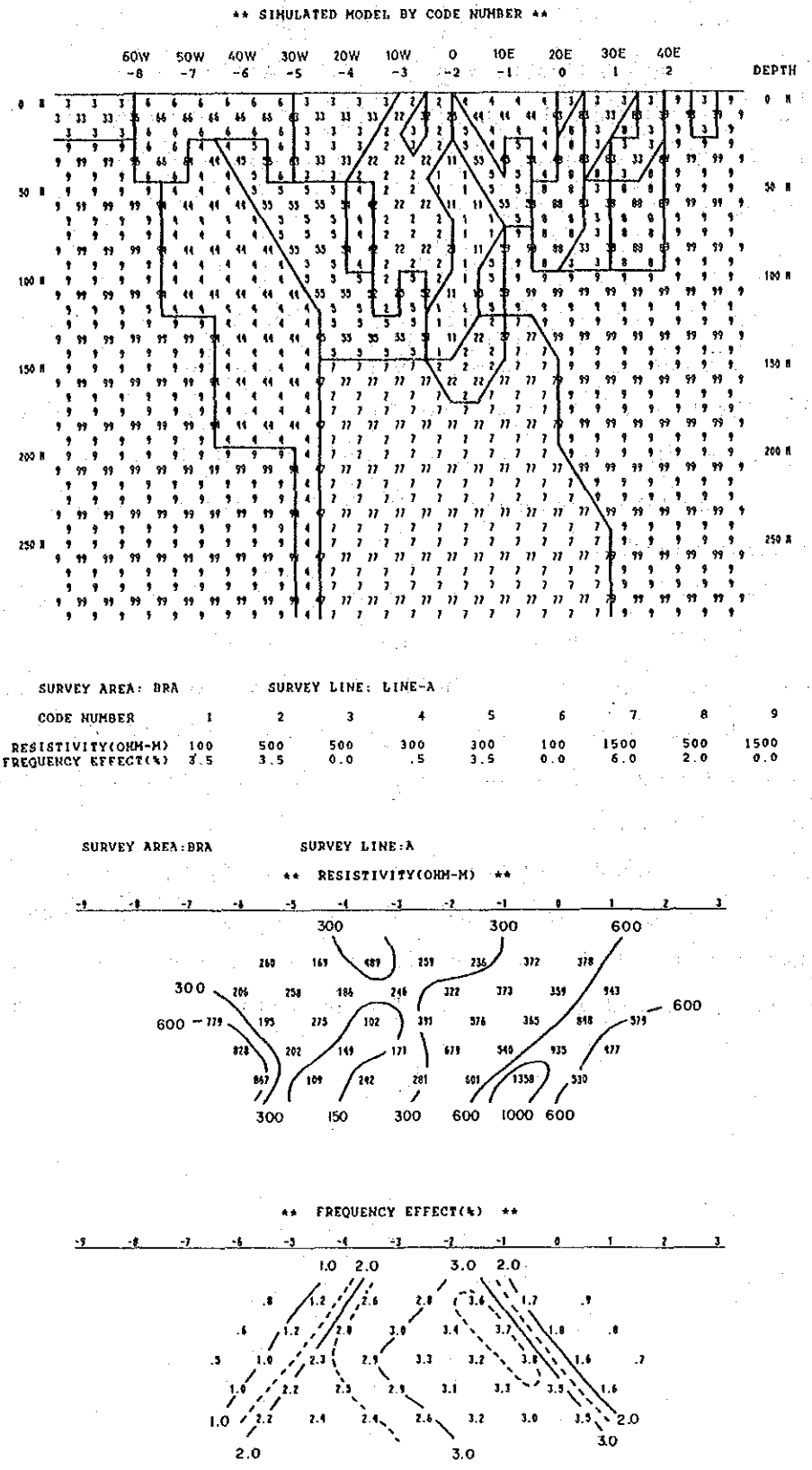

Fig. Ⅲ–27 2–D Model Calculation (Line-15S)

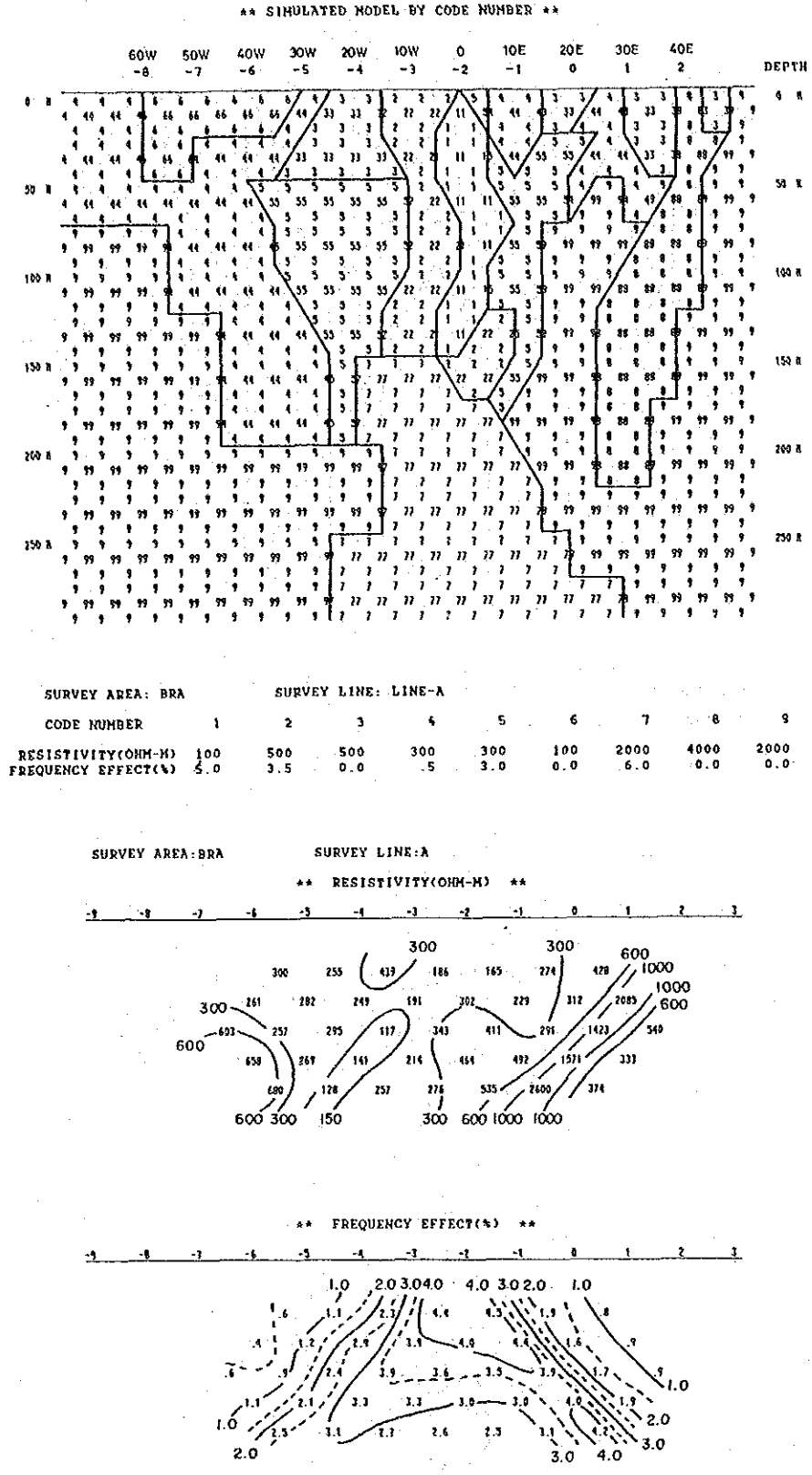

Fig. III–28 2–D Model Calculation (Line-35S)

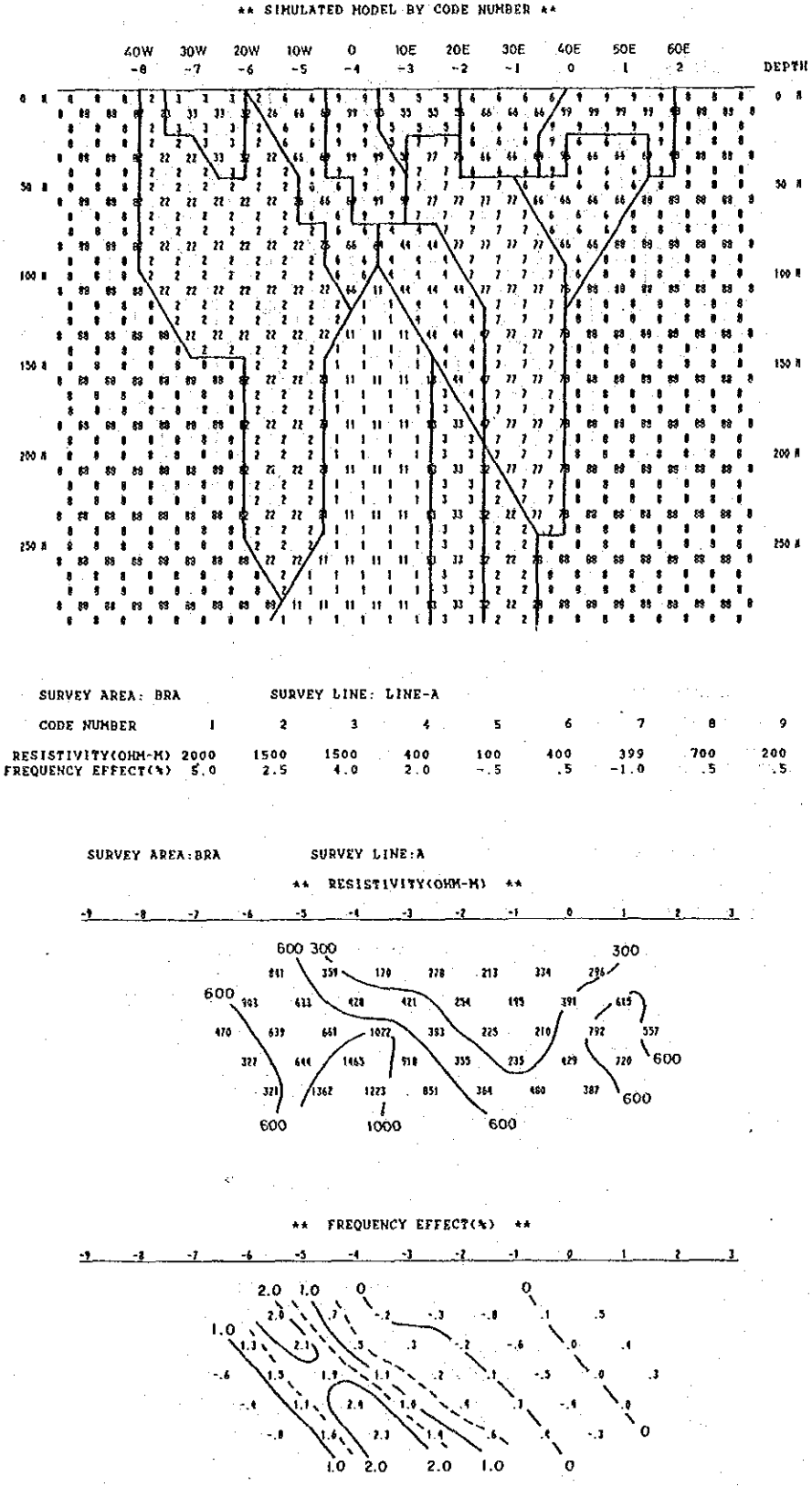

SURVEY AREA: BRA SURVEY LINE: LINE-A

CODE NUMBER	1	2	3	4	5	6	7	8	9
RESISTIVITY(OHM-M)	2000	1500	1500	400	100	400	399	700	200
FREQUENCY EFFECT(%)	5.0	2.5	4.0	2.0	-.5	.5	-1.0	.5	.5

Fig. III–29 2–D Model Calculation (Line-110S)

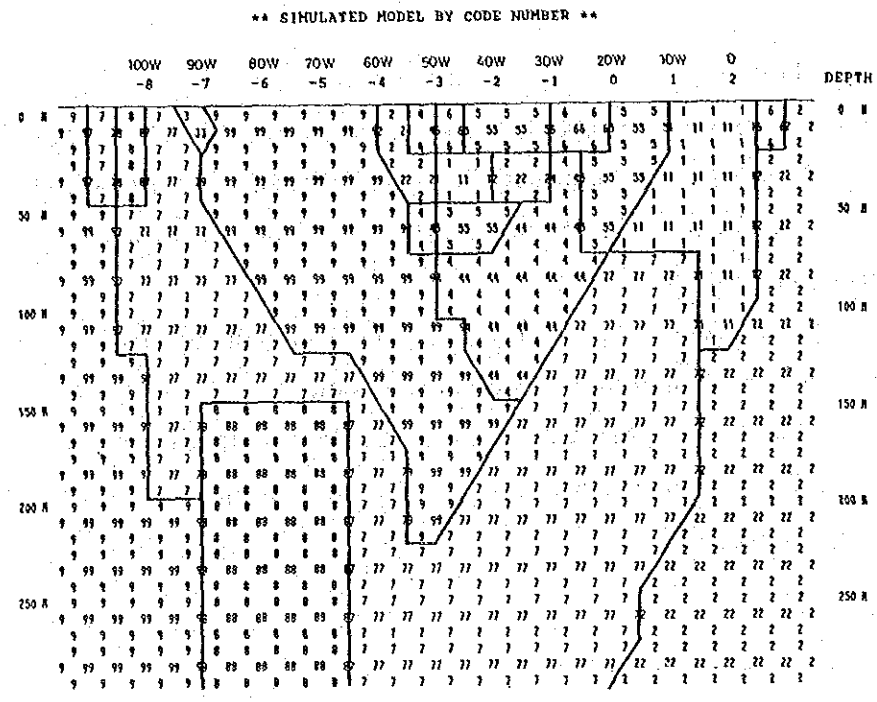

SURVEY AREA: BRA SURVEY LINE: LINE-A

CODE NUMBER	1	2	3	4	5	6	7	8	9
RESISTIVITY(OHM-M)	1000	1000	1000	650	650	300	2000	2000	2000
FREQUENCY EFFECT(%)	2.0	1.0	.5	1.0	2.0	.5	3.0	4.5	1.5

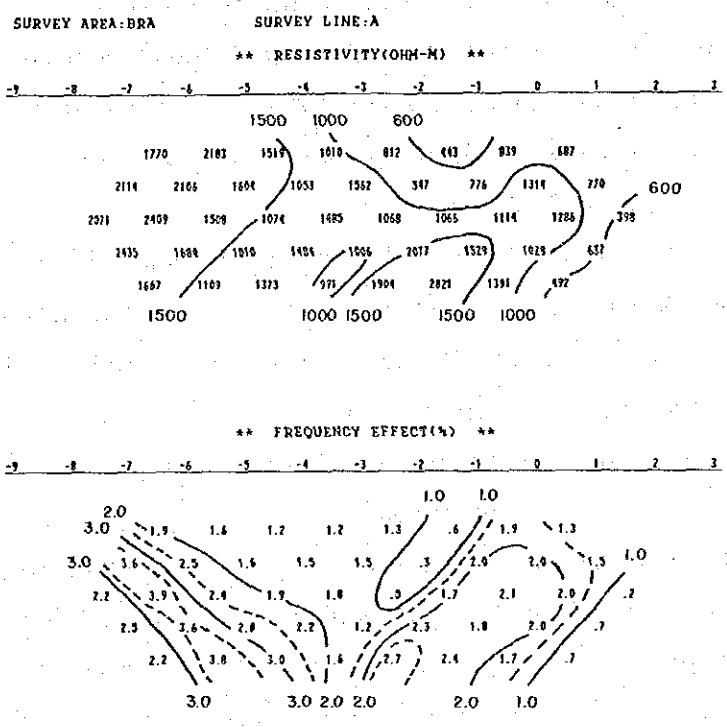

Fig. III–30 2–D Model Calculation (Line-150S)

3–4 Survey Results

3–4–1 Pseudosections

The SIP survey was carried on four survey lines, namely 15S, 35S, 110S and 150S. The first two lines, 15S and 35S, were located on the C-1 ore deposit. The other two, 110S and 150S were set up to clarify not only the southward extension of the C-1 ore deposit, but also to pursue trendings of mineralization.

The pseudosections for each survey line are indicated in Figs. III–31 through III–34, selecting an electrode interval of 100m between Stations.

In the following is given a discussion of the pseudosections for each line based on the information obtained for apparent resistivity, phase, three-point decoupling phase, and percent frequency effect (PFE).

- **LINE–15S**

* Apparent Resistivity Pseudosection (0.125 Hz)

Apparent resistivities of less than 300 Ωm is seen distributed between Stations 50W and 10E. Values of resistivity higher than or equal to 300 Ωm are distributed around the west of 30W at the deeper part measured (n = 3 – 5) and at the east of 10E.

In this survey line, it is considered that the C-1 ore deposit and its surrounding mineralization are located between 10W and 10E with a resistivity of less than 250 Ωm, in particular the resistivity detected in the C-1 ore deposit is lower than 150 Ωm. On the other hand, resistivity of less than 150 Ωm detected between 10W and 20W at the deeper part (n=3–5) may reflect the effect of a low resistivity layer existing around the surface between 00-10E, and 20W-30W.

* Phase Pseudosection (0.125 Hz)

Phase lower than –20 mrad is detected between 10W and 20W and also around 10E which shows a distribution with a strong contrast. Phase less than or equal to –25 mrad is detected from n = 2 to the deeper part of 10E showing a distribution which dips eastward, where the source of the anomalous zone is considered to be located.

Between 00 and 20W it can be seen a distribution of uniform phase from –10 to –20 mrad reflecting a sort of weak mineralization zone.

* 3-point Decoupling Pseudosection (0.125 Hz – 0.375 Hz – 0.625 Hz)

This section shows almost the same distribution form and values as those of the above-mentioned phase pseudosection. Phase of less than –10 mrad is detected between 20W and 10E, and phases between –20 and –30 mrad are detected between Stations 10W and 20E. Same as in the phase pseudosection, phase less than or equal to –25 mrad shows a distribution zone below

10E at depth of (n = 2 – 3) and dips eastward. It is considered as the center of the anomalous zone.

At the east of this anomaly a strong contrast discontinuity line is shown. It suggests either a fault or a boundary of geological structure.

* PFE Pseudo-section (0.125 – 1.0 Hz)

Anomaly of higher than or equal to 2.0% shows almost the same distribution pattern as those of less than or equal to –10 mrad in the previously discussed two pseudo-sections. From this pattern, it is suggested a vertical anomalous source extending from surface to depth.

• **LINE–35S**

* Apparent Resistivity Pseudo-section (0.125 Hz)

This section shows a similar pattern as that of Line-15S. Resistivities higher than or equal to 300 Ωm are widely distributed, with some exceptions such in Station 00 and between Stations 40W and 30W where the resistivities detected were less than 150 Ωm, which reflect the effect of low resistivity layer at shallower depth (n = 1 – 2).

In particular, the resistivity distribution suggests around 30E and 40E the existence of a high resistivity structure dipping westward.

The C-1 ore deposit is considered to be located around Station 00, and with a resistivity of less than 150 Ωm.

* Phase Pseudosection (0.125 Hz)

The distribution pattern in this section looks almost the same as that of Line-15S, strongly reflecting the IP effect. However, the phase lower than or equal to –25 mrad, presents a larger anomaly centered at shallower depth.

* 3-point Decoupling Phase Pseudosection (0.125 – 0.375 – 0.625 Hz)

This section shows the same distribution pattern as that of the phase pseudosection discussed above with the EM coupling not being shown at the low frequency range of 0.125 Hz.

Negative anomaly presented at the depths of (n = 1 – 3) of Stations 30W and 40W is considered to be due to the effect of low resistivity layer existing partly within the high resistivity rocks distributed around the surface.

* PFE Pseudosection (0.125 Hz – 1.0 Hz)

The distribution pattern for the values of PFE higher than or equal to 3.0% suggests the anomalous source dipping eastward and at a scale probably larger than that of Line-15S.

• LINE–110S

* Apparent Resistivity Pseudosection (0.125 Hz)

Values of resistivity lower than 300 Ωm are shown at the depths of (n = 1 – 3) between Stations 10W and 50E, reflecting the effect of a horizontal layer of about 150m depth from the surface, and showing resistivities higher than 300 Ωm at its boundaries. In the deeper part of Stations 00 and 20E a high resistivity distribution of more than 1,000 Ωm suggests the existence of a high resistivity dike going upward to the east.

* Phase Pseudosection (0.125 Hz)

This section compared with the two lines 100S and 35S, shows a small phase with a weak anomaly lower than –10 mrad distributed from the west end of this section to the deeper part of Station 20E.

As a special feature, this line presents a negative anomaly detected around the surface of 20E and dips eastward. This anomaly seems to be due to a geological condition which reflects the effect of a fault or boundary of two structures causing the abrupt change in resistivity.

* 3-point Decoupling Phase Pseudosection (0.125 – 0.375 – 0.625 Hz)

This section shows also the same distribution pattern as that of the phase pseudosection with the EM coupling not being shown at the low frequency range. The distribution form detected in this section is considered to be due to a weak mineralization.

* PFE Pseudosection (0.125 Hz – 1.0 Hz)

Between Stations 30W and 20W an anomaly higher than 1.0% appears and trends to the deeper part by dipping eastward. It is difficult to assure that this distribution pattern suggests an anomalous source. It may, however, be considered the existence of a horizontal layer at a shallow depth of 20-30 m with a weak IP effect.

• LINE–150S

* Apparent Resistivity Pseudosection (0.125 Hz)

This section shows a different resistivity distribution as compared to the other three sections mentioned above. Resistivity of higher than 1,000 Ωm is detected in almost all over the survey line. However, resistivity of less than 600 Ωm is seen only in the east of Station 10W, and at n = 1 between Stations 40W and 10W. It is considered that around Station 00, a fault or boundary layer is suggested which seems to be in correspondence with the other three sections. This can be interpreted as a structural line extending along the N-S direction.

* Phase Pseudosection (0.125 Hz)

In this section, it is almost general to see phase values of less than –10 mrad, showing a distribution pattern caused by a probable weak disseminated anomalous source.

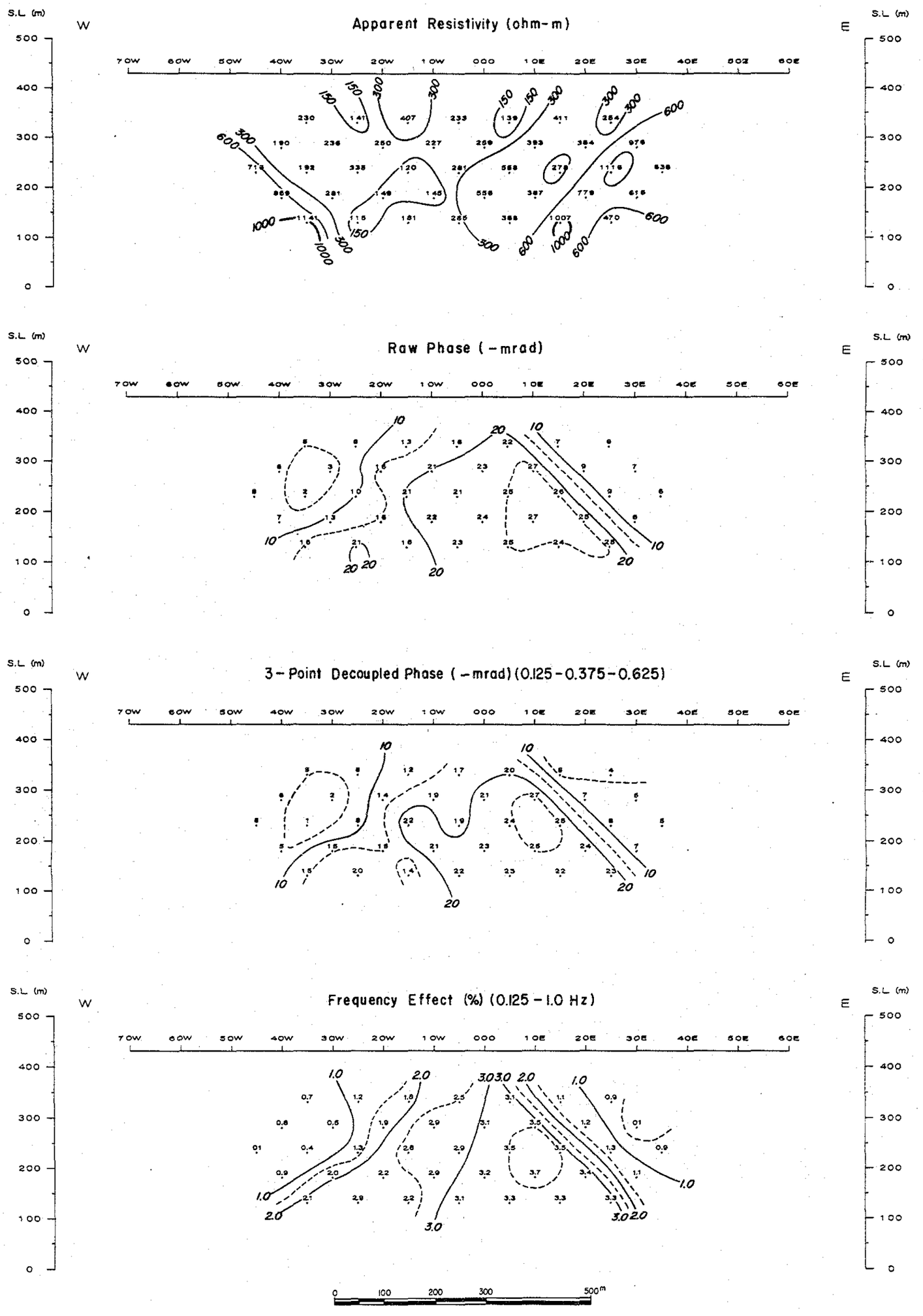

Fig. III–31 SIP Pseudo-Section (Line-15S)

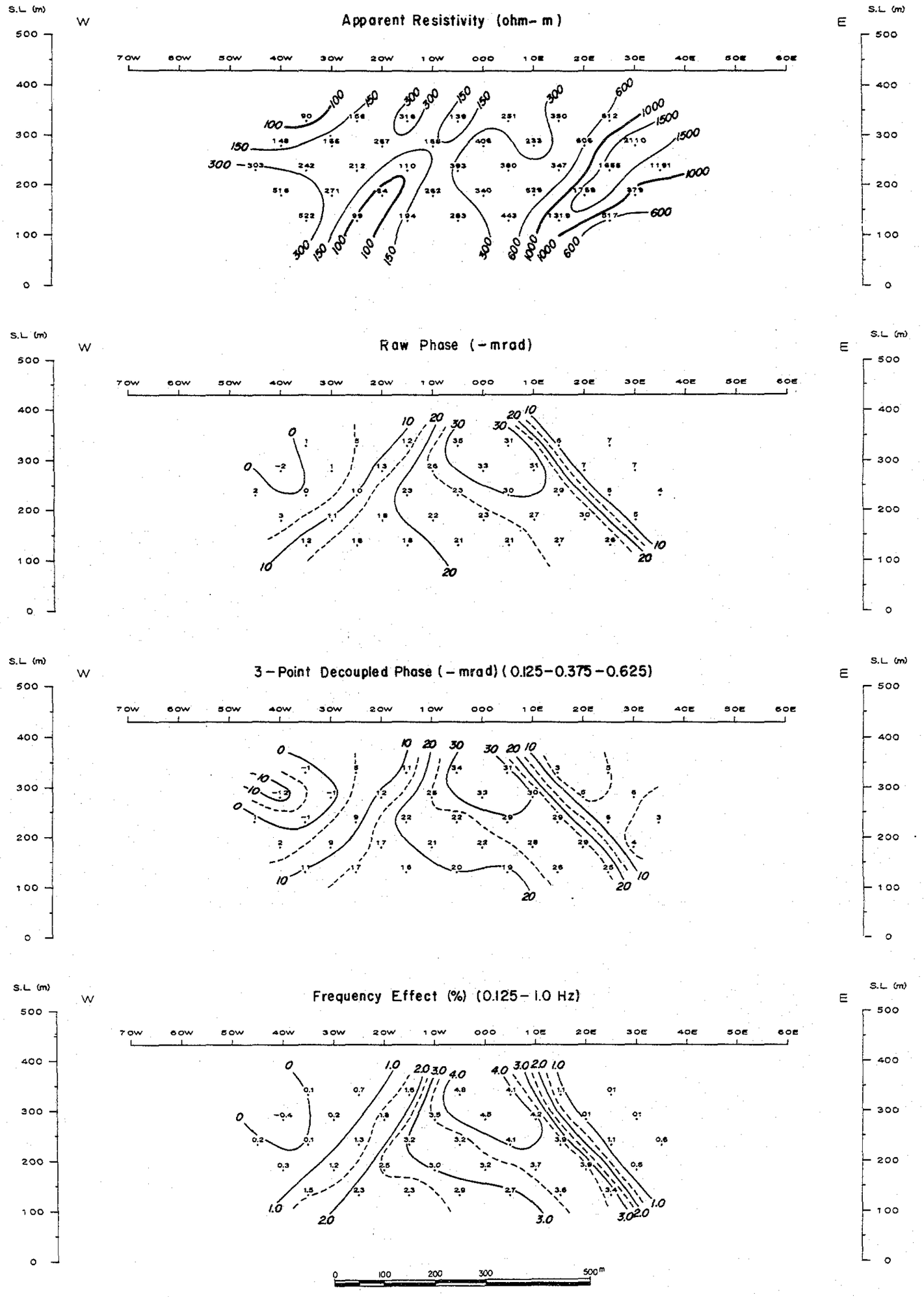

Fig. III–32 SIP Pseudo-Section (Line-35S)

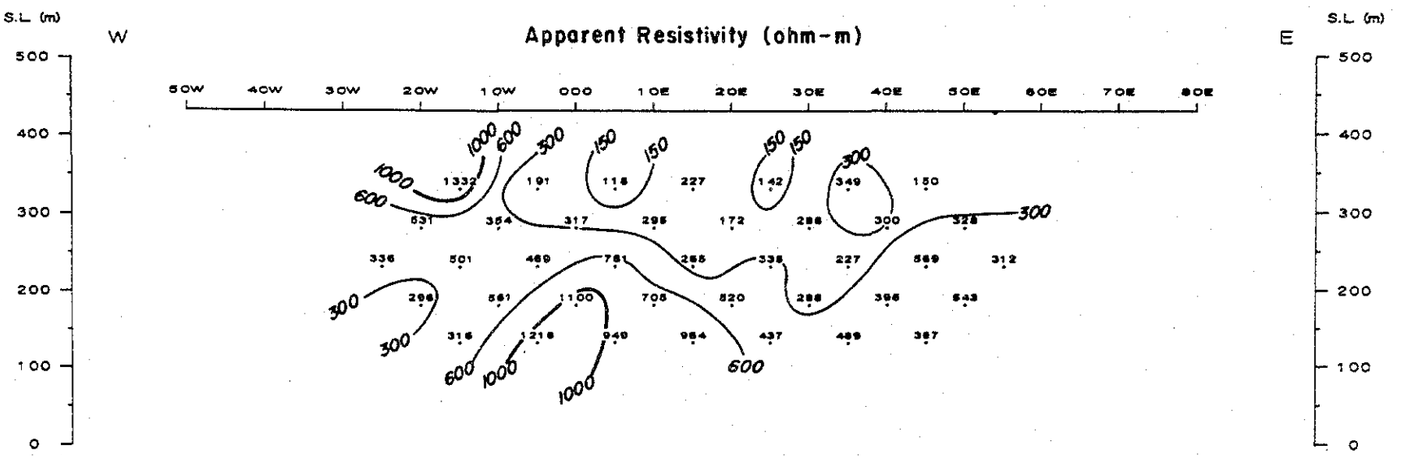

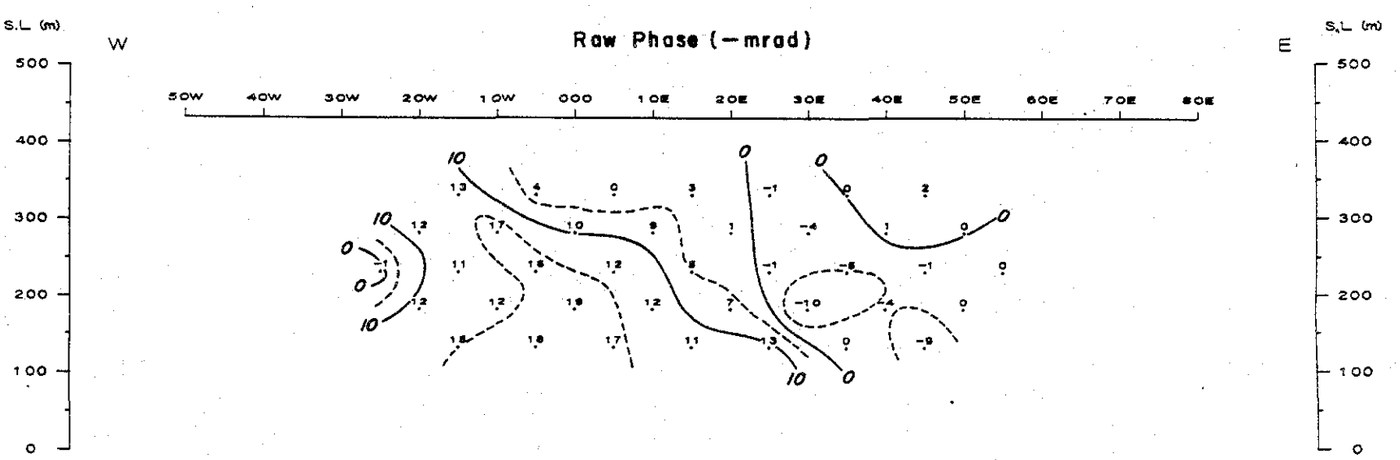

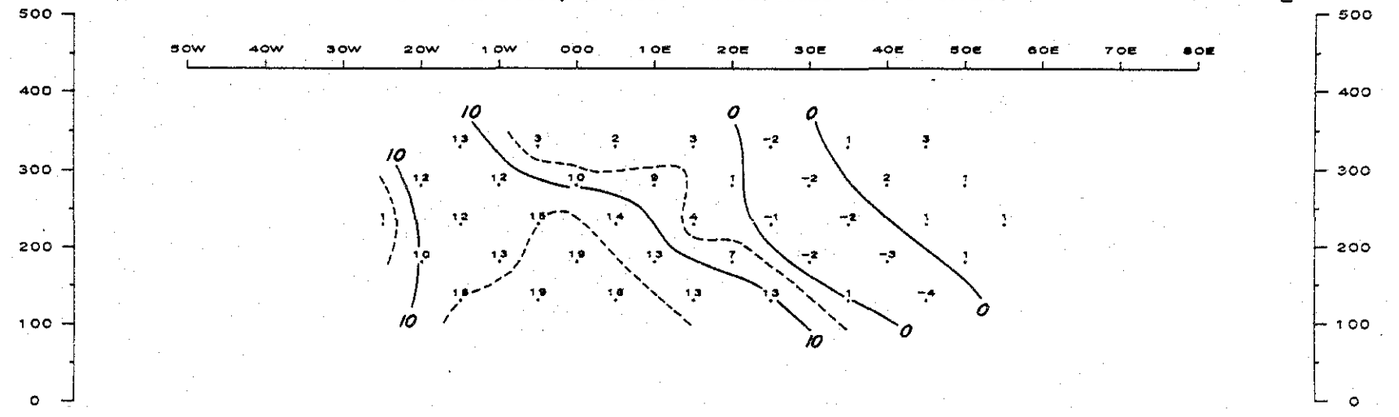

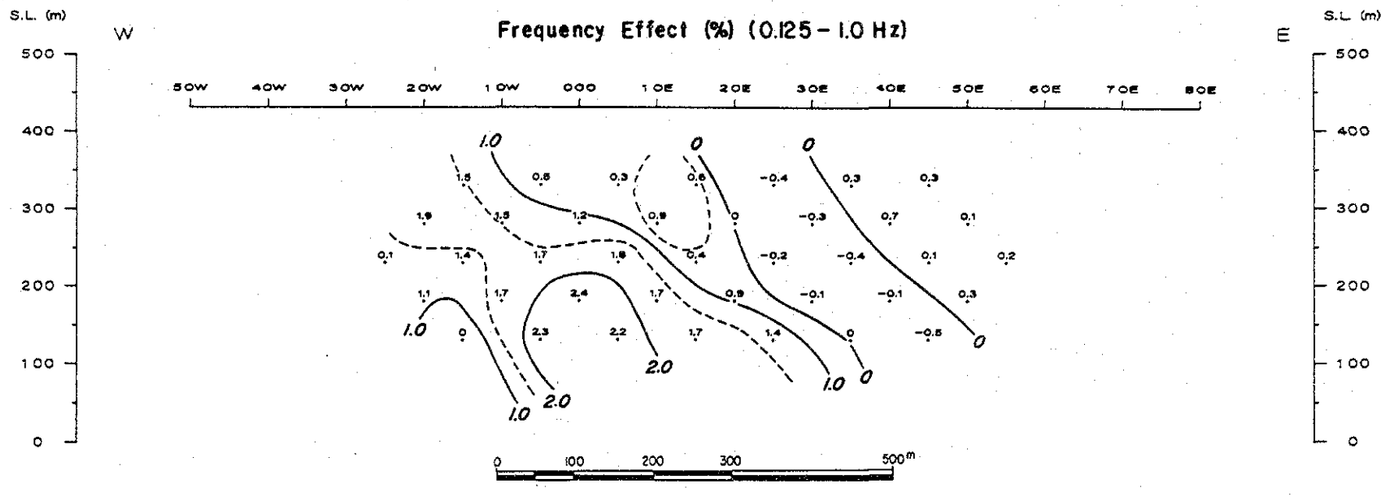

Fig. III–33 SIP Pseudo-Section (Line-110S)

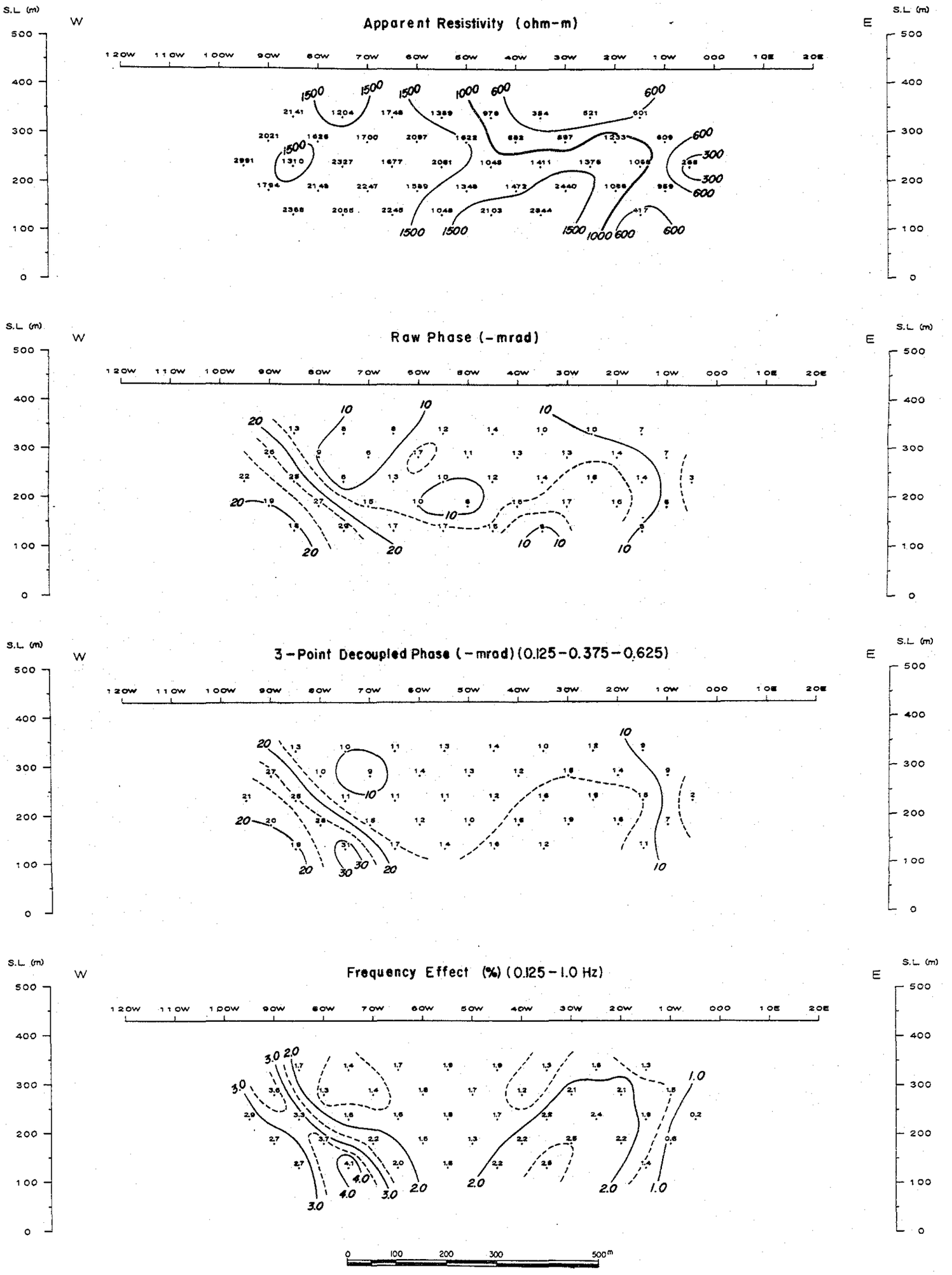

Fig. III–34 SIP Pseudo-Section (Line-150S)

Notwithstanding the above, at the west end of this line, the IP anomaly presumed to be due to the existence of an anomalous source shows a strong IP effect. From the distribution pattern of this anomaly, the center of the source is assumed to be around 100W-120W. However, it is difficult to assure whether this anomaly is due to a massive or vein type anomalous source because this line did not possible cover the whole anomaly.

Another weak anomaly shown at the deeper part of 30W and 20W seems to be dipping westward and due probably to the mineralization related to the C-1 ore deposit because this anomaly shows similar pattern as those of Line-15S, 35S and 110S.

* 3-point Decoupling Phase Pseudosection (0.125 Hz – 0.375 Hz – 0.625 Hz)

This section shows the same distribution pattern as that of the above phase pseudosection. Phase lower than –20 mrad is shown at the west end of the survey line, indicating a distribution pattern associated with the center of an anomaly located around 110W. Different point from the phase pseudosection is that the phase value changes lower than –10 mrad up to (n = 1 – 2) of 80W-60W.

* PFE Pseudosection (0.125 Hz – 1.0 Hz)

IP anomalies higher than 2.0% are detected at the west end of the survey line and at deeper part of the Stations 40W to 20W. The former contains PFE of higher than 4.0% and its origin is assumed around the ground surface. The latter is considered to reflect the effect of the weak disseminated anomalous source at 10W-20W dipping westward.

3–4–2 Plan Maps

In order to further analyze the IP anomalies, a set of plan maps was prepared based on the information obtained at three different depths: 100, 200 and 300 m, which correlates with the n-factors of 1, 3 and 5, respectively. And two different sets of maps were prepared, of which one set, indicated by Figs. III–35 through 37 shows the apparent resistivity, and the other, illustrated by Figs. III–38 through 40, shows the PFE. In the following, the apparent resistive plan maps will first be described, and thereafter the PFE plan maps, both of them for n = 1, 3 and 5.

Apparent Resistivity Plan Map (0.125 Hz)

The two survey Lines 15S and 35S located on the C-1 ore deposit presented a resistivity of less than 500 Ωm amply distributed with the exception in the deeper part (n = 5) where only a small high resistivity distribution is seen. The other two survey lines, 110S and 150S do not show a high contrast in resistivity at all the analyzed depths.

On the other hand, the approximated 800m separation between the two lines located on the C-1 ore deposit and the other two southern lines presented difficulties in clearly defining the resistivity distribution between both groups.

n = 1

Resistivity distribution around Line-15S and 35S shows that the resistivity lower than 300 Ωm has a tendency to extend along the N-S direction around the C-1 ore deposit. To the west of Station 20W a low resistivity, almost the same as that around the C-1 ore deposit, is distributed showing a trend to extend along the N-S direction.

In relation to the other two lines (110S and 150S), the resistivity distribution suggests a different response from the two previous lines. High resistivity of more than 1,000 Ωm is detected in the west of 10W of Line-110S continuing to the west of 50W of Line-150S and expanding widely to the west. In this area the high resistivity detected reflects the Pip_3 formation which is thought to be mainly amphibolite.

In these lines a resistivity contrast is also shown extending along the NE-SW direction and considered to be caused by a fault or boundary layer.

n = 3

The resistivity values at this depth are higher than those of n = 1. Resistivity higher than 300 Ωm is notably detected in the three Lines 15S, 35S and 110S, whereas in Line-150S resistivities higher than 1,000 Ωm are mainly detected. From the above, it is considered that between three lines of 15S, 35S and 110S, and Line-150S a structural change takes place along the N-S direction.

A high resistivity which is detected in Station 20E of lines 15S and 35S, but not detected at n = 1, suggests the existence of a high resistivity layer of 700 m width and a presumed fault or boundary layer in the vicinity of 20E.

The similar pattern in the resistivity distribution of the Line-110S with lines 15S and 35S reflects a layer distributed horizontally.

On the other hand, the high resistivity detected between 20E and 40E of lines 15S and 35S and not found in Line-110S, reflects a high resistivity distributed along the SE direction.

As compared with n = 1, the high resistivity distributed to all over the area of Line-150S is seen expanded in this map. A strong resistivity contrast shown in this line suggests the existence of a fault or structural boundary around 10W.

n = 5

A discontinuity in the resistivity distribution bewteen 10W and 20E of Line-15S reflects the existence of a fault or the boundary of a geological structure. From the resistivity distribu-

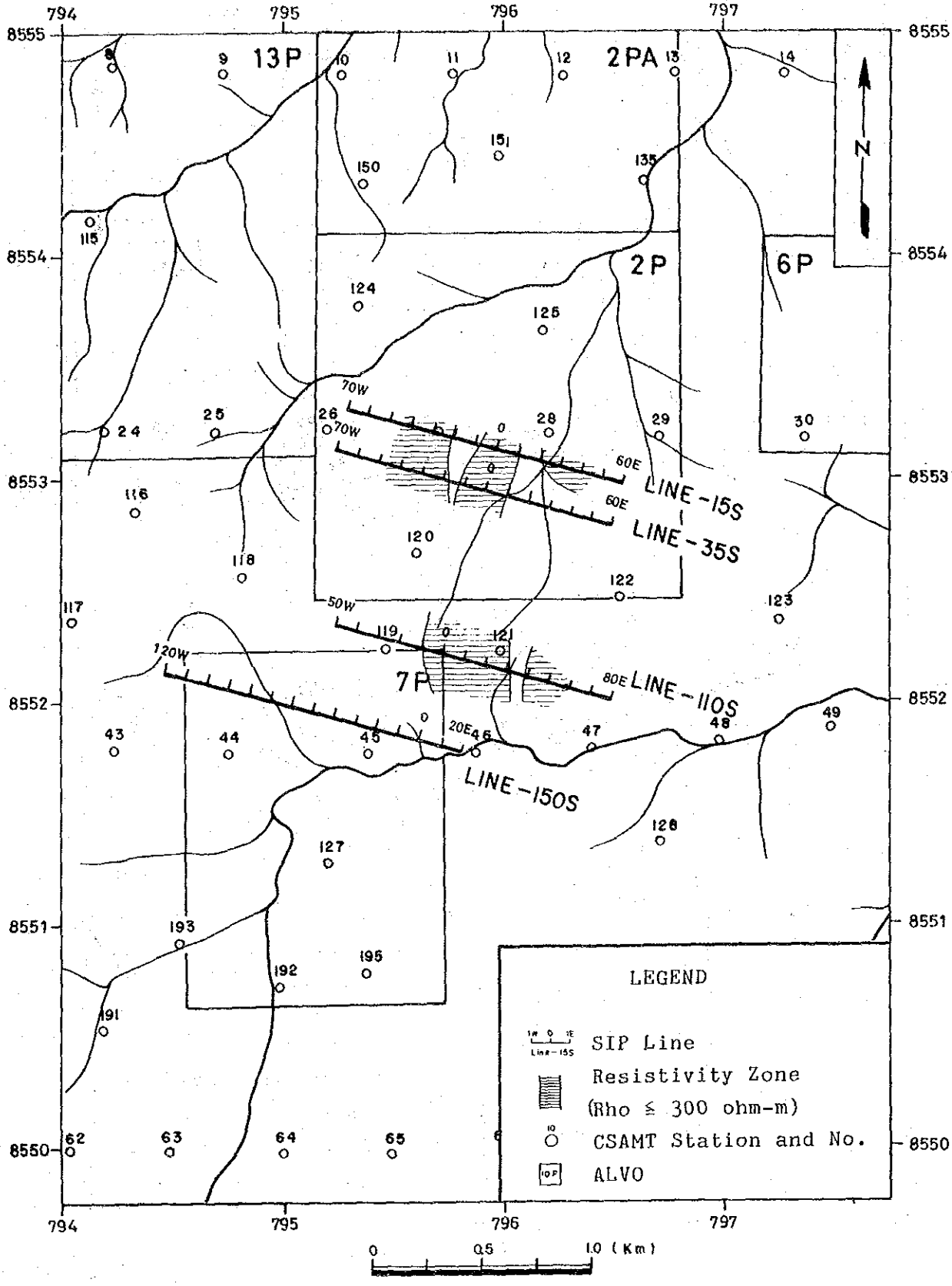

Fig. III—35 Apparent Resistivity Map [SIP (n-spread 1)]

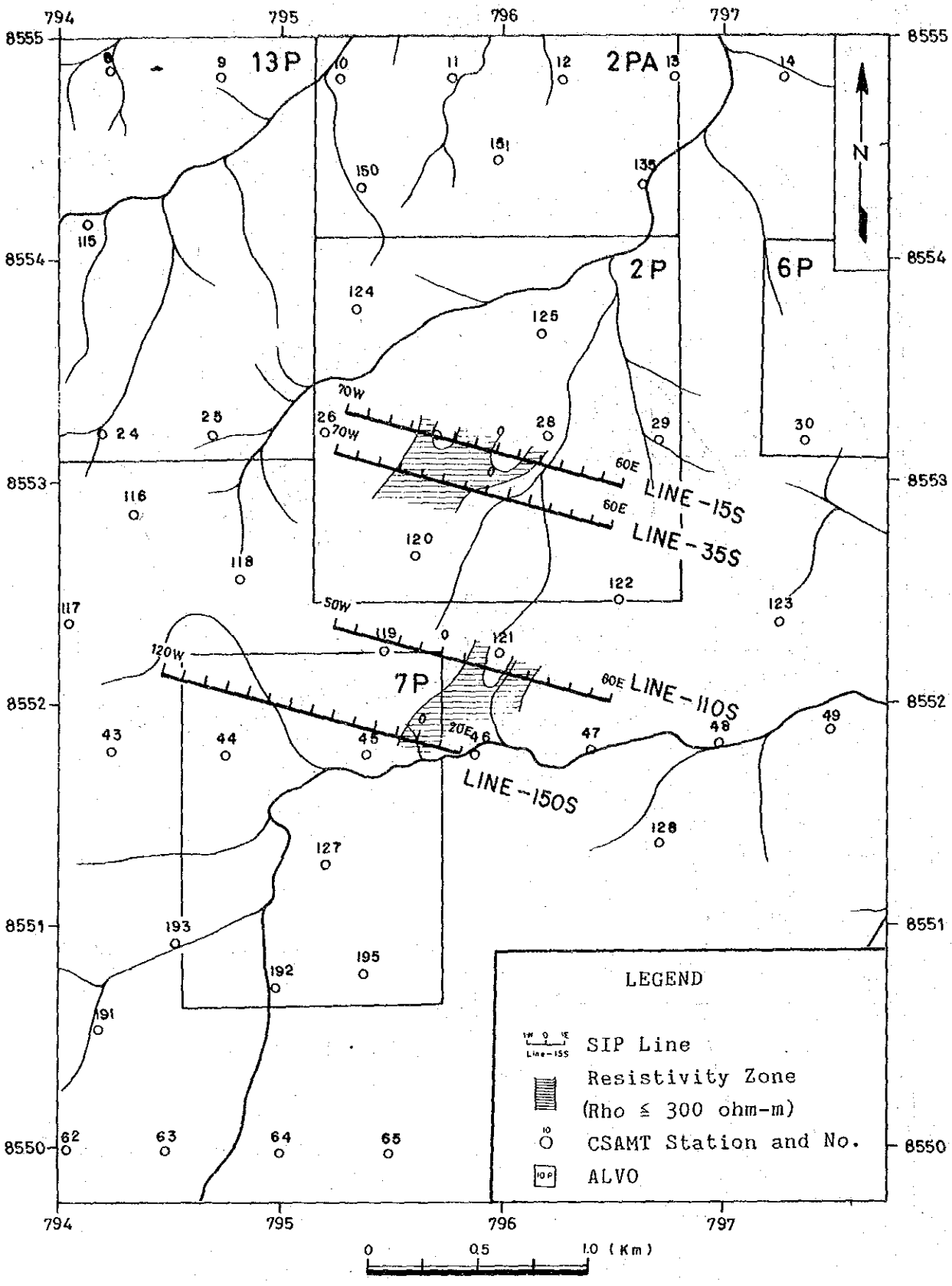

Fig. III–36 Apparent Resistivity Map [SIP (n-spread 3)]

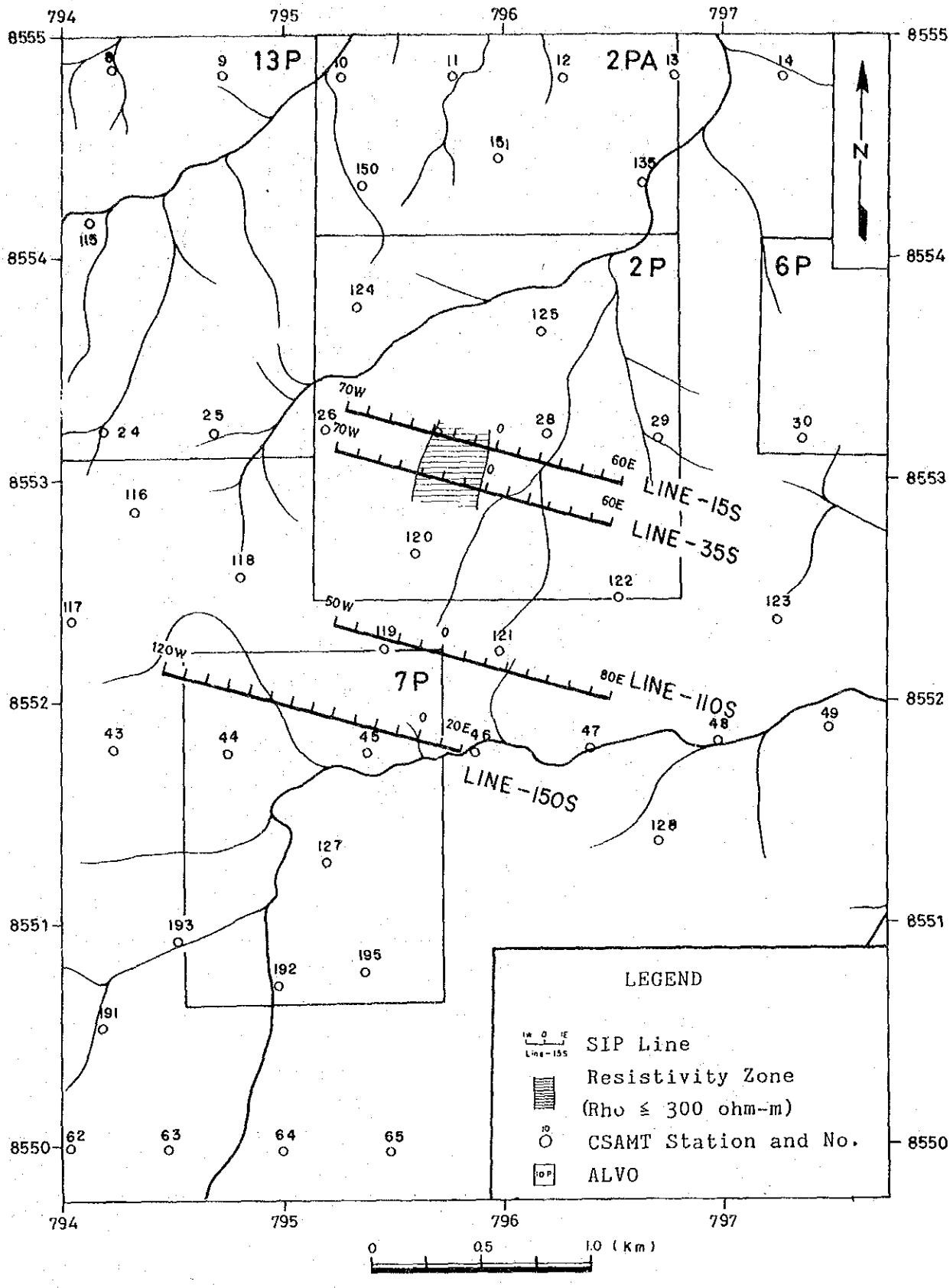

Fig. III–37 Apparent Resistivity Map [SIP (n-spread 5)]

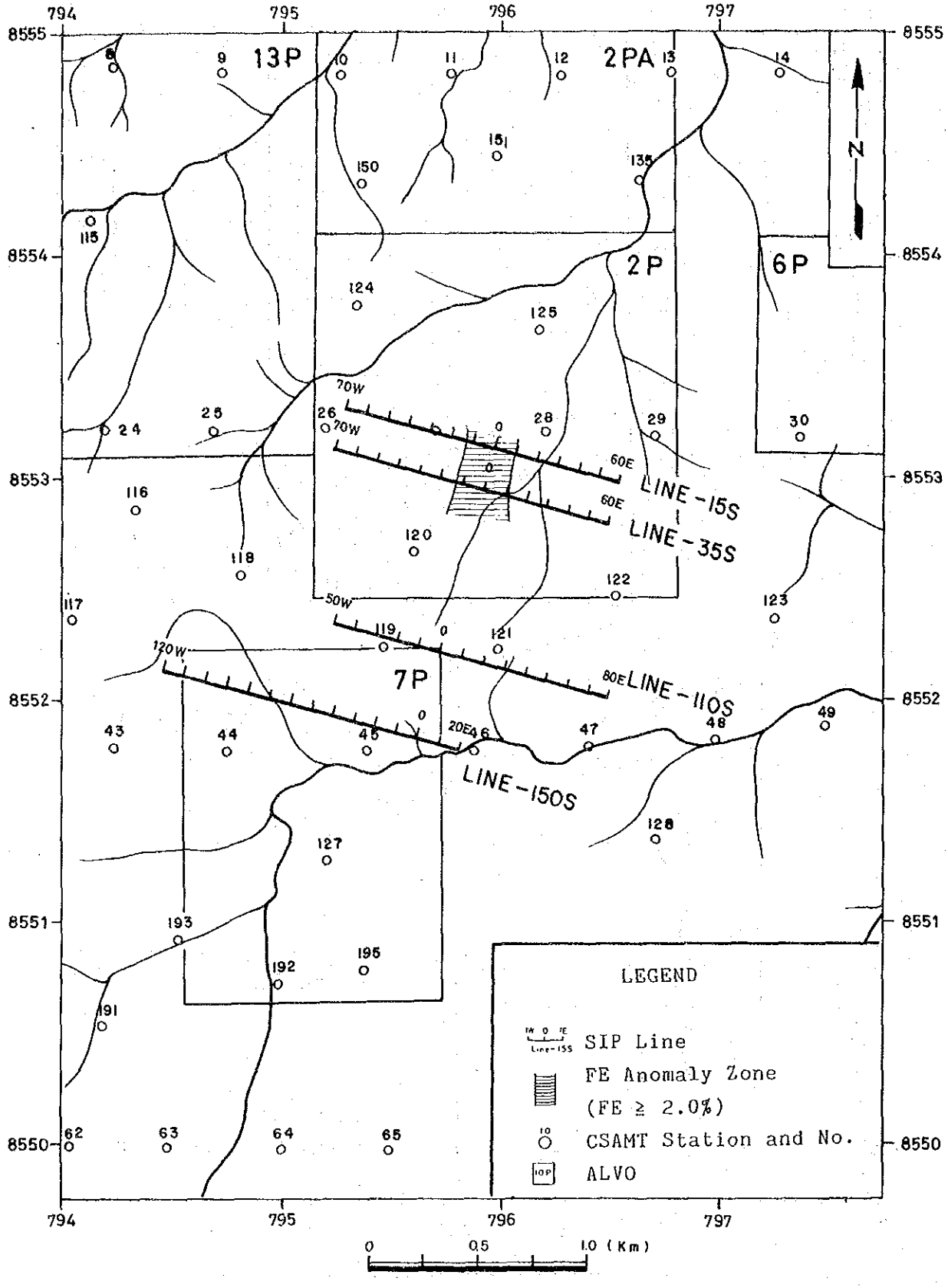

Fig. III–38 Frequency Effect Map [SIP (n-spread 1)]

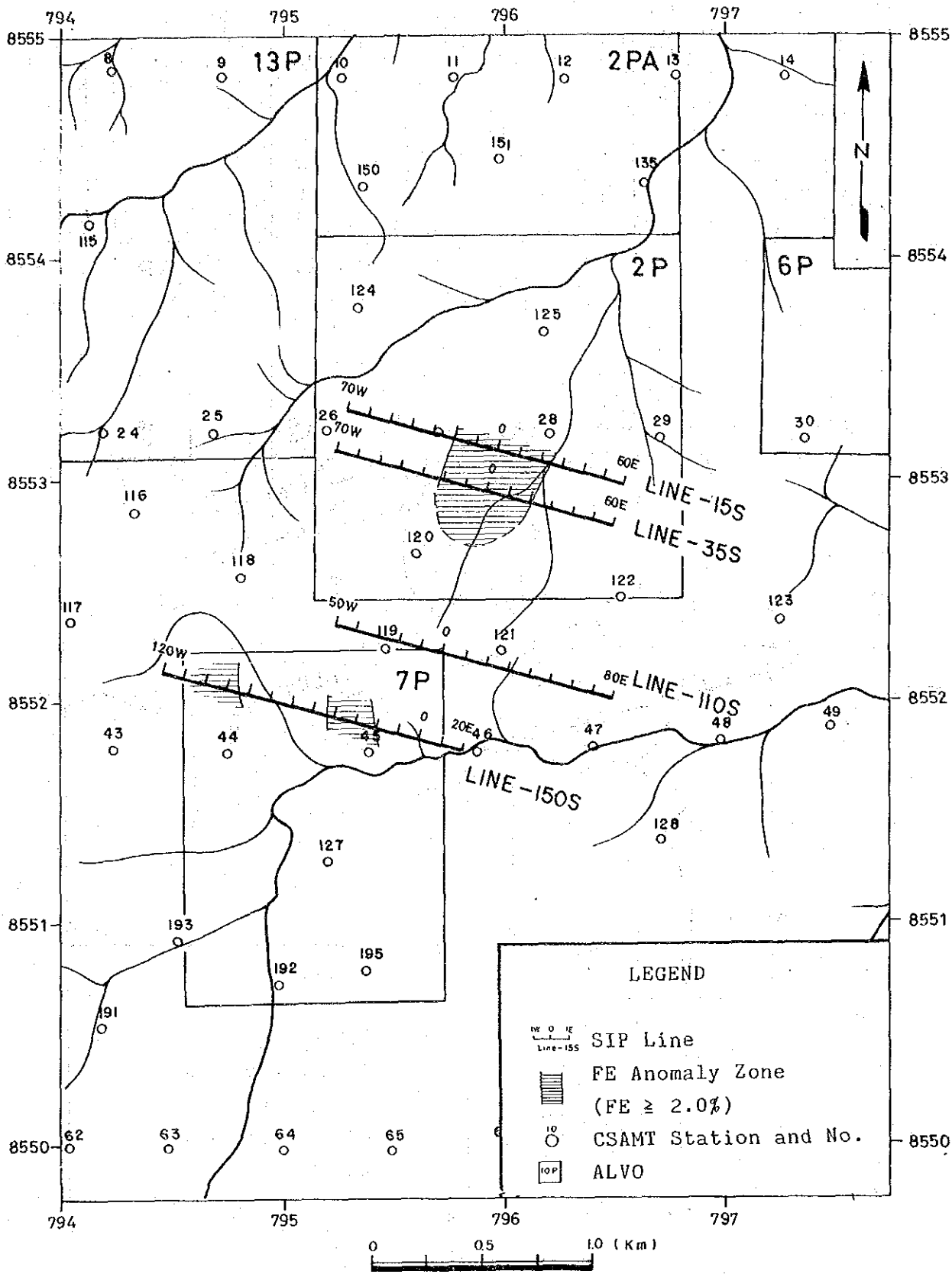

Fig. III–39 Frequency Effect Map [SIP (n-spread 3)]

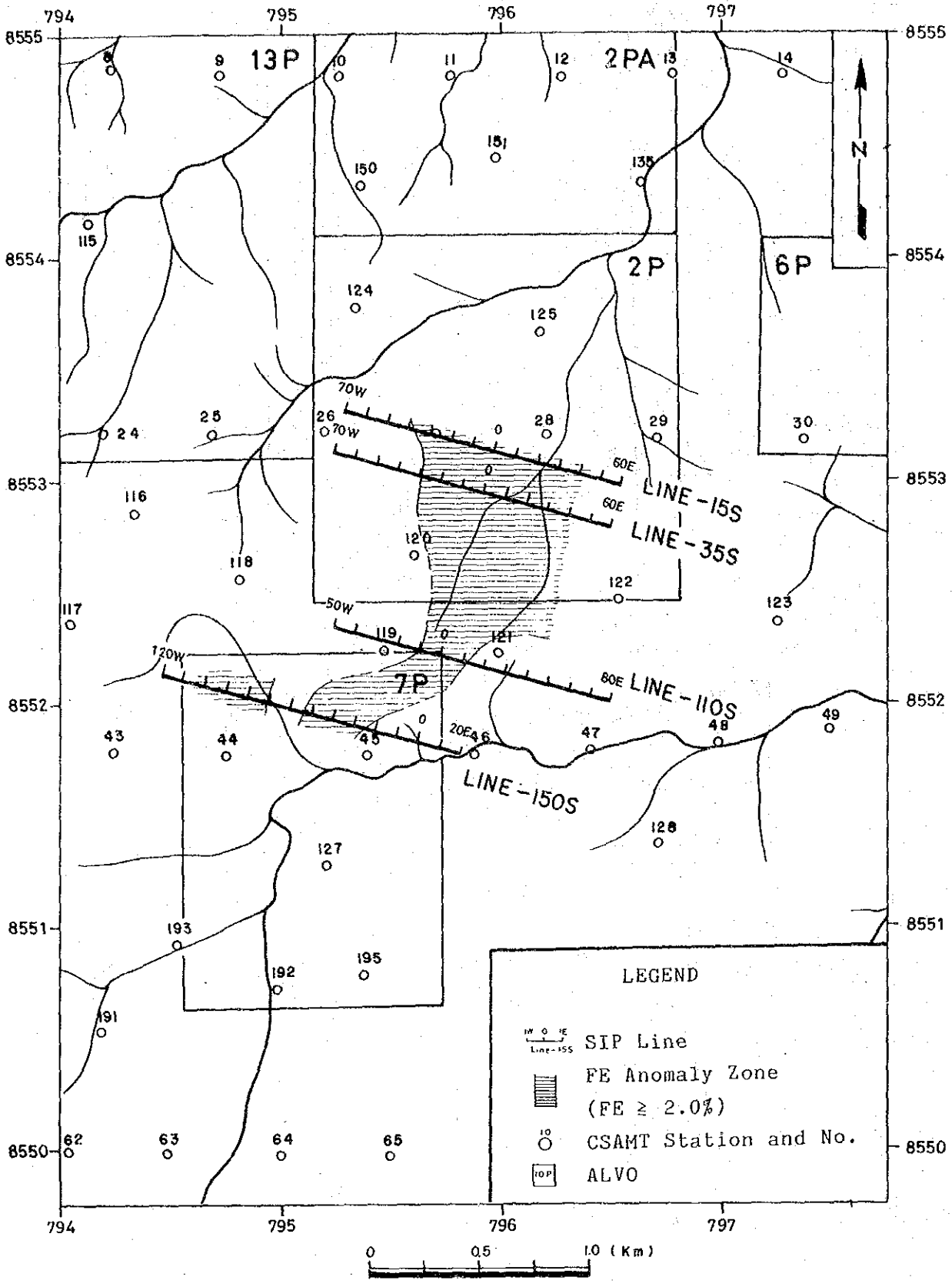

Fig. III-40 Frequency Effect Map [SIP (n-spread 5)]

tion for n=3 and n=5, the above mentioned structure is seen to dip westward.

PFE Plan Maps

IP anomalies were detected around the C-1 ore deposit and at the west end of Line-150S.

n = 1

PFE values higher than 2.0% are detected in lines 15S and 35S, however, they are not seen in lines 110S and 150S.

Anomaly of more than 2.0% detected in lines 15S and 35S defines an anomalous zone extending along the NE-SW direction, with their highest value of 4.8% being detected around Station 00 of Line-35S. This anomaly is considered to be due to the C-1 ore deposit with the possibility that this deposit or the mineralization formed around the deposit be distributed along the NE-SW direction. It is not clear at this time whether or not the C-1 ore deposit or mineralization is continued around Line-110S.

n = 3

IP anomaly higher than 2.0% is shown in two zones, i.e., between 10W and 20E of Line-15S and 35S, and in the west of 80W and between 20W and 40W of Line-150S. The former zone presents an anomalous zone extending to the NE-SW direction just the same as n = 1, however, it shows higher PFE values. This fact assures the existence of a stronger anomalous source than the one found at n = 1. The latter zone was not detected at n = 1.

n = 5

PFE values higher than 2.0% are indicated all over the lines, but showing a distribution pattern which reflects the effect of a weak mineralization zone.

PFE values between 2.0 and 4.0% can be recognized in Line-15S and 35S, however, it is impossible from this pattern, to determine the center of the anomaly.

IP anomaly detected between 70W and 90W of Line-150S shows a high contrast IP anomalous distribution larger than the one at the previous depth of n = 3. It can not be considered that the anomaly detected for Line-15S and 35S represents a continuation of this anomaly. Taking also into account the physical property of the rocks, it can be said that these anomalies may belong to the same geological horizon.

3–4–3 Spectral Analysis

The raw phase spectrum, magnitude spectrum, and Cole-Cole diagrams represent the main tools to give a close analysis to the spectral response of the geological structure under study. They may enable us to discriminate among several kinds of minerals or types of ore deposits.

These diagrams are shown in Figs. III−41 through III−43.

In this survey area, three kinds of spectral type were detected. They are:

* Spectral type A: associated with sulphide mineralization and reflects the strong IP anomalous source.
* Spectral type B: associated also with sulphide mineralization, but reflects the weak IP anomalous source.
* Spectral type C: shows no IP effect and refects only electromagnetic coupling.

In the following will be discussed the characterizations of the spectral responses due to the geological structure using the above mentioned diagrams obtained for all the survey lines.

• LINE−15S

As already mentioned, this line was located on the C-1 ore deposit, giving indications of an anomaly with a strong IP effect around Station 00. As shown in Fig. III−41, i.e. in the phase spectrum diagram, an anomaly of spectral type A is detected around Station 00 reflecting the C-1 ore deposit. This spectrum shows a gentle upward concave curve at a high frequency range, with phase differences of about −3 mrad between 0.125 and 9.0 Hz. This type of curve is presumed to be due to sulphide mineralization.

Spectral type A is found at n = 1 to 2 around the Station 00 but with spectral type B reflecting the surrounding zone. Actually, spectral type B is almost the same as type A, but seems to reflect dissemination of sulphide minerals.

The analysis of the magnitude spectrum diagram reflects the effect of a low resistivity in the high frequency range. The distribution pattern of this type is the same as spectral type B.

In relation to the Cole-Cole diagram, an anomaly at n = 1 to 3 between Stations 00 and 10E dipping westward was able to detect. This characteristic type shows a large change in the imaginary part at the high frequency range, being able to reflect the C-1 ore deposit.

• LINE−35S

In this line, the IP anomaly detected is stronger than the one in the Line-15S but is being continued to deeper depth. Spectral type A is detected around n = 1 to 3 of Station 00 as a center, with spectral type B distributed in the surroundings of type A.

Judging from the trending shown by this distribution, both spectral types A and B are presumed to be due to the C-1 ore deposit which is considered to extends to the southern direction.

In magnitude spectrum and Cole-Cole diagrams, a characteristic pattern seems to reflect the IP anomaly seen in the same distribution areas as the one previously indicated by spectral type B. This pattern is of the same kind as the one shown in Line-15S.

• LINE−110S

A quite different spectrum was detected between Stations 00 and 20E, due most certainly, to some unknown artificial noise. Spectral type B, considered to be due to weak IP anomalous source, is found between Stations 10W and 00. However, spectral type C is seen to be the dominant one in this line.

In both, the magnitude spectrum and Cole-Cole diagrams, the patterns detected are considered to reflect only electromagnetic coupling and no IP anomaly is found.

The above results lead to assume the existence in this line of sulphide minerals of the same quality as that of the C-1 ore deposit.

• LINE−150S

A characteristic type of spectrum was found beneath Station 40W and the west of 90W.

Spectral type A is detected to the west of 90W with a pattern dipping eastward. This type shows also a trend distributed westward, however, the whole aspect of its distribution area is still unknown.

Spectral type beneath 40W is similar to type B, showing phase differences between 0.125 and 1.125 Hz. It is probably due to the sulphide mineralization which induced a weak IP effect, as same as the one seen at the west of 90W. In magnitude spectrum and in Cole-Cole diagrams, the distribution area of the pattern is mostly due to IP anomaly similar to spectral type B.

PHASE SPECTRUM
LINE-15S

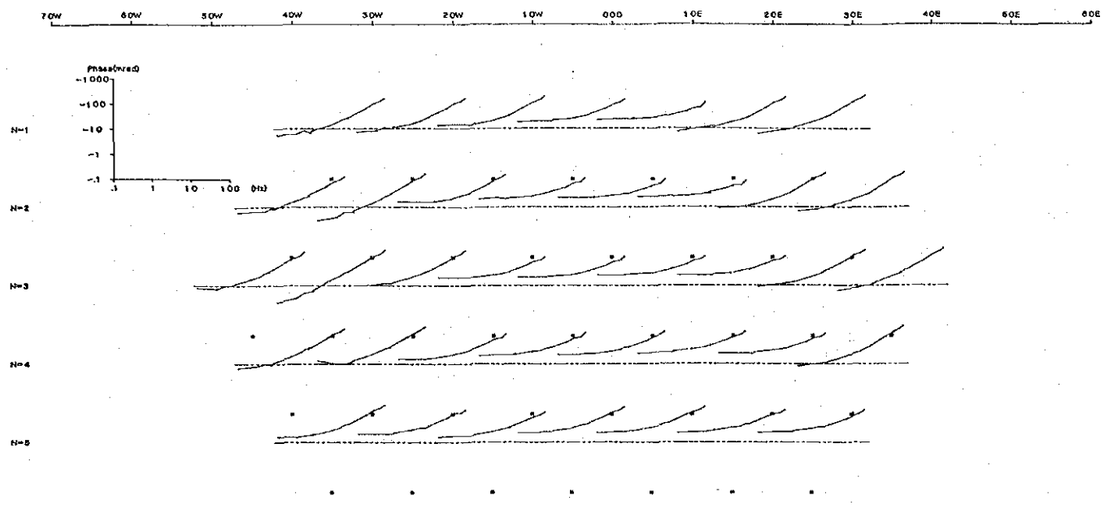

PHASE SPECTRUM
LINE-110S

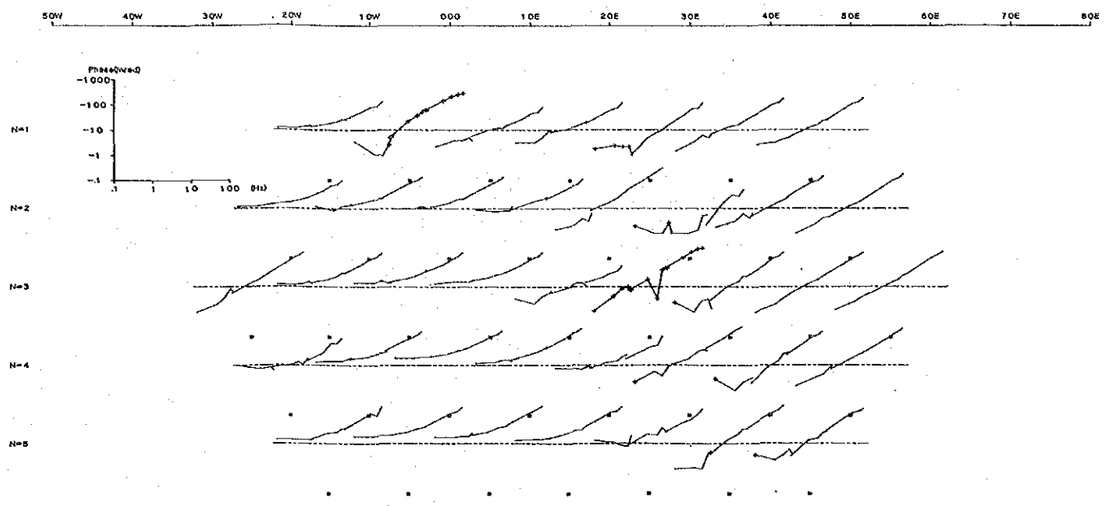

PHASE SPECTRUM
LINE-35S

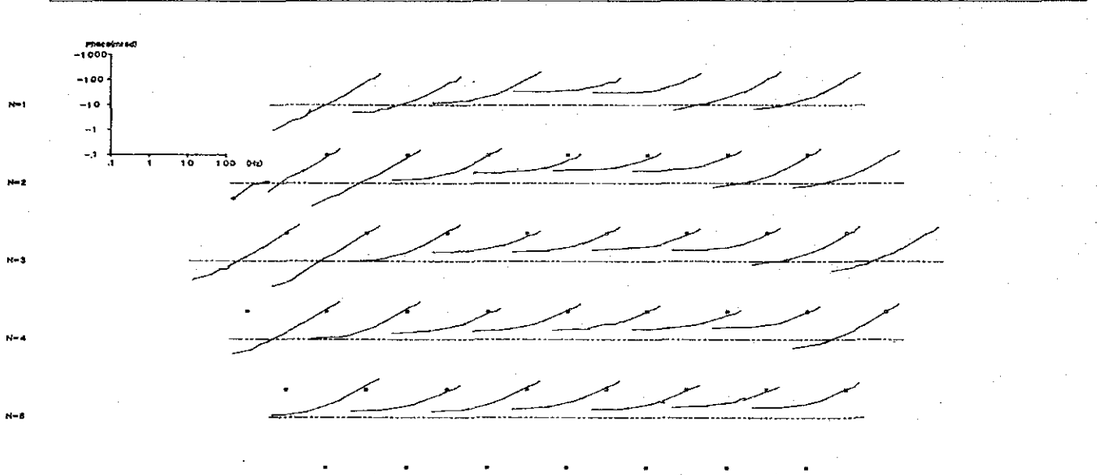

PHASE SPECTRUM
LINE-150S

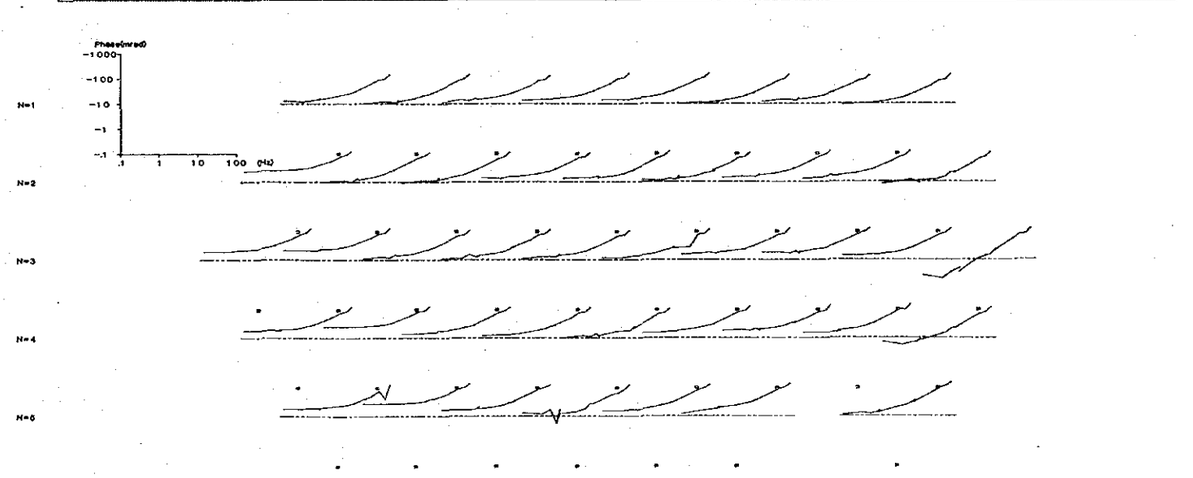

Fig. III–41 Phase Spectrum Diagram

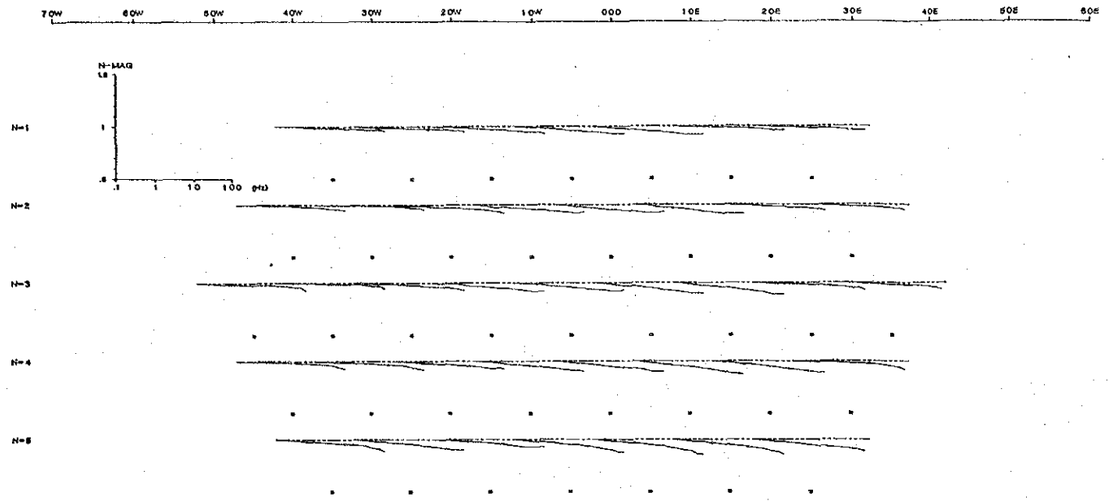

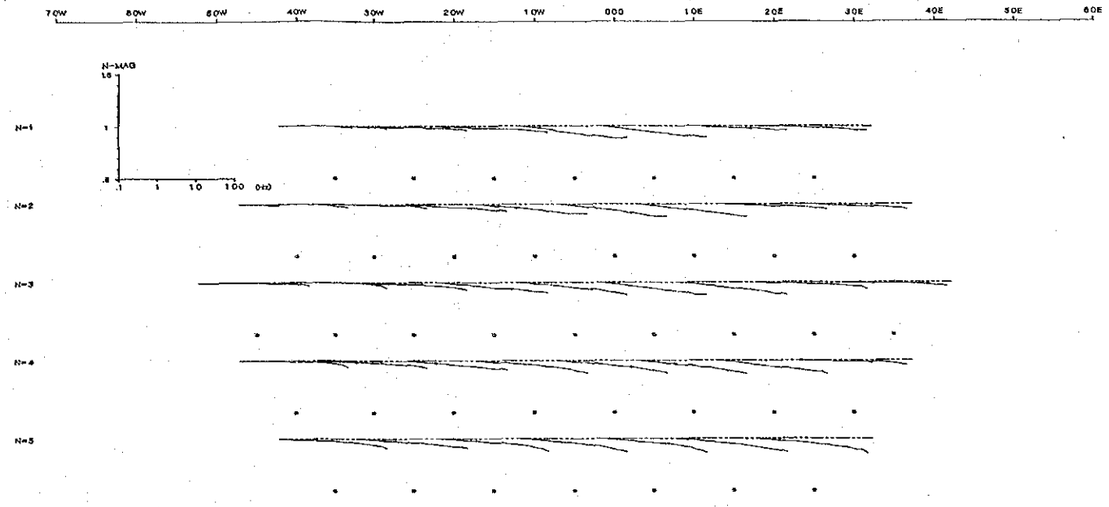

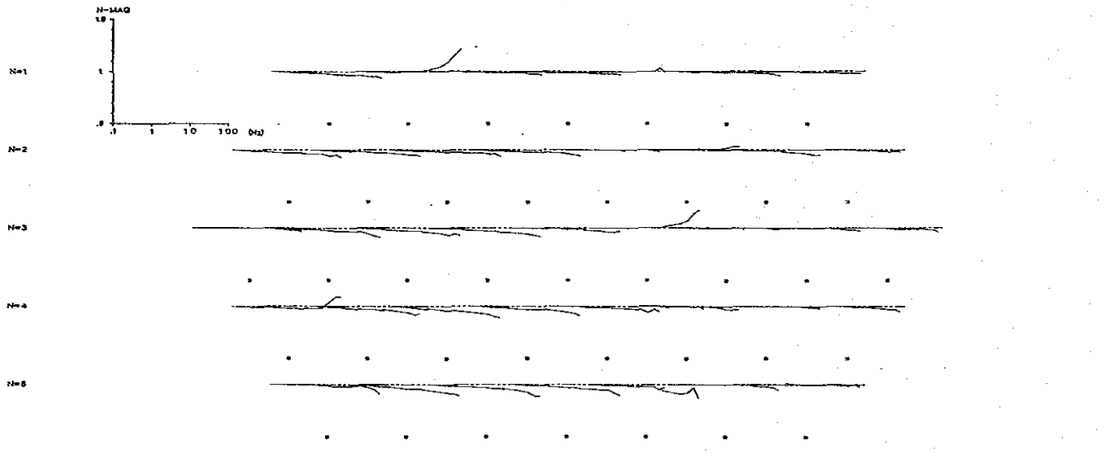

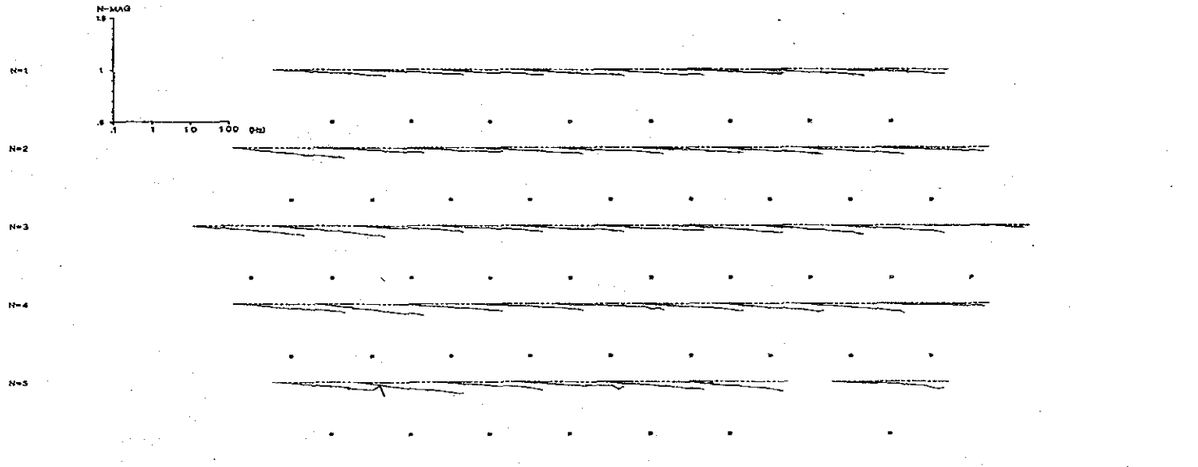

Fig. Ⅲ–42 Magnitude Spectrum Diagram

COLE-COLE DIAGRAM
LINE-15S

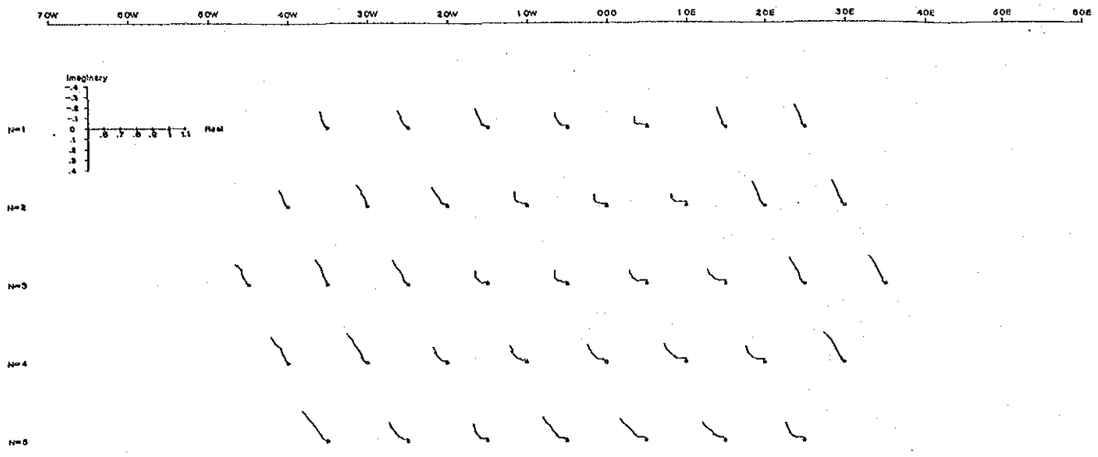

COLE-COLE DIAGRAM
LINE-110S

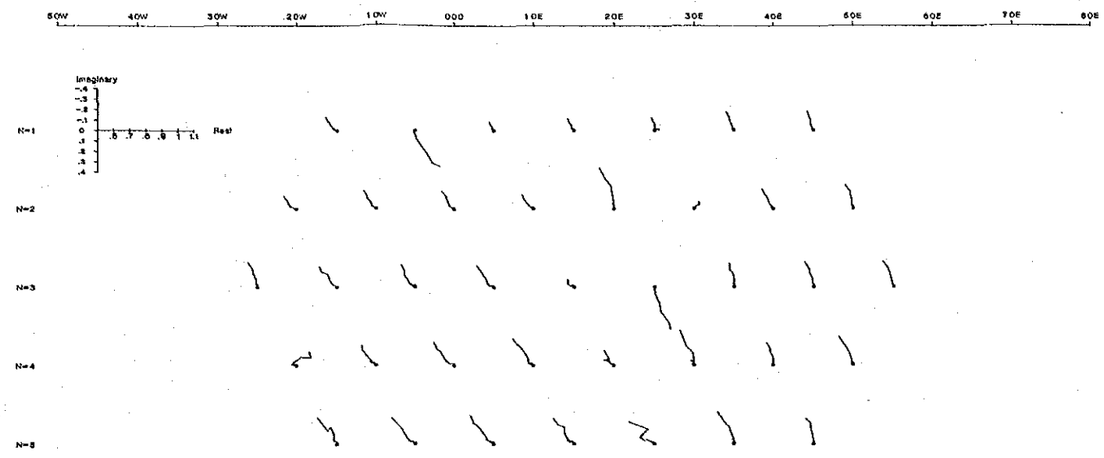

COLE-COLE DIAGRAM
LINE-35S

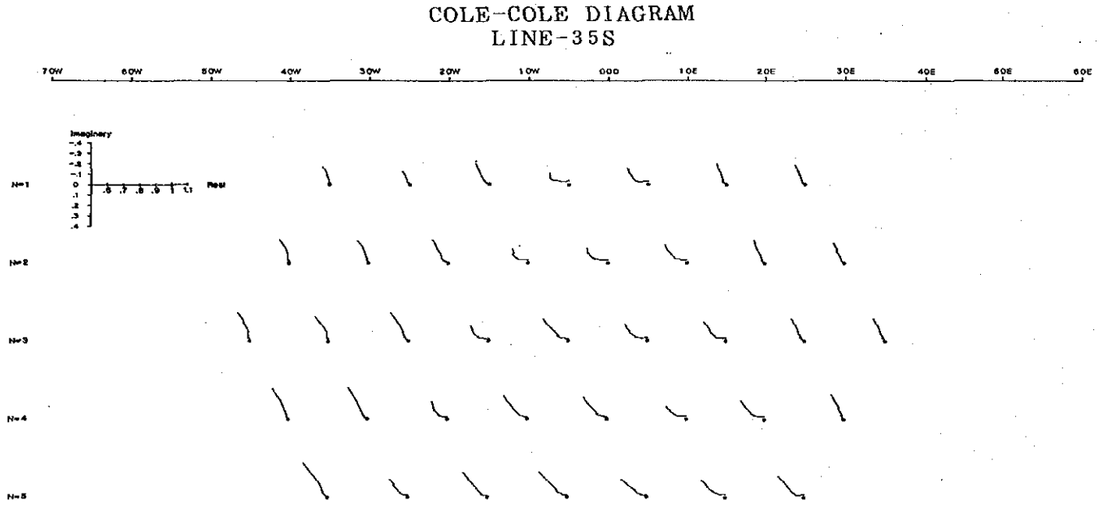

COLE-COLE DIAGRAM
LINE-150S

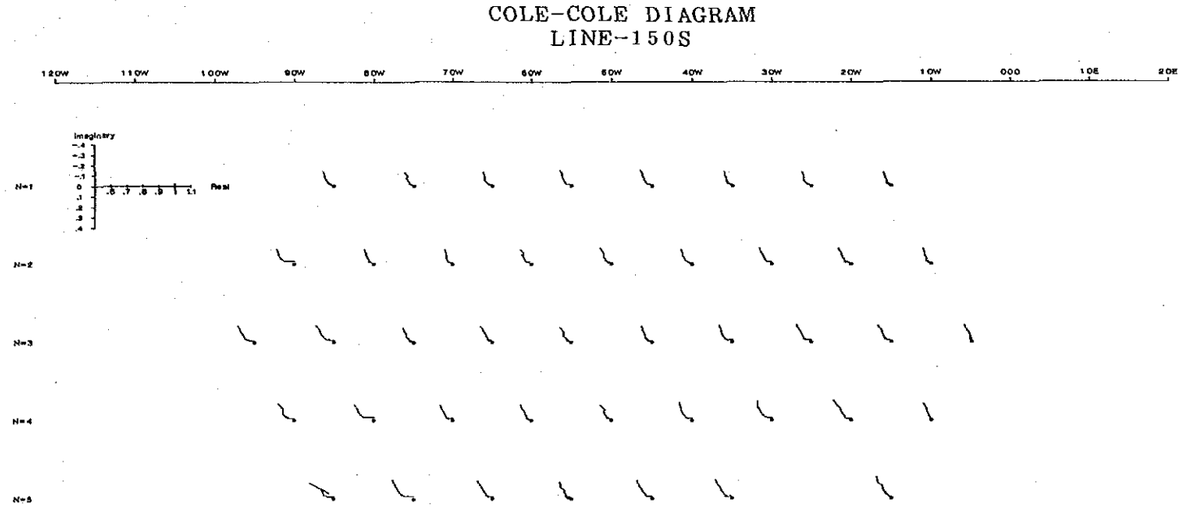

Fig. Ⅲ–43 Cole-Cole Diagram

3–5 Discussion

As a result of this survey, anomalous zones around the C-1 ore deposit are found to be originated from two kinds of anomalous source. At the west end of Line-150S an unconfirmed anomaly was detected, however, it needs to be further investigated.

The resistivity structure around the C-1 ore deposit is clarified to be composed of two or three layers, the first layer being 50m in thickness and 100 Ωm.

The next layers appeared to be with a higher resistivity, as it was concluded from the CSAMT survey. The C-1 ore deposit, already known, is therefore in the first layer.

As a result of the SIP survey, the resistivity at the estimated depth between 100 to 150m appeared to be around 300 Ωm. At deeper depth, high resistivity of more than 1,000 Ωm is found distributed. IP anomaly is shown at resistivities higher than 300 Ωm, showing a stronger IP effect as the resistivity gets higher.

The distribution form of observed IP anomaly is not due to massive anomalous source, but is considered to be due to anomalous source of fine vein (stockwork structure) or to dissemination. Judging from the spectral response and physical properties of the rocks, this anomalous source is considered to be caused by disseminated sulphide mineralization within the high resistivity rocks.

Therefore, the massive ore deposit (C-1 ore deposit), which is already confirmed and which is distributed at shallow depth, seems to be the most probable reason of the change at deeper part of stockwork disseminated ore deposit within amphibolite. The IP anomaly detected at the center of Line-15S and Line-35S are considered to be due to the anomalous source which reflects the stockwork assembling of disseminated sulphide minerals developed beneath the C-1 ore deposit. This anomalous source decreases towards the south.

A new anomaly detected in this survey shows also a strong IP effect, with a spectral type almost the same as the one obtained around the C-1 ore deposit and reflects sulphide mineralization. This detected anomalous source is seen to be due to the same geological horizon as that of C-1 ore deposit, but is not the southern extension of the C-1 ore deposit. Therefore, this source seems to be another mineralization zone.

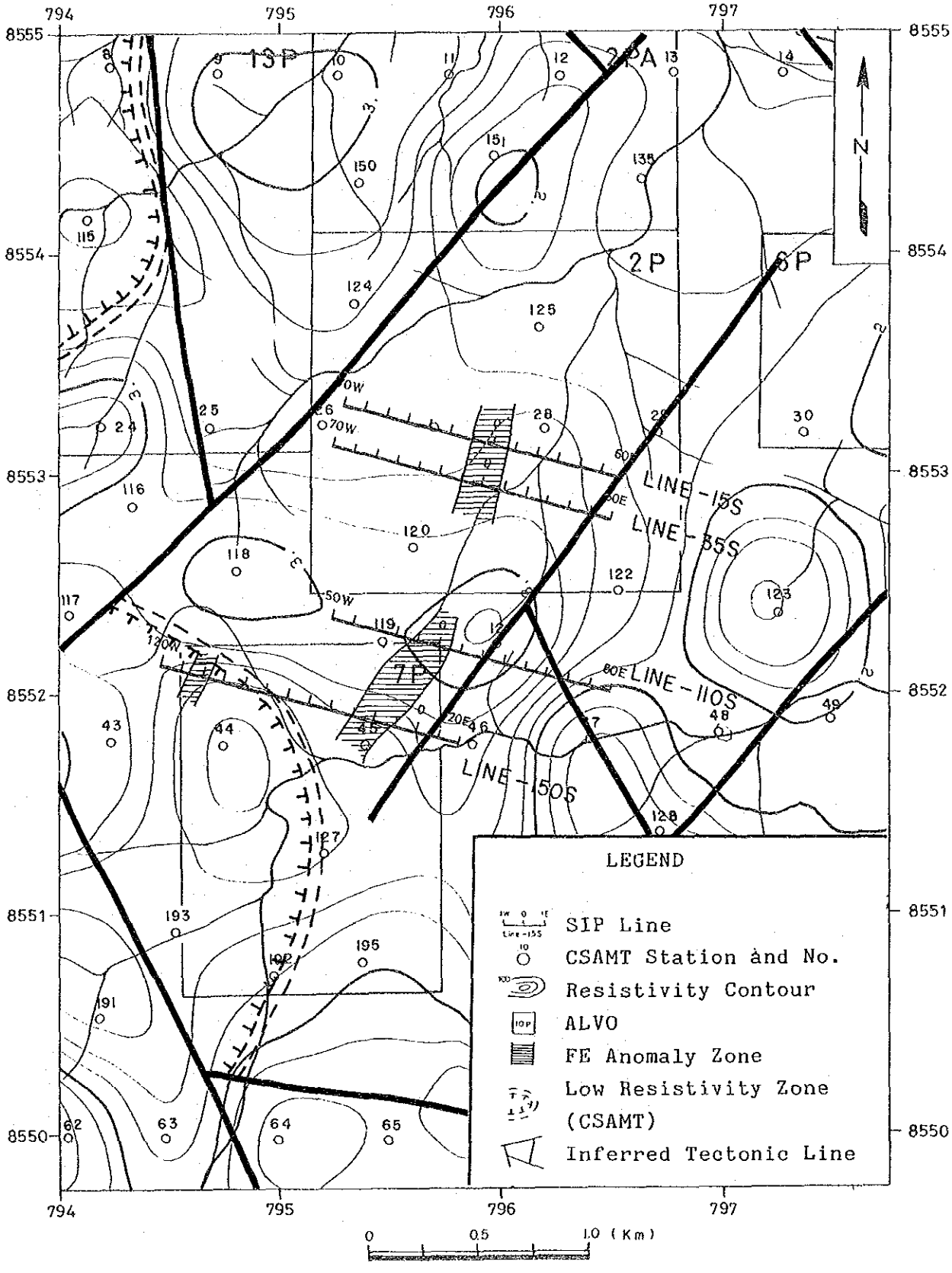

Fig. III–44 SIP Interpretation Map

IV CONCLUSION AND RECOMMENDATION

CHAPTER 1 Conclusions

In order to grasp more clearly the relation between the geologic structure and the field of emplacement of ore deposit in the survey area, the geochemical survey (stream sediment) was conducted for the regional survey area in parallel with check the survey of geology, the geochemical (soil) and geophysical (CSAM method and SIP method) surveys which were conducted covering the semi-detailed survey area.

The results of these surveys are as follows:

1. The geology of the survey area consists of the Precambrian groups such as Archaean (Cana Brava basic to ultrabasic massif) and Proterozoic (the lower part: Palmeirópolis volcano-sedimentary sequence, the middle part: Serra da Mesa Group, the upper part: Rio Maranhão cataclastic zone and paranoá Group), and the intrusive rocks such as granitic rocks and basic to ultrabasic rocks. Among these, the Palmeirópolis volcano-sedimentary sequence, in which copper, lead and zinc deposits are emplaced, are classified, from the base upward, into amphibolite (Pip_1 formation), pyroclastic rocks and schistose rocks (Pip_2 formation), amphibolites (Pip_3 formation), intermediate to acidic schistose rocks (Pip_4 formation) and pelitic schistose rocks (Pip_5 formation).

Metamorphic grade of the rocks of the sequence belongs to the amphibolite facies, and the temperature and pressure of metamorphism are considered to be 300° to 600°C and six to 10 atms respectively.

2. The Palmeirópolis deposit (C-1 Ore Deposit) is a stratiform to lenticular copper, lead and zinc deposit harmoniously emplaced between the Pip_3 formation which is the country rock in the footwall, and the Pip_4 formation which is the country rock in the hanging wall.

The type of ore belongs to massive ore and disseminated ore. The ore minerals are composed of the assemblage of sphalerite, pyrrhotite, pyrite, chalcopyrite and galena.

The host rocks of the C-1 ore deposit plunge toward the southwest to continue to the lower part of Alvo 7P, 9P and 10P.

3. The results of statistical processing of 1,031 samples (four components of Cu, Pb, Zn and As) collected in the field showed the threshold values of 47 ppm in copper, 22 ppm in lead, 63 ppm in zinc and 8 ppm in arsenic. Multivariate analysis resulted in obtaining a Pb-Zn factor considered to be caused by mineralization, a Cu-Zn factor which seems to have reflected the characteristic of the basic rock, and an As-Pb factor considered to have reflected hydrothermal effect along fault.

Single component analysis and multivariate analysis led to extract the six geochemically

anomalous areas as follows:

① Alvo 2P, 7P, 9P, 10P, east of 11P and 1P in the semi-detailed survey area (Cu-Pb-Zn).

② The area underlain by the Pip_4vs formation in the central part of the regional survey area (Cu-Pb-Zn).

③ The area underlain by the Pip_1 and Pip_3 formations in the northeast of the central part of the regional survey area (Cu-Zn).

④ The area underlain by the Pip_5 formation in the northwest of the central part of the regional survey area (Cu-Pb-Zn).

⑤ The area underlain by the Pm_1xt and Pmsm formations in the western part of the regional survey area (As-Pb).

⑥ The area underlain by the Pip_3 and Pip_5 formations in the southern part of the regional survey area (As-Pb(-Cu-Zn)).

Putting aside the semi-detailed survey area, the area ② is considered to be the most important one for future surveys, because it is distributed by the geologic setting to be correlated to the same horizon as that of the country rocks emplaced by the Palmeirópolis deposit, which is assumed to be the geochemically anomalous area caused by Cu-Pb-Zn mineralization similar to the known deposit.

4. As the result of statistical processing of the 2,555 soil samples (four components) collected in the field, single component analysis showed the threshold values of 105 ppm in Cu, 35 ppm in Pb, 114 ppm in Zn and 6 ppm in As for the whole samples.

The values are 104 ppm in Cu, 35 ppm in Pb, 126 ppm in Zn and 6 ppm in As for the soil derived from amphibolite, and 72 ppm in Cu, 33 in Pb, 91 ppm in Zn and 5 ppm in As for the soil derived from schistose rocks.

Multivariate analysis resulted in extracting a Cu-Zn factor considered to have reflected both the characteristics of basic rock and mineralization, and a As-Pb factor seems to have reflected the later hydrothermal effect.

As a result of analysis of the data obtained in the soil geochemical survey, Pb-Zn anomalous zones arranged in the direction of NE-SW were extracted in the schistose rocks (Pip_4 Formation) in Alvo 7P, southeast of 9P, 13P and 10P, and Cu-Zn anomalous zones in the eastern part of Alvo 11P, in addition to the Cu-Pb-Zn high anomalous zone in the vicinity of the C-1 ore deposit.

5. As the result of analysis of the CSAMT method, high resistivity zones are distributed in the eastern and western parts of the area showing a two-layered structure.

Moderate to low resistivity zones are distributed in the central part of the area in the direction of N-S showing a three to four-layered structure. The distribution pattern is consistent

with that of the schistose rocks (Pip_4 formation).

Regarding the low resistivity structure, the trend of NW-SE system is dominant in the western part, while that of NE-SW system is dominant in the central to eastern part.

A low resistivity structure showing a subsiding structure by crossing of the two directions as mentioned above predominates is recognized in the central part.

The resistivity structure in the vicinity of the C-1 ore deposit shows a gentle gradient of resistivity. The similar structures are concentrated around the NE-SW tectonic line through Alvo 7P and 10P.

6. The result of the SIP method shows that resistivity layer lower than 300Ωm corresponding to schistose rock (Pip_4vxt_1 Formation) is distributed in the vicinity of the C-1 ore deposit to about 100 meters below the surface, and further below, another layer of high resistivity corresponding to amphibolite (Pip_3 Formation) is distributed.

The result of analysis of IP effects and spectrum types in the deeper part of the C-1 ore deposit led to an assumption that the massive ore would change to a network to dissemination.

Distinct continuity of the C-1 ore deposit could not be confirmed along the survey line 150S. However, an IP anomaly was newly detected at the western end of the survey line 150S, and the anomaly is considered to be the one caused by sulfide minerals based on its spectral characteristics.

CHAPTER 2 Recommendations for the Phase II Surveys

The following surveys are recommended for the second year based on the results and conclusions of the Phase I surveys.

1. Semi-detailed Area

As the result of comprehensive analysis of the data obtained in the geological, geochemical and geophysical surveys, it is considered that a area from Alvo 7P to the southeast of Alvo 9P has the highest potentiality.

It is be necessary in future surveys in this area to conduct a geophysical survey by means of both IP and SIP methods as well as drilling.

2. Regional Survey Area

Both soil geochemical survey and geological survey are needed for the target of promising Cu-Pb-Zn geochemically anomalous zone extracted in the area underlain by schistose rocks (Pip_4 vs Formation) in the lower valley of Rio Dois de Junho in the central part of the regional survey area.

LIST OF ILLUSTRATION

LIST OF TABLES

APPENDIX

LIST OF PLATE

REFERENCE

(1) Almeida F.F.M., Hasui Y., Brito Neves B.B. and Fuck R.A. – 1981 – Brasilian structural provinces; an introduction, Earth-Sci, Rev., 17: 1-29.

(2) Almeida F.F.M. e Hasui, Y. – 1984 – O Precambriano do Brasil.

(3) CNEN/DNPM/CPRM – 1973 – Levantamento Aerocintilometrico Projeto Serra da Mesa.

(4) CNEN/DNPM/CPRM – 1977 – Projeto Serra da Mesa II-Goias, Relatorio Final.

(5) CPRM – 1984 – Projeto Palmeirópolis Informe Tecnico.

(6) DNPM – 1975 – Carta Geologica do Brasil ao Miliodesimo, Folha Goias SD-22.

(7) DNPM/MME – 1981 – Projeto RADAMBRASIL, Vol. 25.

(8) DNPM – 1981 – Geologia e Inventario dos Recursos Minerais do Regiao Central do Estado de Goias – Projeto Brasilia –.

(9) DNPM – 1981 – Os Principais Depositos Minerais do Região Centro-Oeste.

(10) DNPM/CPRM – 1983 – Projeto Palmeirópolis, Etapa Preliminar.

(11) DNPM – 1983 – Levantamento Aerogiofisico do Projeto Palmeiropolis-GO.

(12) DNPM – 1983 – Garimpos do Brasil.

(13) DNPM – 1984 – Garimpos do Brasil.

(14) DNPM – Projeto Mapas Metalogeneticos e de Previsão de Recursos Minerais – Porangatu – Folha SD-22-X-D.

(15) DNPM – Projeto Mapas Metalogeneticos e de Previsão de Recurais Minerais – Alvorada – Folha SD-22-X-B.

(16) Girardi A.V. and Kurat G. – 1982 – Precambrian Mafic and Ultramafic Rock of the CANABRAVA Complex, Brasil.

(17) Hasui Y. et al. – 1980 – Datacoes Rb-Sr e K-Ar Centro Norte do Brasil e seu Significado Geologico-Geotectonico, XXXI Congresso Brasileiro de Geologia.

(18) Louis L. – 1978 – Aspectos Geotectonicos da Africa Ocidental a Leste do Golfo da Guine com Refrencia as Conexoes Estruturais e Litoloficas Brasil e Africa, XXX Congresso Brasileiro de Geologia.

(19) Ishikawa, H., Sawaguchi, T., Iwaya, S. and Horiuchi, M. – 1976 – Delineation of Prospecting Targets for Kuroko Deposits Based on Modes of Volcanism of Underlying Dacite and Altoration Haloes, Mining Geology, 26, 105-117 (abstract in Japanese)

(20) Meyers, R.E. and MacLean, W.H. – 1983 – The geology of the New Inco copper deposit, Noranda district, Quebec, CAN. J. EARTH SCI., Vol. 20, 1291-1304.

(21) MMAJ – 1985 – Report on Morro Agudo and Palmeirópolis Project, Brasil.

(22) Severin, P.W.A. – 1982 – Geology of the Sturgeon Lake Copper -Zinc- Lead -Silver- Gold Deposit, CIM. Bull., Vol. 75, 107-123.

(23) Suszczynski E. – 1981 – South America, Structural Framework, Chapter 13 of Precambrian of the Southern Hemisphere.

APPENDICES

Photo A–1 Microphotograph of Thin Section

Abbreviations

q, qtz	:	quartz
pl	:	plagioclase
K–f	:	potash felspar
mc	:	microcline
bt	:	biotite
mv	:	muscovite
sc	:	sericite
hb	:	hornblende
gnt	:	garnet
str	:	staurolite

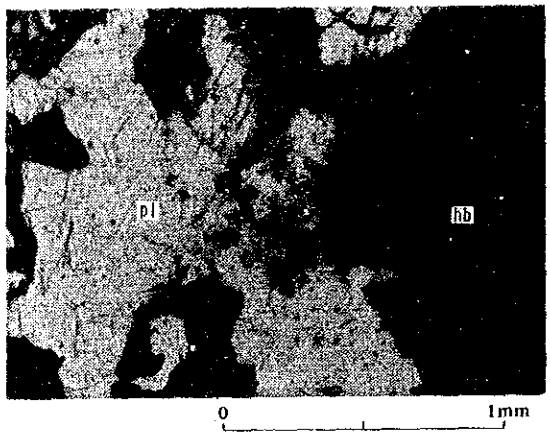

Sample No. : TS0010
Rock name : Coarse amphibolite (Pip_1)
Location : 802.95, 8549.80
Texture : granoblastic

(only lower polar)

(crossed polars)

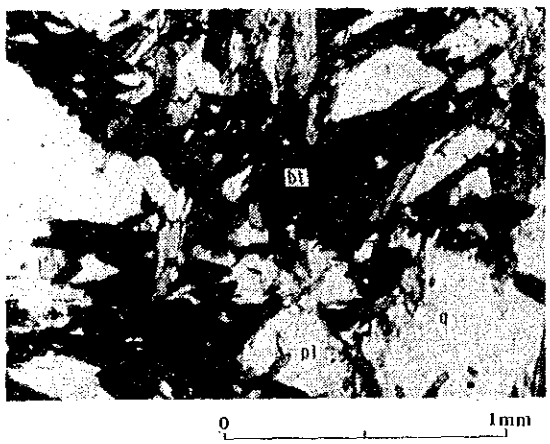

Sample No. : NI0063
Rock name : sc-pl-bt-qtz schist (Pip_2vc)
Location : 803.35, 8533.15
Texture : lepidoblastic

(only lower polar)

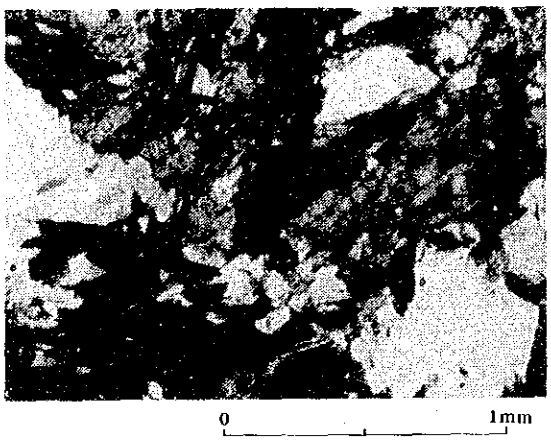

(crossed polars)

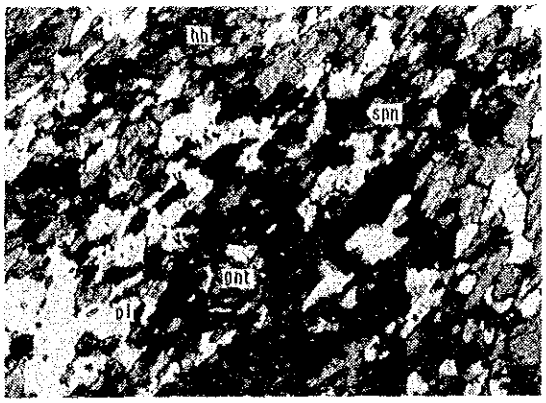

Sample No. : NI0060
Rock name : gnt-amphibole schist (Pip_3)
Location : 798.15, 8539.85
Texture : nematoblastic

(only lower polar)

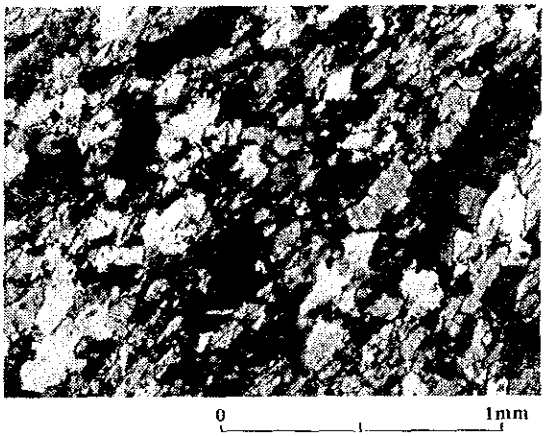

(crossed polars)

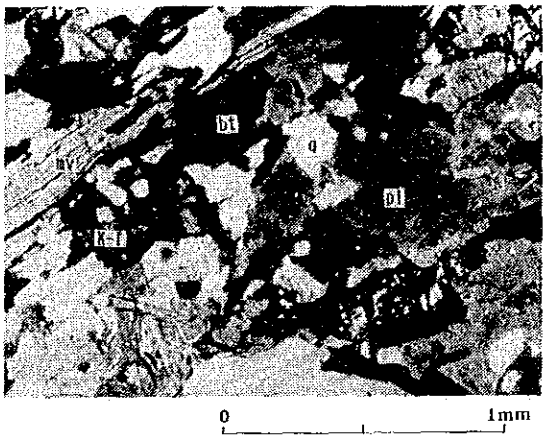

Sample No. : NI0059
Rock name : gnt-pl-mv-bt-qtz schist (Pip_4 vxt_1)
Location : 795.50, 8555.40
Texture : lepidoblastic

(only lower polar)

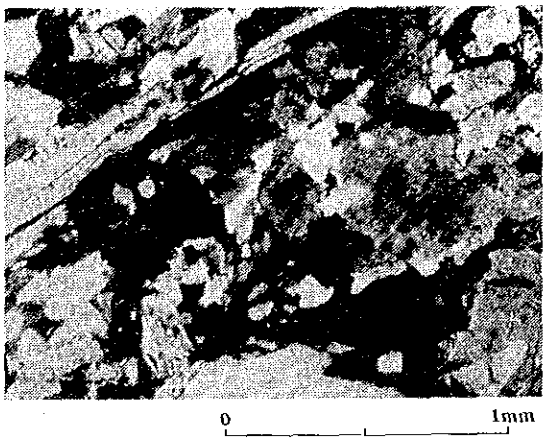

(crossed polars)

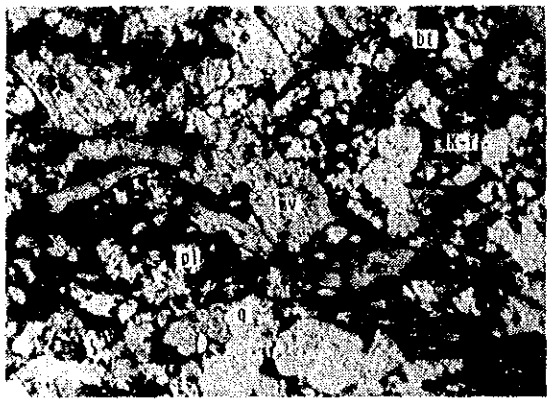

Sample No. : NI0037
Rock name : mc-pl-mv-bt-qtz schist (Pip_4vxt_2)
Location : 792.40, 8547.90
Texture : lepidoblastic

(only lower polar)

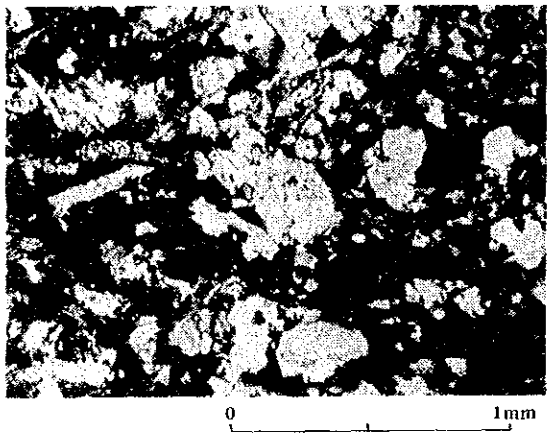

(crossed polars)

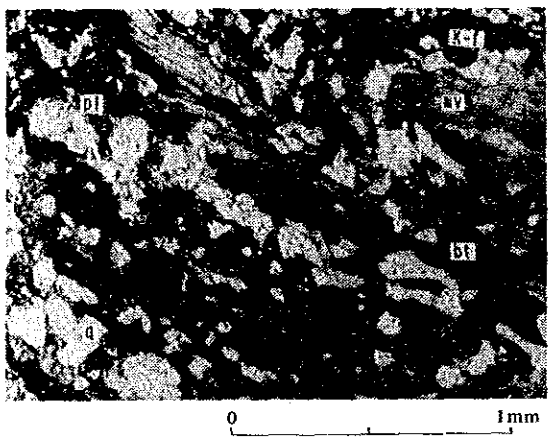

Sample No. : NI0035
Rock name : mc-pl-mv-bt-qtz schist (Pip_4vxt_3)
Location : 792.90, 8549.45
Texture : lepidoblastic

(only lower polar)

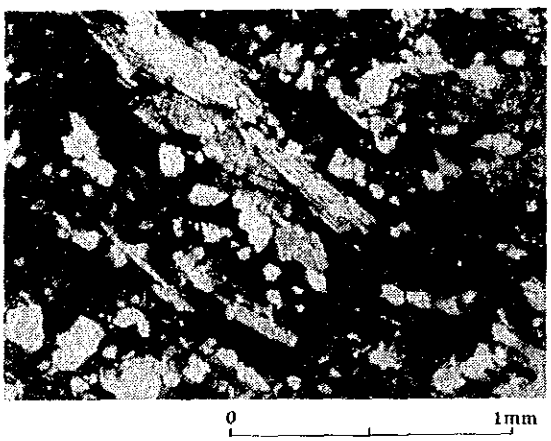

(crossed polars)

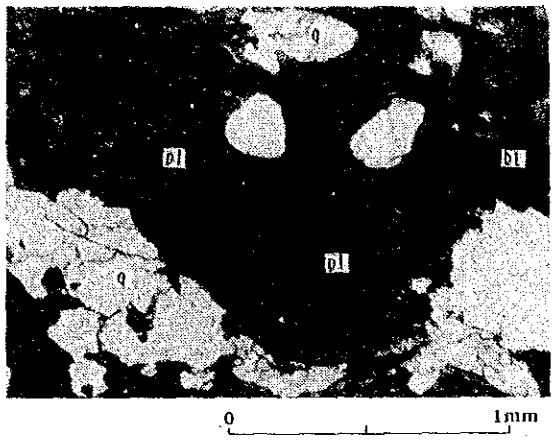

Sample No. : NI0068
Rock name : gnt-bt-pl-qtz schist (Pip_4vs)
Location : 792.70, 8524.85
Texture : lepidoblastic

(only lower polar)

(crossed polars)

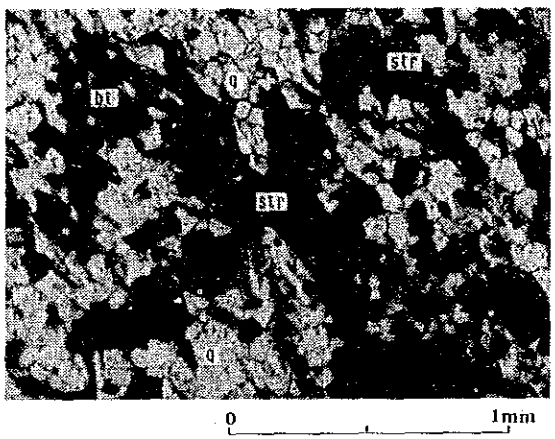

Sample No. : NI0021
Rock name : gnt-str-bt-mv-qtz schist (Pip_5)
Location : 788.55, 8559.50
Texture : lepidoblastic

(only lower polar)

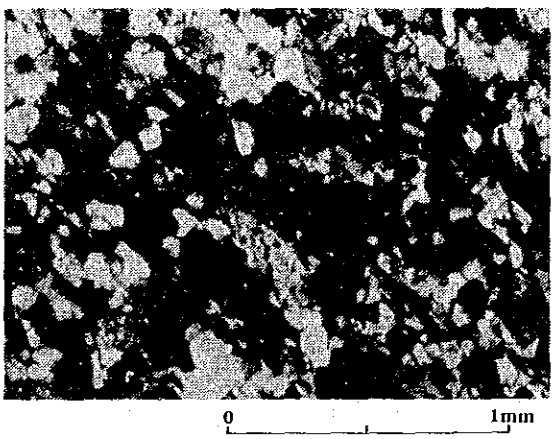

(crossed polars)

Photo A–2 Microphotograph of Polished Section

Abbreviation

sp	:	sphalerite
po	:	pyrrhotite
py	:	pyrite
cp	:	chalcopyrite
gn	:	galena
Ti	:	titanium minerals
g	:	gangue minerals

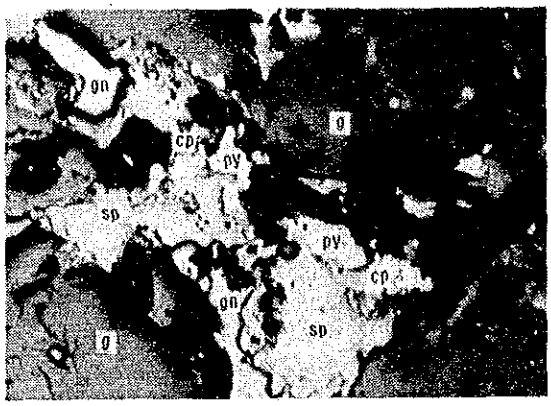

Sample No. : NI0025
Ore name : Sphalerite-pyrite-chalcopyrite ore
Location : Inclined shaft of C-1 ore body, 0.8 – 2.0 m

(only lower polar)

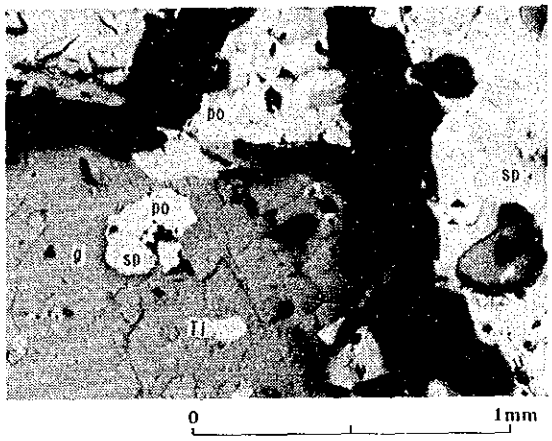

Sample No. : NI0124
Ore name : Sphalerite-pyrrhotite ore
Location : Inclined shaft of C-1 ore body, 3.0 – 4.0 m

(only lower polar)

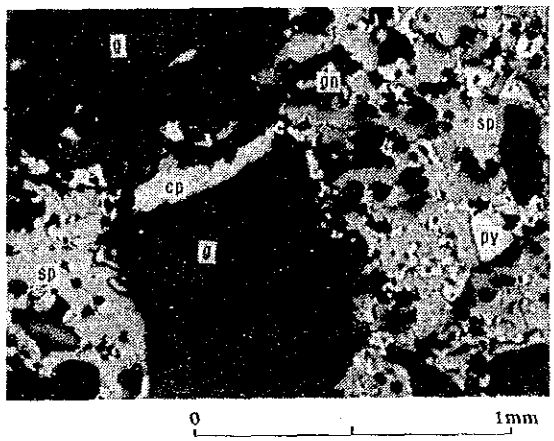

Sample No. : NI0137
Ore name : Sphalerite-pyrite ore
Location : D/D No. PM-68, 40.8 m

(only lower polar)

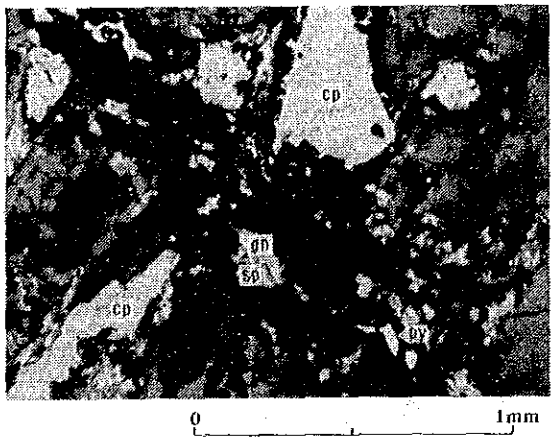

Sample No. : NI0138
Ore name : Chalcopyrite-sphalerite ore
Location : D/D No. PM-68, 41.3 m

(only lower polar)

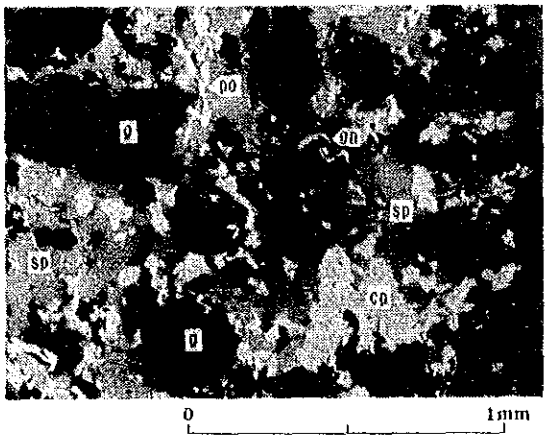

Sample No. : NI0158
Ore name : Sphalerite-chalcopyrite-pyrrhotite ore
Location : D/D No. PM-23, 34.5 m

(only lower polar)

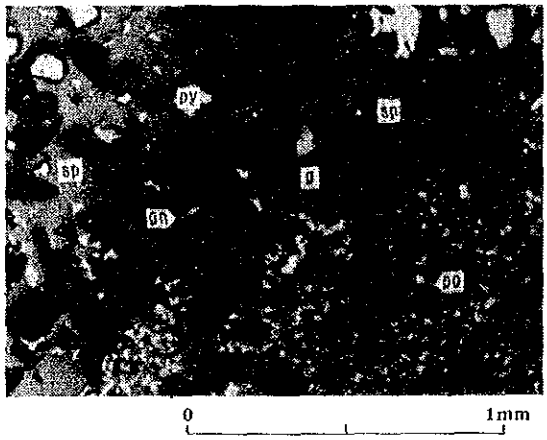

Sample No. : NI0166
Ore name : Sphalerite-pyrrhotite ore
Location : D/D No. PM-93, 56.1 m

(only lower polar)

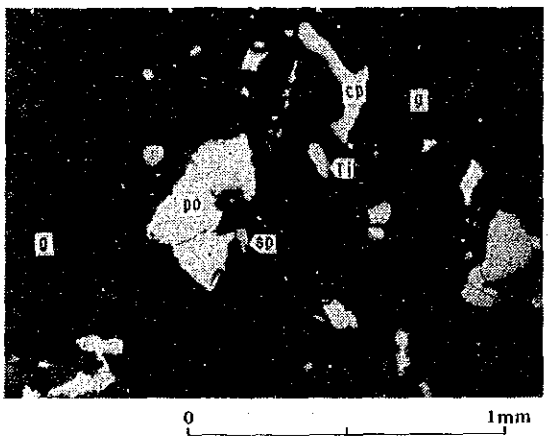

Sample No. : NI0196
Ore name : Pyrrhotite-chalcopyrite ore
Location : D/D No. PM-06, 30.0 m

(only lower polar)

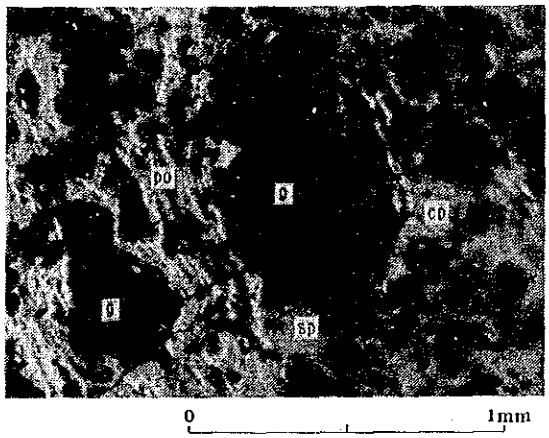

Sample No. : NI0229
Ore name : Sphalerite-pyrrhotite-chalcopyrite ore
Location : D/D No. 17, 73.5 m

(only lower polar)

Table A–1 Microscopic Observations (Thin Section)

No.	Sample No.	Coordinates X	Coordinates Y	Geological Unit	Rock Name	Texture	quartz	plagioclase	K-feldspar	biotite	muscovite	clinopyroxene	orthopyroxene	tremolite	actinolite	hornblende	garnet	opaque mineral	andalusite	staurolite	zircon	sphene	apatite	graphite	sericite	chlorite	zoisite	epidote	carbonate mineral	serpentine	
1	NI0079	798.60	8501.85	Acbsp	sepentinite	acicular-foliated serpentine																								*	serpentine (asbest) vein
2	NI0084	799.35	8501.75	Acbmb	metabasic rock	cataclastic, porphyroblastic																							o		quartz segregation
3	NI0085	795.55	8503.60	Acbmg	hb-opx metagabbro	granoblastic																									
4	TS0010	802.95	8549.80	Pip1	coarse amphibolite	do.																									
5	NI0064	803.20	8533.50	do.	do.	nematoblastic																									plagioclase-clay mineral
6	YT0020	799.10	8556.90	Pip2gv	mv-qtz schist	lepidoblastic																									
7	NI0004	802.50	8553.70	do.	sc-mv-qtz schist	do.																									
8	NI0063	803.35	8533.15	Pip2vc	sc-pl-bt-qtz schist	do. , porphyroblastic																									
9	TS0004	798.25	8550.50	Pip3	fine amphibole schist	nematoblastic																									
10	YT0011	795.85	8560.55	do.	do.	do.																									carbonate (ankerite?)-epidote rock
11	NI0191	PM-24	70.00 m	do.	do.	do.																									
12	NI0060	798.15	8539.85	do.	gnt-amphibole schist	do.																									
13	NI0067	791.25	8524.65	do.	fine amphibole schist	do.																									
14	NI0070	788.15	8526.20	do.	gnt-amphibole schist	do.																									
15	NI0059	795.50	8555.40	Pip4vxt1	gnt-pl-mv-bt-qtz schist	lepidoblastic																									
16	NI0119	inclined shaft	58.85 ~ 60.20 m	do.	gnt-mv-bt-qtz schist	do.																									clay mineral:
17	NI0120	do.	60.20 ~ 61.24 m	do.	gnt-amp sch/gnt-qtz-mv-bt schist	do. , nematoblastic																									
18	NI0188	PM-24	50.05 m	do.	epidote-qtz rock	do. , granoblastic																									altered rock
19	TS0009	794.30	8551.85	Pip4vxt2	pl-mv-bt-qtz schist	do.																									
20	NI0037	792.40	8547.90	do.	mc-pl-mv-bt-qtz schist	do.																									
21	NI0261	PM-52	104.10 m	do.	qtz-pl-amp-bt schist	do.																									
22	NI0035	792.90	8549.45	Pip4vxt3	mc-pl-mv-bt-qtz schist	do																									
23	NI0040	793.00	8549.75	do.	mc-mv-pl-bt-qtz schist	do.																									
24	NI0068	792.70	8524.85	Pip4vs	gnt-bt-pl-qtz schist	do.																									
25	NI0069	790.95	8524.80	do.	mv-bt-qtz schist	do.																									
26	NI0013	788.50	8554.60	Pip5	trm-dp-pl-mc-qtz schist	do.																									impure dolostone?
27	NI0021	788.55	8559.50	do.	(gnt)-str-bt-mv-qtz schist	do.																									
28	NI0030	787.85	8560.65	do.	mv-bt-mgt-qtz schist	do.																									iron formation
29	NI0039	789.30	8547.40	do.	str-sc-mv-qtz schist	do.																									
30	NI0045	785.80	8547.40	Pm1f1	graphite-mv-sc-qtz schist	do.																									
31	NI0001	804.65	8554.75	ct	oc-sc-mv-bt-qtz schist	do. , cataclastic																									
32	YT0025	794.40	8560.35	granite intrusive	bt (gneissose) granite	granoblastic																									
33	NI0032	793.60	8560.40	do.	bt-mv granite	do.																									
34	NI0077	773.95	8501.80	do.	mv-bt granite	do.																									
35	YT0029	788.95	8552.45	basic intrusive	amphibolite	nematoblastic																									

qtz: quartz
pl : plagioclase
oc : orthoclase
mc : microcline
bt : biotite
mv : muscovite
cpx: clinopyroxene
dp : diopside
trm: tremolite
hb : hornblende
amp: amphibole
gnt: garnet
str: staurolite
sc : sericite

* abundant
o common
\- a little
. rare

Table A–2 Microscopic Observations (Polished Section)

No.	Sample No.	Location		Ore Mineral Assemblage	Type	G/S	Minerals					
		No.	Depth (m)				Ti oxide	Pyrite	Pyrrhotite	Chalcopyrite	Sphalerite	Galena
		(Stockpile of ore)										
1	NI0025	drift	0.8 - 2.0	Sp>Py=Cp=Ga>Po	B	≈		o	x	o	*	-
2	NI0026	"	3.0 - 4.0	Py>Cp	B	≫	#	*	x	*	x	x
3	NI0121	"	0.0 - 0.8	Sp>Po=Py>Cp=Ga	B	≫	#	o	o	-	*	-
4	NI0122	"	0.8 - 2.0	Sp≫Py>Po=Cp=Ga	A	>		o	-	-	*	·
5	NI0123	"	2.0 - 3.0	Sp>Cp>Py>Ga>Po	A	≫		o	x	o	*	-
6	NI0124	"	3.0 - 4.0	Sp≫Po≫Ga	A	≫	#	x	o	x	*	-
7	NI0125	"	4.0 - 4.8	Sp≫Po>Ga≫Cp	A	>		x	*	·	*	-
8	NI0126	"	4.8 - 5.6	Sp≫Po>Ga≫Py>Cp	A	>	#	·	*	·	*	-
9	NI0127	"	5.6 - 6.5	Sp=Po>Ga>Py>Cp	B	≈	#	·	*	·	*	-
10	NI0128	"	6.5 - 7.3	Sp=Po≫Ga>Cp=Py	A	>	#	·	*	·	*	-
11	NI0129	"	7.3 - 8.0	Po>Sp≫Ga>Py>Cp	B	>	#	·	*	·	*	-
12	NI0130	"	8.0 - 8.5	Sp>Po>Py>Ga	A	>		-	*	·	*	-
		(Drilling core)										
13	NI0137	PM-68	40.8	Sp>Py>Ga	A	=		o	x	·	*	-
14	NI0138	"	41.3	Cp>Sp>Ga=Py	B	≫	#	-	x	*	o	-
15	NI0154	PM-23	26.0	SP=Py≫Cp=Ga	B	≫	#	*	x	·	*	·
16	NI0155	"	27.0	Sp>Py>Po=Ga	A	>		o	-	x	*	·
17	NI0157	"	32.2	Sp≫Py≫Po>Cp=Ga	B	>		o	·	·	*	·
18	NI0158	"	34.5	Sp>Cp>Po>Py=Ga	A	>		o	-	o	*	-
19	NI0165	PM-93	55.3	Sp>Po≫Py>Ga	A	<		-	*	x	*	-
20	NI0166	"	56.1	Sp>Po>Py=Ga	A	<		-	*	x	*	-
21	NI0184	PN-31	83.7	Sp>Po≫Ga	B	>	#	x	*	·	*	-
22	NI0189	PM-24	57.95	Sp>Po≫Ga	B	≈		x	*	x	*	-
23	NI0196	PM-6	30.0	Po>Cp≫Sp	B	≫	#	x	*	o	·	x
24	NI0198	"	35.0	Sp>Po>Cp≫Ga	B	≫	#	x	o	o	*	·
25	NI0229	PM-17	73.5	Sp>Po>Cp	A	≈		x	o	o	*	·
26	NI0233	"	81.0	Sp>Po≫Ga>Cp	A	≈	#	x	*	-	*	-
27	NI0236	"	89.0	Sp=Cp>Po>Ga	B	>	#	x	o	*	*	-
28	NI0243	"	120.0	Cp>Po≫Sp	B	>	#	x	*	*	-	x

#: Commonly found
*: Major and very abundant
o: Major and abundant
-: Minor but common
·: Very little
x: None or neglegible

G/S: Ratio of gangue and sulfide minerals

Table A--3 Assay Results of Ore

No.	Sample No.	Location		Description	Assay Results				
					g/t Au	g/t Ag	% Cu	% Pb	% Zn
1	NI0022	Coordination X: 786.95, Y: 8557.85		Hm-Lm. gossan	Tr	Tr	0.06	0.09	0.05
2	NI0025	Stockpile of ore; No. drift	Depth (m) 0.8 ~ 2.0 m	Sp > Py = Cp = Ga > Po bre. ore	0.3	74.9	1.03	5.22	22.27
3	NI0026	〃	3.0 ~ 4.0	Py > Cp band.-diss. ore.	0.5	21.5	2.75	0.06	0.16
4	NI0051	Coordination X: 792.85, Y: 8545.75		Hm - Lm gossan	Tr	0.4	0.05	0.08	0.16
5	NI0089	Pit; No. 37	Depth (m) 2.5 ~ 4.5 m	weathered mica-qtz schist	Tr	2.6	0.13	0.16	0.31
6	NI0090	〃	4.5 ~ 7.5	do.	Tr	2.5	0.17	0.09	0.26
7	NI0091	〃	7.5 ~ 10.5	do.	Tr	1.9	0.22	0.08	0.46
8	NI0093	No.19	1.0 ~ 3.0	do.	Tr	2.5	0.44	0.49	1.39
9	NI0094	〃	3.0 ~ 6.0	do.	0.1	4.7	0.54	0.49	0.77
10	NI0095	〃	6.0 ~ 9.0	do.	Tr	2.7	1.13	0.93	1.70
11	NI0096	〃	9.0 ~ 12.0	do.	Tr	4.0	0.95	0.72	1.60
12	NI0097	No.5	3.0 ~ 6.0	weathered amphibolite	Tr	1.2	0.18	0.25	0.52
13	NI0098	〃	6.0 ~ 9.0	do.	Tr	1.0	0.26	0.26	0.77
14	NI0099	〃	9.0 ~ 12.0	do.	Tr	0.9	0.30	0.49	1.19
15	NI0121	Stockpile of ore; No. drift	Depth (m) 0.0 ~ 0.8	Sp > Po = Py > Cp = Ga ore	0.3	49.5	1.30	3.38	13.21
16	NI0122	〃	0.8 ~ 2.0	Sp ≫ Py > Po = Cp = Ga ore	0.4	48.1	2.20	2.62	9.74
17	NI0123	〃	2.0 ~ 3.0	Sp > Cp > Py > Ga > Po ore	0.3	25.3	0.96	1.41	5.58
18	NI0124	〃	3.0 ~ 4.0	Sp ≫ Po ≫ Ga ore	0.5	51.6	1.12	3.28	11.84
19	NI0125	〃	4.0 ~ 4.8	Sp ≫ Po > Ga ≫ Cp ore	0.5	52.2	1.02	3.85	13.84
20	NI0126	〃	4.8 ~ 5.6	Sp ≫ Po > Ga ≫ Py > Cp ore	0.4	37.6	1.71	2.81	7.05
21	NI0127	〃	5.6 ~ 6.5	Sp = Po > Ga > Py > Cp ore	0.3	43.6	1.33	2.81	12.05
22	NI0128	〃	6.5 ~ 7.3	Sp = Po ≫ Ga > Cp = Py ore	0.4	48.3	1.44	3.47	12.58
23	NI0129	〃	7.3 ~ 8.0	Po > Sp ≫ Ga > Py > Cp ore	0.5	42.7	2.04	2.29	7.58
24	NI0130	〃	8.0 ~ 8.5	Sp > Po > Py > Ga ore	0.2	30.5	0.85	2.14	9.37
25	NI0136	Drilling core; No. PM-68	Depth (m) 40.1 ~ 40.13	diss. ore	Tr	1.4	0.18	0.08	0.11
26	NI0137	〃	40.8 ~ 41.1	Sp > Py > Ga msv. ore	0.4	79.1	0.14	5.89	21.95
27	NI0138	〃	41.3 ~ 41.4	Cp > Sp > Ga = Py diss. ore	0.2	38.3	0.36	2.02	3.32
28	NI0154	PM-23	26.0 ~ 26.5	Sp = Py ≫ Cp = Ga bre. msv. ore	0.4	29.0	0.28	2.25	10.74
29	NI0155	〃	27.0 ~ 27.3	Sp > Py > Po = Ga do.	0.5	39.4	0.53	2.61	11.48
30	NI0157	〃	32.20 ~ 32.40	Sp ≫ Py ≫ Po > Cp = Ga msv. ore	0.3	25.5	0.49	1.83	8.74
31	NI0158	〃	34.5 ~ 35.4	Sp > Cp > Po > Py = Ga bre. msv. ore	0.3	52.2	1.71	2.71	9.64
32	NI0165	PM-93	55.3 ~ 55.7	Sp > Po ≫ Py > Ga msv. ore	0.4	94.1	0.08	7.07	24.00
33	NI0166	〃	56.1 ~ 56.2	Sp > Po > Py = Ga do.	0.6	87.0	0.39	5.52	18.95
34	NI0184	PM-31	83.7 ~ 83.9	Sp > Po ≫ Ga diss. ore	Tr	3.0	0.75	0.08	1.16
35	NI0189	PM-24	57.95 ~ 58.15	Sp > Po ≫ Ga msv. ore	0.6	26.4	0.13	0.73	15.90
36	NI0190	〃	59.4 ~ 59.6	diss. ore	0.6	94.6	0.24	1.56	4.32
37	NI0196	PM-6	30.0 ~ 30.05	Po > Cp ≫ Sp diss. ore	0.1	2.9	0.42	0.18	0.32
38	NI0197	〃	32.7 ~ 32.8	diss. ore	0.5	70.7	0.36	2.54	8.63
39	NI0198	〃	35.0 ~ 35.05	Sp > Po > Cp ≫ Ga msv. ore	0.1	15.5	0.22	0.90	1.68
40	NI0199	〃	37.5 ~ 37.6	diss. ore	0.1	5.4	1.07	0.24	1.53
41	NI0200	〃	40.0 ~ 40.05	do.	Tr	4.4	0.69	0.09	0.16
42	NI0223	PM-17	47.5 ~ 47.6	do.	0.1	8.7	0.33	0.32	2.32
43	NI0224	〃	50.2 ~ 50.3	do.	0.1	11.7	0.22	0.16	1.21
44	NI0225	〃	52.5 ~ 52.6	do.	0.4	11.8	0.97	0.16	0.84
45	NI0229	〃	73.5 ~ 73.6	Sp > Po > Cp diss. ore	0.4	105.1	0.25	6.84	25.00
46	NI0232	〃	79.0 ~ 80.0	diss. ore	0.3	27.3	0.59	1.83	2.95
47	NI0233	〃	80.0 ~ 81.0	Sp > Po ≫ Ga > Cp msv. ore	0.3	52.8	2.34	2.61	7.26
48	NI0235	〃	87.0 ~ 88.0	msv. ore	0.4	26.0	0.51	1.89	4.26
49	NI0236	〃	88.0 ~ 89.0	Sp = Cp > Po > Ga msv. ore	0.4	44.3	0.88	2.43	10.53
50	NI0237	〃	89.0 ~ 90.0	diss. ore	0.5	27.3	0.62	1.27	6.84
51	NI0243	〃	114.50 ~ 123.30	Cp > Po ≫ Sp diss. ore	0.1	4.3	0.37	0.17	0.26
52	NI0244	〃	123.3 ~ 124.5	diss. ore	Tr	1.1	0.06	0.16	0.21
53	NI0260	PM-52	81.7 ~ 82.05	msv. ore	0.4	28.2	0.08	0.68	4.84
54	TS0014	Coordination X: 794.95, Y: 8543.50		Hm - Lm gossan	Tr	0.6	0.07	0.07	0.05

Abbreviation

Py: Pyrite
Po: Pyrrhotite
Cp: Chalcopyrite
Sp: Sphalerite
Ga: Galena
Hm: Hematite
Lm: Limonite
msv.: massive
diss. : disseminated
bre. : brecciated
band.: banded

Table A–4 Results of X-ray Diffractive Analysis

(1)

No.	Sample No.	Coordination X	Coordination Y	Rock Name		quartz	plagioclase	k-feldspar	hornblende	tremolite	actinolite	edenite	anthophyllite	gedrite	epidote	muscovite	biotite	calcite	chlorite	kaolinite	gibbsite	goethite	pyrite	majorite	Remarks
1	NI0001	804.65	8554.75	oc-sc-mv-bt-qtz schist	Ct	29.5	9.5									3.9	3.9								
2	NI0002	803.30	8554.15	gnt-pl-bt schist	P_3	16.4	3.8								2.1	6.3									
3	NI0004	802.50	8553.70	sc-mv-qtz schist	P_3	35.1										3.6			3.1						
4	NI0006	800.95	8554.30	gnt-qtz schist	P_2	30.3										4.6			6.0						
5	NI0007	800.25	8554.10	gabbro	P_1	6.7	1.5		6.3	6.3									1.3						
6	NI0008	795.55	8552.65	mica-qtz schist	P_4	36.4										5.0				1.1	1.4				
7	NI0009	795.70	8552.65	amphibolite	P_3	0.7	6.0		6.4	6.4															
8	NI0011	792.80	8553.20	amphibolite	P_3	-	8.3		6.4	6.4															
9	NI0015	803.10	8548.30	volcaniclastics	P_2vc	39.6										2.2				1.0					
10	NI0016	795.85	8545.60	gnt-mica-qtz schist	P_4	23.9										4.8				1.1					
11	NI0017	794.70	8548.25	bt-qtz schist	P_4	26.0	9.4	8.0								8.3		0.7							
12	NI0018	791.25	8549.20	str-mica-qtz schist	P_5	11.7										12.6			0.7	0.7					
13	NI0019	788.30	8559.55	graphite schist	Pm_1fl	44.3	1.0									8.4									
14	NI0021	788.55	8559.50	str-gnt-bt-mv-qtz schist	P_5	22.0										3.9									staurolite (2.9)
15	NI0029	787.20	8561.20	sc-qtz schist	P_5	27.1										8.5					0.5				staurolite (0.5)
16	NI0033	793.40	8561.10	amphibolite	P_3	6.3	7.3		6.4	6.4															
17	NI0035	792.90	8549.45	mc-pl-mv-bt-qtz schist	P_4	25.2	4.9	6.6								5.3	5.3			20.4					
18	NI0036	792.45	8548.70	amphibolite	P_3		4.7		4.2	4.2	2.9							0.5							
19	NI0037	792.40	8547.90	mc-pl-mv-bt-qtz schist	P_4	35.9	8.8	2.9								2.7	2.7	0.7							
20	NI0038	792.60	8547.50	feld-mv-qtz schist	P_4s	22.8	11.9									3.2	3.2								
21	NI0039	789.30	8547.40	ser-mv-qtz schist	P_5	28.0										5.0				0.5	1.0				
22	NI0040	793.00	8549.75	mc-mv-pl-bt-qtz schist	P_4	29.5	11.3	9.7								5.3	5.3	1.0							
23	NI0041	794.65	8547.15	amphibolite	P_3	1.3	4.6	1.7	4.2	4.2	2.9							0.5							
24	NI0043	785.80	8547.95	graphy. phyllite	Pm_1fl	58.3										7.0									
25	NI0045	785.80	8547.40	graphite-mv-sc-qtz schist	Pm_1fl	30.3										10.5				1.1					
26	NI0046	790.55	8544.60	gnt-mv-qtz schist	P_5	11.6										12.7				2.1	2.8				
27	NI0048	790.10	8543.40	mv-qtz schist	P_5	28.8										6.0				1.8	3.4				staurolite (0.8)
28	NI0049	794.35	8547.85	mv-qtz schist	P_4	34.0	13.3	4.5								3.9	3.9								
29	NI0050	793.80	8547.75	amphibolite	P_3				4.2	4.2	1.8														
30	NI0052	791.80	8545.30	mv-qtz schist	P_5											6.7				1.1	1.1				
31	NI0053	794.10	8547.30	amphibolite	P_3	0.7	10.5		4.3	4.3	2.5														
32	NI0054	793.70	8549.15	feld-mica-qtz schist	P_4	32.7										7.1				1.1	2.9				
33	NI0056	794.75	8554.90	amphibolite	P_3	5.9	6.0		4.3	4.3	2.7														
34	NI0058	795.50	8555.40	amphibolite	P_3	6.9	4.5		4.3	4.3	1.8														
35	NI0059	795.50	8555.40	gnt-pl-mv-bt-qtz schist	P_4	26.0	13.3	8.1								6.3	6.3								

(2)

No.	Sample No.	Coordination		Rock Name		quartz	plagioclase	k-feldspare	hornblende	tremolite	actinolite	edenite	anthophyllite	gedrite	epidote	muscovite	biotite	calcite	chlorite	kaolinite	gibbsite	goethite	pyrite	majorite	Remarks
		X	Y																						
36	NI0060	798.15	8539.85	amphibolite	P_3	3.1	8.8	2.1	6.4	6.4															
37	NI0061	802.80	8537.45	gabbro	db		10.9			10.5									0.7						
38	NI0062	803.40	8534.90	gnt-mv-qtz schist	P_2	23.6										6.2				2.2					
39	NI0063	803.35	8533.15	gnt-sc-pl-bt-qtz schist	P_2	9.9	3.9									12.9			1.5						
40	NI0064	803.20	8533.50	amphibolite	P_1	2.4	7.1		4.3	4.3	2.4								3.6						
41	NI0065	783.35	8532.15	amphibolite	db	5.0	6.4		6.4	6.4									0.7						
42	NI0067	791.25	8524.65	amphibolite	P_3		5.0		3.6	3.6															
43	NI0068	792.70	8524.85	bt-mc-pl-qtz schist	P_4	26.7	11.2										12.7								
44	NI0069	790.95	8524.80	bt-mc-pl-qtz schist	P_4	27.1														2.9	5.6	0.8			
45	NI0070	788.15	8526.20	amphibolite	P_3	9.7			4.2	4.2	2.7														
46	TS0001	794.10	8554.00	pl-bt-qtz schist	P_4	31.9											12.7		0.5						
47	TS0002	794.20	8554.50	pl-bt-qtz schist	P_4	27.6											3.9			4.1	1.1				
48	TS0004	798.25	8550.50	amphibolite	P_3	0.7	7.0		6.4	6.4															
49	TS0006	797.35	8554.20	amphibolite	P_3		9.8		6.4	6.4									0.4						
50	TS0007	794.55	8555.20	gnt-bt-qtz schist	P_4	49.0										6.0	6.0								serpentine (8.0)
51	TS0008	794.25	8553.60	gnt-feld-bt-qtz schist	P_4	27.1	9.5	8.8								2.7			2.8						
52	TS0009	794.30	8551.85	pl-mv-bt-qtz schist	P_4	28.0	15.5									6.3	6.3								
53	TS0010	802.95	8549.80	amphibolite	P_1	2.8	12.2									6.4	6.4	0.7							
54	TS0011	796.75	8547.55	amphibolite	P_3	2.1	3.6									6.4	6.4	0.7							
55	TS0012	802.80	8543.30	mica schist	P_4	35.9										2.9				1.7	3.5				
56	TS0013	795.20	8543.55	mica-qtz schist	P_4	1.3	2.8									12.7									
57	YT0007	795.27	8559.28	amphibolite	P_3		11.5		6.4	6.4					1.0				0.4						
58	YT0010	785.75	8560.30	amphibolite	P_3	6.3	5.0		6.4	6.4															
59	YT0011	795.86	8560.53	amphibolite	P_3		5.9			11.9					1.4										
60	YT0018	797.75	8556.91	amphibolite	P_1		7.3		6.4	6.4									0.7						
61	YT0020	799.12	8556.88	mica-qtz schist	P_2	18.3	0.8									9.2				1.7	1.7				
62	YT0024	794.78	8557.43	amphibolite	P_3		4.6		4.6	4.6															
63	YT0031	787.20	8552.60	qtz-mica schist	P_5	22.8	1.7	1.8								12.6				2.1	2.5				
64	YT0032	789.00	8554.03	mica-qtz schist	P_5	20.0	1.4	1.8								12.6				0.8					
65	YT0033	792.16	8554.20	gnt-str-mica-qtz schist	P_5	29.5	1.3	1.3								7.0				1.4	3.8				
66	YT0036	785.46	8552.68	gnt-qtz-mica schist	P_5	13.6	2.1	3.1								12.9				1.0	2.7				
67	YT0039	803.45	8545.62	amphibolite	P_1				6.4	6.4						0.7			2.8						
68	YT0040	803.70	8543.02	amphibolite	P_3	1.4	4.9		6.4	6.4									0.8						
69	YT0041	800.38	8543.36	amphibolite	P_3		11.2		6.4	6.4									1.4						

No.	Sample No.	Pit and inclined shaft	Depth (m)	Rock Name	quartz	plagioclase	k-feldspar	hornblende	tremolite	actinolite	edenite	anthophyllite	gedrite	epidote	muscovite	biotite	calcite	chlorite	kaolinite	gibbsite	goethite	pyrite	majorite	Remarks
		(pit)																						
1	NI0089	37	2.5 ~ 4.5	mica-qtz schist	9.9		1.0								1.0				1.4		0.7			
2	NI0090	37	4.5 ~ 7.5	mica-qtz schist	13.1										1.1				1.1		0.7			
3	NI0091	37	7.5 ~ 10.5	mica-qtz schist	18.0										0.7				2.0		0.8			
4	NI0092	37	7.8	clay mineral	12.7										0.7				3.2					bassanite (2.8)
5	NI0093	19	1.0 ~ 3.0	mica-qtz schist	11.0														1.8					
6	NI0094	19	3.0 ~ 6.0	mica-qtz schist	13.6																2.4			
7	NI0095	19	6.0 ~ 9.0	mica-qtz schist	10.5														1.1		1.8			jarosite (0.5) brookite (1.7)
8	NI0096	19	9.0 ~ 12.0	mica-qtz schist	20.8														0.7		0.4			jarosite (0.5)
9	NI0097	5	3.0 ~ 6.0	amphibolite ?	4.2														1.1					
10	NI0098	5	6.0 ~ 9.0	amphibolite ?	3.2														1.0					
11	NI0099	5	9.0 ~ 12.0	amphibolite ?	2.5														1.0					
		(inclined shaft)																						
12	NI0100		40.8 ~ 41.6	gnt-qtz-bt schist	12.4	3.2										12.4		1.5				1.0		
13	NI0101		41.6 ~ 42.4	gnt-qtz-bt schist	25.2	9.0		0.7								10.8		0.4						staurolite (0.5)
14	NI0102		42.4 ~ 43.5	gnt-qtz-bt schist	18.3	10.8	3.4	3.6								3.6		0.4						staurolite (0.8)
15	NI0103		43.5 ~ 44.2	gnt-qtz-bt schist	24.8	9.2		1.5								7.1		2.1						staurolite (1.1)
16	NI0104		44.2 ~ 45.3	amphibolite		4.9		4.2	4.2	1.3						12.4		3.2						talc (1.8)
17	NI0105	1	45.3 ~ 46.0	amphibolite	21.5	13.1		1.4								12.3		8.0				1.5		basaluminite (5.6)
18	NI0106	2	46.0 ~ 46.85	amphibolite		9.0		0.5								12.4		4.2				3.5		basaluminite (2.5) siderite (5.3)
19	NI0107	3	46.85 ~ 47.5	amphibolite		13.1		1.7								12.6		3.9				2.1		basaluminite (4.6)
20	NI0108	4	47.5 ~ 48.24	amphibolite	1.3	9.5					13.0					12.4		1.4						basaluminite (5.2) siderite (0.5)
21	NI0109	5	48.24 ~ 48.9	amphibolite	4.1	13.1					3.8					6.4		1.0						
22	NI0110	6	48.9 ~ 49.8	amphibolite gnt-amp-bt bt-amp gnt-bt-qtz schist	12.4	2.4					2.4					12.6		0.5						
23	NI0111	7	49.8 ~ 50.7	gnt-amp-bt bt-amp gnt-bt-qtz schist	13.1						2.8					12.4		1.8						
24	NI0112	8	50.7 ~ 52.0	amphibolite	11.2	3.2		1.4	1.4							12.6		3.4						
25	NI0113	9	52.0 ~ 52.9	gnt-amp-bt bt-amp gnt-bt-qtz schist	2.0			6.3	6.3							12.6		1.0						
26	NI0114	10	52.9 ~ 54.4	gnt-amp-bt bt-amp gnt-bt-qtz schist	46.6	3.9										2.2		0.8					2.5	
27	NI0115	11	54.4 ~ 55.9	gnt-amp-bt bt-amp gnt-bt-qtz schist	15.9	4.3		1.5	1.5							12.3		0.5					3.9	
28	NI0116	12	55.9 ~ 56.5	gnt-amp-bt bt-amp gnt-bt-qtz schist	31.2	4.8		0.3								6.2		0.8					3.2	
29	NI0117	13	56.5 ~ 57.5	gnt-amp-bt bt-amp gnt-bt-qtz schist	23.9	4.8			1.5							12.9		3.9						
30	NI0118	14	57.5 ~ 58.85	amphibolite	51.3											1.0		3.6					1.4	
31	NI0119	15	58.85 ~ 60.2	gnt-amp-bt bt-amp gnt-bt-qtz schist	32.0	3.9										8.5		0.3					1.3	
32	NI0120	16	60.2 ~ 61.24	gnt-amp-bt bt-amp gnt-bt-qtz schist	2.0			2.1	2.1							3.4		2.0					4.8	

No.	Sample No.	Drill hole No.	Depth (m)	Rock Name		quartz	plagioclase	k-feldspar	hornblende	tremolite	actinolite	odenite	anthophyllite	gedrite	epidote	muscovite	biotite	calcite	chlorite	kaolinite	gibbsite	goethite	pyrite	majorite	Remarks
1	NI0131	(10N) PM-18	40.0	amphibolite	P_3		13.4		5.9	5.9									0.5						
2	NI0132	"	60.0	amphibolite	P_3	5.3	11.2		6.4	6.4							13.0		1.4						
3	NI0133	"	80.0	amphibolite	"	2.1	6.6		6.4	6.4									1.5						
4	NI0134	PM-68	25.0	amphibolite	"		2.1		4.6	4.6									0.8						montmorillonite (1.3)
5	NI0135	"	35.0	amphibolite	"	3.2	5.9		6.4	6.4									0.4						
6	NI0139	"	45.0	gnt-bt-qtz schist	P_4	13.1			5.3								12.6		3.2						diopsite (0.8)
7	NI0140	"	50.0	gnt-bt-qtz schist	"	35.1	1.7		0.3								11.6		0.5					3.2	
8	NI0141	"	55.0	gnt-bt-qtz schist	"	46.6	0.8										9.1							1.1	
9	NI0142	"	60.0	gnt-bt-qtz schist	"	23.1	2.2		0.7								12.6		0.8					5.2	
10	NI0143	"	65.0	amphibolite	P_3	1.4	1.8		6.4	6.4							0.7	13.4	1.0						
11	NI0144	PM-26	40.0	amphibolite	"		9.5		6.4	6.4								7.0	1.0						
12	NI0145	"	60.0	amphibolite	"	4.8	11.7		6.3	6.3								10.9	0.5						
13	NI0146	"	80.0	amphibolite	"	2.4	7.4		6.4	6.4								1.8	0.4						
14	NI0147	"	100.0	amphibolite	"		9.4		6.4	6.4								8.0	1.0						
15	NI0148	(10S) PM-29	40.0	amphibolite	"		13.4		6.4	6.4					3.2			0.8	1.4						
16	NI0149	"	60.0	amphibolite	"	17.5	16.9		4.5	4.5					1.8			1.1	0.5						
17	NI0150	"	80.0	amphibolite	"	8.8	10.2		4.9	4.9								12.3	1.7						
18	NI0151	"	100.0	amphibolite	"	1.3	8.7		6.4	6.4								3.1							
19	NI0152	PM-23	22.0	amp-bt schist	P_4	35.9	5.0										3.8		1.4						
20	NI0153	"	25.0	amp-bt schist	"	1.5	16.8		2.4	2.4							12.7		1.1						
21	NI0156	"	30.0	amphibolite	P_3	10.2			3.9	3.9					3.1										
22	NI0159	"	40.0	gnt-amp-bt schist	P_4	18.0			6.4	6.4					1.3		2.5		0.8						
23	NI0160	"	45.0	gnt-amp-bt schist	"	50.1	1.0										2.8							4.2	analcime (2.9)
24	NI0161	"	50.0	amphibolite	P_3	23.9	13.3										1.0	3.2							nesquehonite (2.2)
25	NI0162	"	60.0	amphibolite	"	10.8	13.3		2.4	2.4							6.3		1.1						
26	NI0163	PM-93	35.0	amphibolite	"		2.5		6.6	6.6					2.2			2.5	0.8						
27	NI0164	"	45.0	amphibolite	"	2.4	11.7		6.4	6.4							1.7								
28	NI0167	"	65.0	amphibolite	"	5.6	8.5		6.4	6.4							0.4		1.3						
29	NI0168	"	75.0	amphibolite	"		10.3		6.4	6.4								2.5							
30	NI0169	PM-27	40.0	amphibolite	"		9.7		6.4	6.4							3.2		0.5						
31	NI0170	"	60.0	amphibolite	"	1.3	12.9		6.4	6.4								13.4	0.4						
32	NI0171	"	80.0	amphibolite	"	5.5	11.5		6.4	6.4								7.6							
33	NI0172	(30S) PM-34	50.0	str-gnt-bt-qtz schist	P_3				3.1								9.1		11.9						
34	NI0173	"	60.0	str-gnt-bt-qtz schist	"	29.5	5.7										12.6		0.7						
35	NI0174	"	70.0	str-gnt-bt-qtz schist	"	24.3	6.7		0.7								12.6								brookite (0.4)

(5)

No.	Sample No.	Drill hole No.	Depth (m)	Rock Name		quarz	plagioclase	k-feldspar	hornblende	tremolite	actinolite	edenite	anthophyllite	gedrite	epidote	muscovite	biotite	calcite	chlorite	kaolinite	gibbsite	goethite	pyrite	majorite	Remarks
36	NI0175	(30S) PM-34	80.0	str-gnt-bt-qtz schist	P_4	46.6	5.3		0.5								6.3		0.4					2.0	
37	NI0176	"	90.0	str-gnt-bt-qtz schist	P_4	16.4											12.4		1.5					2.8	
38	NI0177	"	102.2	amphibolite	P_3	17.2	1.5		1.1								9.8		2.4					8.7	hydrocalcite (1.3)
39	NI0178	"	120.0	amphibolite	"	0.7	8.0		6.4	6.4															
40	NI0179	PM-31	50.0	str-gnt-bt-qtz schist	P_4	62.9											2.7		2.0					1.0	
41	NI0180	"	60.0	str-gnt-bt-qtz schist	"	19.6											12.6	0.4	1.5					4.3	ilmenite (1.7)
42	NI0181	"	70.0	str-gnt-bt-qtz schist	"	6.3			0.7								11.7		6.4					2.5	
43	NI0182	"	75.0	str-gnt-bt-qtz schist	"	11.6	1.3										12.6		13.1						
44	NI0183	"	80.0	str-gnt-bt-qtz schist	"	23.1								1.7			12.6		0.8						
45	NI0185	"	90.0	amphibolite	P_3		12.2		6.4	6.4									0.5						
46	NI0186	PM-24	40.1	gnt-amp-bt schist	P_4	1.7			6.4	6.4				2.8					5.3						
47	NI0187	"	45.1	gnt-amp-bt schist	"	4.5				2.4				7.0			0.7		2.4						
48	NI0188	"	50.05	gnt-amp-bt schist	"	7.6	11.0		5.3	5.3					1.1		1.1		3.1						
49	NI0191	"	70.0	amphibolite	P_3	2.2	13.4		6.4	6.4									0.7						
50	NI0192	"	80.0	amphibolite	"		13.4		5.3	5.3					1.4		0.7	4.5	3.1						
51	NI0193	"	90.1	amphibolite	"	3.2	9.4		6.4	6.4									0.7						
52	NI0194	"	100.0	amphibolite	"		7.3		6.4	6.4									0.7						
53	NI0195	"	110.4	amphibolite	"	1.0	13.4		6.4	6.4								2.9	0.5						
54	NI0201	PM-6	43.0	gnt-amp-bt schist	P_4	14.4								4.5			6.2		1.8						
55	NI0202	"	50.0	amphibolite	P_3		9.2		6.4	6.4															
56	NI0203	"	60.0	amphibolite	"		9.2		6.4	6.4					1.3			5.6	0.4						
57	NI0204	"	70.0	amphibolite	"	1.1	5.9		5.6	5.6					2.2			9.0							
58	NI0205	"	80.0	amphibolite	"	1.4	6.6		6.4	6.4								4.2	0.7						
59	NI0206	"	100.0	amphibolite	"		17.9		6.4	6.4								1.7	0.4						
60	NI0207	PM-19	50.0	amphibolite	"		8.8		6.4	6.4					1.3			13.8	0.8						
61	NI0208	"	70.0	amphibolite	"		10.3			13.4	0.5				4.4			6.0	1.0						
62	NI0209	"	90.0	amphibolite	"	1.7			4.6	4.6					1.8			4.3							
63	NI0210	(50S) PM-33	50.0	gnt-bt-qtz schist	P_4	15.2	3.5		3.8								12.2		3.1						
64	NI0211	"	70.0	gnt-amp-bt schist	"	20.0	1.5							6.4			12.9		1.4					2.7	
65	NI0212	"	90.0	gnt-amp-bt schist	"	15.2								4.2			3.6		0.7					5.6	
66	NI0213	"	110.0	gnt-bt-qtz schist	"	27.1											12.9		1.1						
67	NI0214	PM-20	30.0	amphibolite in schist	"	12.9	1.8		6.6	6.7					1.3		1.3		1.1						
68	NI0215	"	40.0	str-amp-bt schist	"	19.6											12.7			1.1					nacrite ? (0.5)
69	NI0216	"	50.0	str-amp-bt schist	"	34.8			0.5								12.9		1.3						
70	NI0217	"	60.0	str-amp-bt schist	"	25.2	4.8										12.7		1.8					2.1	

(6)

No.	Sample No.	Drill hole No.	Depth (m)	Rock Name		quartz	plagioclase	k-feldspar	hornblende	tremolite	actinolite	edenite	anthophyllite	gedrite	epidote	muscovite	biotite	calcite	chlorite	kaolinite	gibbsite	goethite	phyrite	majorite	Remarks
71	NI0218	(50S) PM-20	70.0	str-amp-bt schist	P_4	38.3	8.8									5.3	5.3		1.3						
72	NI0219	"	80.0	str-amp-bt schist	P_4	18.7										10.6	10.6		0.8					5.3	
73	NI0220	"	90.0	str-amp-bt schist	"	29.9	3.2									12.7	12.7		1.0	1.0					
74	NI0221	PM-17	30.2	amphibolite	P_3	65.3											0.7	3.6					1.1		
75	NI0222	"	40.0	amphibolite	"	0.8			6.3	6.3								8.3							
76	NI0226	"	60.0	gnt-amp-bt schist	P_4	12.7				3.8					6.3	6.3	6.3						1.8		
77	NI0227	"	64.0	gnt-amp-bt schist	"	62.9	6.2		0.8						3.5				1.4						
78	NI0228	"	68.0	gnt-amp-bt schist	"	3.2	2.2		1.4							12.6	12.6		2.4				0.8		
79	NI0230	"	74.0	gnt-amp-bt schist	"	14.0										12.7	12.7		1.3					3.9	
80	NI0231	"	78.0	gnt-amp-bt schist	"	4.3										12.7	12.7		0.7					2.9	alunite (1.3)
81	NI0234	"	84.0	amphibolite	P_3	23.9	1.5			3.1							0.7								
82	NI0238	"	95.0	str-amp-bt schist	P_4	23.6	1.0									12.7	12.7		0.4						
83	NI0239	"	100.0	str-amp-bt schist	"	3.6							8.8			11.9	11.9		2.9					2.4	
84	NI0240	"	105.0	str-amp-bt schist	"	25.2	3.2						2.5				1.0		0.8					1.3	
85	NI0241	"	110.0	str-amp-bt schist	"								8.0			5.0	5.0		1.3					2.0	
86	NI0242	"	115.0	str-amp-bt schist	"	4.8							7.1			12.7	12.7		1.1						
87	NI0245	"	125.0	gnt-amp-bt schist	"	20.4							4.5				2.2		1.0					1.5	
88	NI0246	"	130.0	gnt-amp-bt schist	"	15.5	4.6									12.7	12.7		1.5					1.0	
89	NI0247	"	135.0	gnt-amp-bt schist	"	4.8	5.6						10.6				2.2		0.8					2.4	
90	NI0248	"	140.0	amphibolite	P_3		11.2		6.4	6.4									1.1						
91	NI0249	"	145.0	gnt-amp-bt schist	P_4	6.4	7.8			3.2						13.0	13.0		0.7						
92	NI0250	PM-25	50.0	amphibolite	P_3		9.0		6.4	6.4								12.9	1.5						
93	NI0251	"	60.0	amphibolite	"	2.4	8.3		6.6	6.6							1.4		2.2						
94	NI0252	"	70.0	amphibolite	"	0.8	12.2		6.6	6.6							0.4		0.7						
95	NI0253	"	80.0	amphibolite	"	0.4	13.6		6.6	6.6								0.7	4.8						
96	NI0254	"	90.0	amphibolite	"	4.3	12.2		4.8	4.8								13.6	0.8						
97	NI0255	"	100.0	amphibolite	"		9.8		6.2	6.2							0.4	7.0	1.1						
98	NI0256	"	110.0	amphibolite	"	1.4	8.1		6.6	6.6								9.4	0.5						
99	NI0257	"	120.0	amphibolite	"		8.8		6.6	6.6									1.1						
100	NI0258	"	130.0	amphibolite	"	1.7	7.6		6.4	6.4					1.3			8.0	0.4						
101	NI0259	"	140.0	amphibolite	"		4.9		6.6	6.6								2.4	0.7						
102	NI0261	(10P) PM-52	104.1	bt-qtz schist	P_4	2.2	7.4		6.6	6.6							0.4		1.4						